Universitat Autònoma de Barcelona

RF Filters and Multiplexers Based on Acoustic Wave Technologies with Ladder-Type and Cross-Coupled Topologies

Alfred Raul Giménez Bonastre

Universitat Autònoma de Barcelona

Department of Telecommunications and Systems Engineering

RF Filters and Multiplexers Based on Acoustic Wave Technologies with Ladder-Type and Cross-Coupled Topologies

Designing Under a Systematic Strategy

Ph.D. Dissertation in Electrical and Telecommunications Engineering by

Alfred Raul Giménez Bonastre
E-mail: AlfredRaul.Gimenez@uab.cat

Thesis Advisor: Prof. Pedro de Paco Sánchez
E-mail: Pedro.DePaco@uab.cat
Universitat Autònoma de Barcelona (UAB)
Escola d'Enginyeria

September, 2016

"The truths are easy to understand once they are discovered. The point is to discover them."

Galileo Galilei

Abstract

The mobile technology has emerged as the most successful platform for the introduction of innovative services and user applications from both a technological and economical perspective. Mobile devices are changing the habits of the people and it is possible to see how, in this sense, our society is continuously improving. With the 4G network in process of deployment and the future 5G standards under development, global demand for broadband data services has been subjected to a series of unstoppable growth. And it will continue increasing pushed by the ubiquity of the service, according to Cisco's forecasts. The most important is that this growth undoubtedly demonstrates the importance of broadband services for the people, society, and economy, while it is drawing a major challenge for the network service providers.

The aim of this work is to develop synthesis techniques for the design of filtering devices based on micro-acoustic technologies, focusing therefore the great challenge of frequency spectrum management in the user segment. In general, the design of these filtering devices is based on optimization techniques because of the stringent requirements imposed by the technological feasibility of acoustic resonators and the tight performance specifications of the device. For this reason, the design and manufacture of filters and duplexers based on acoustic resonators becomes a huge challenge increasingly difficult to achieve. In this work, systematic methodologies are presented in order to improve and make more efficient the design of filtering devices based on micro-acoustic technologies.

The most important consideration during the synthesis of filters and duplexers is that the resonators must be technologically feasible. The methodologies presented in this work are useful for the design of ladder-type filters and cross-coupled prototypes in which the technological feasibility is an essential requirement for all the provided solutions. The effective coupling coefficient of each resonator, the resonant frequencies, the quality factor, the stored energy, or the chip size are parameters to consider during the design of micro-acoustic filters. By means of the techniques provided in this work, all these restrictions are analytically managed, and optimum results are obtained with a minimum time and computational effort.

Moreover, the use of these synthesis techniques allows the control of the phase parameters, which are essential for the design of multiplexer devices. These are considered the main device for the future radio-frequency front-end modules ready to work with Carrier Aggregation and the 4G-Advanced and 5G standards. Stand-alone filtering devices, duplexers, and multiplexers, ready to accommodate the micro-acoustic technological requirements and satisfying the frequency mask specifications, as long as possible, are the result of the proposed methodologies in this work.

Resum

La tecnologia mòbil ha emergit com la plataforma de major èxit per a la implantació de serveis innovadors i aplicacions d'usuari tant des d'un punt de vista tecnològic com econòmic. Els dispositius mòbils estan modificant els hàbits de comportament de les persones i veiem contínuament com, en aquest sentit, la nostra societat millora dia a dia. Amb la xarxa 4G en ple procés de desplegament i els futurs estàndards 5G en ple desenvolupament, la demanda global per al servei de dades de banda ampla ha estat sotmesa a un cicle de creixement imparable. I continuarà així alimentat per la ubiqüitat del servei, segons les previsions del Cisco. El més important és que aquest creixement indubtablement demostra la importància de la banda ampla per als ciutadans, la societat i l'economia, mentre dibuixa un gran repte als proveïdors de serveis de xarxa.

L'objectiu d'aquest treball està centrat en el desenvolupament de tècniques de síntesi per al disseny de dispositius filtrants basats en tecnologies micro-acústiques, enfocant així el gran repte de gestió de l'espectre freqüencial en el segment d'usuari. En general, el disseny d'aquest tipus de dispositius es basa en tècniques d'optimització degut a les rigoroses limitacions imposades per la viabilitat tecnològica dels ressonadors acústics, així com a les exigents especificacions de rendiment del dispositiu. És per aquests motius que el disseny i fabricació de filtres i duplexors basats en tecnologia acústica creen un gran repte cada cop més difícil d'assolir. En aquest treball es proporcionen metodologies sistemàtiques enfocades en millorar i fer més eficient el disseny de dispositius filtrants basats en ressonadors acústics.

El més important durant el disseny de filtres i duplexors basats en tecnologia acústica és que els ressonadors siguin viables tecnològicament. Les diferents metodologies presentades en aquest treball són útils per a la síntesi de topologies en escalera o xarxes amb acoblaments creuats on la viabilitat tecnològica és un requisit indispensable en totes les solucions proporcionades. El coeficient d'acoblament de cada ressonador, les freqüències de ressonància, el factor de qualitat, l'energia emmagatzemada, o l' àrea del xip són paràmetres que es tenen en compte durant el disseny d'aquest tipus de dispositius. Mitjançant les tècniques de síntesi proporcionades en aquest treball, no només es controlen analíticament aquestes restriccions, sinó que s'obtenen resultats òptims en el mínim temps i cost computacional.

L'ús d'aquestes tècniques, a més, permet un control dels paràmetres de fase essencial per al disseny de multiplexors, els quals estan en el punt de mira com a dispositiu indispensable dins les capçaleres dels futurs sistemes sense fils preparats per treballar amb el protocol de *Carrier Aggregation* dins els estàndards 4G-Advanced i 5G. Dispositius filtrants, duplexors i multiplexors viables tecnològicament i complint amb les especificacions de màscara freqüencials són resultat de l'ús de les metodologies proposades en aquest treball.

Acknowledgements

I am indebted with many people who have contributed to this work with their support, collaboration, and guidance. First of all, I would like to express my sincere gratitude to my supervisor, Prof. Pedro de Paco, for his kind support and patience. He gave me the opportunity to start my research in the fascinating world of micro-acoustic filters, and his encouragement and guidelines throughout this work have been very valuable during these years. He shared his immense knowledge and kept me motivated through tough times. His door was always open whenever I needed him.

Besides my supervisor, I would like to thank the rest of Antenna and Microwave Systems Group members for their insightful comments and encouragement. Specially to Jordi Verdú and Edén Corrales for their inputs and passionate participation. I also want to thank Dr. Óscar Menéndez, who introduced me to the field of BAW filters and encouraged me to start my Ph.D. degree. Ernesto Díaz must also be mentioned here, for his constant assistance in the laboratory.

I would like to thank my current and past roommates Mercedes, Iuliia, Ángel, Mónica, and Jordi for all the fun we have had during these years. In particular, I am grateful to Sergi for his continuous happiness and friendship. I would like to extend my gratitude to my other colleagues Alex, Marc, Martí, Pau, Dani, Yi, Guillermo, Jose, David, Vicente, Toni, Sergi, Úrsula, and everyone who have made the time I spent in the university something nice and fun.

My sincere thanks to EPCOS AG, a TDK group company, for funding and follow this work with great interest. Thanks to Dr. Karl Wagner, Vice-President of Advanced Development Discrete Components Systems, Acoustics, Waves Business Group, for giving me the opportunity to make an internship in his group. I would like to give a special mention to Dr. Thomas Bauer for his support, knowledge, and interest in my work. Work apart, he also offered all his help and support during my stay in Munich. Thank you, Thomas and Emi.

Last but not the least, I would like to acknowledge my family. Thanks to my parents, Rosa and Josep, and my grandparents Pilar and Alfredo, for providing me with unfailing support and continuous encouragement throughout my years of study and research. Thanks to Magda, Paqui, Jose, and my sisters Meri and Ester for being always there. And of course, to Montse and Mariano and all my cousins, uncles, and aunts for supporting me spiritually throughout my life in general.

I hope not to miss anyone, but I want to thank everybody who offered me his unconditional support, time, and love. This accomplishment would not have been possible without you. Thanks.

ALFRED

Contents

List of Figures

List of Tables

CHAPTER 1

Introduction

Mobile communications technology has evolved into the most successful enabling platform for innovative services and user applications. Mobile devices, such as smartphones, tablets, and wearable devices among others, have changed the society life-style and they have become essential in the daily lives of many people. Talking, text messaging, checking for e-mail, surfing the Internet, watching movies, or playing games are some of the most common utilities that people use routinely on their mobile devices.

According to Cisco's report [1], more than half a billion mobile devices and connections were added in 2015, most of them being smartphones. It represents a grew up to 7.9 billion connections and it is expected to be of 11.6 billion by 2020. As shown in Figure 1.1 (a), by 2020, there will be over 8 billion personal mobile-ready devices and over 3 billion machine-to-machine (M2M) connections, the basis of the Internet of Things (IoT). Such an increasing number of devices, along with the rising rate of data being transmitted throughout the world, generates an exponential growth of data traffic as measured and predicted by Cisco based on the increase in data moving through its routers. Overall mobile data traffic is therefore expected to grow to 30.6 exabytes per month by 2020, an eightfold increase over 2015, as shown in Figure 1.1 (b). Among different mobile applications, video content has much higher bit rates than other mobile content types, thus generating much of the overall mobile traffic growth. In fact, video streaming accounted for more than half of all mobile data traffic and it will grow to three-fourths by 2020.

Another important trend is the projected increase at the global mobile network connection speeds. Whereas the average downstream speed for smartphones grew nearly 26% to 7.5 megabits per second (Mbps) in 2015, the quantity is anticipated to reach 12.5 Mbps by 2020. Nowadays, the fourth generation (4G) is still being deployed in many parts of the world and represent just 20% of global mobile connections [1]. However, intensive research is going on towards future

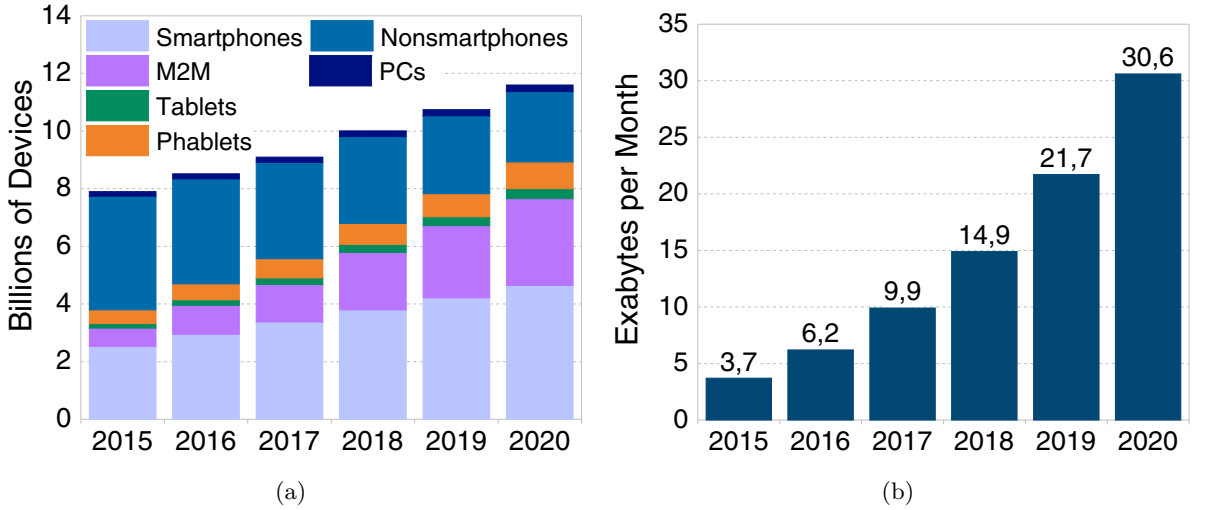

Figure 1.1: Global mobile forecast: (a) mobile devices and connections and (b) data traffic growth as measured by Cisco [1]. Source: Cisco Visual Networking Index Mobile, 2016.

mobile systems, and fifth generation (5G) system deployments are expected around 2020 [2].

Long Term Evolution (LTE) and its extension, LTE-Advanced, as the most up-to-date deployed standards, provide high throughput data transmission with peak data rates up to 3 Gbps and 1.5 Gbps for downlink (DL) and uplink (UL), respectively [3]. LTE was also designed for reduced service latency, simplified implementation complexity for cost reduction, optimized packet transmission, and so on. Furthermore, LTE introduced for the first time Internet Protocol (IP) packets for communication and enables a better usage of the spectrum. The main new features and improvements of LTE-Advanced with respect to LTE are Carrier Aggregation (CA) and the enhanced use of multi-antenna techniques [4].

An approach to satisfy the demanded peak data rates is to simply extend the transmission bandwidth using a single carrier, as stated in Shannon's theorem [5]. In practice, because of the overcrowded spectrum at frequencies of MHz and a few GHz, such a large portion of bandwidth is rarely available. CA becomes an attractive alternative because multiple component carriers of smaller bandwidth are aggregated, thus increasing the efficiency of the current fragmented spectrum [6,7]. In intraband CA, contiguous or non-contiguous carriers are allocated in one band, whereas in interband CA carrier combination is realized among two to five different bands. In 4G systems the number of aggregated bands is limited to 5, each of 20 MHz, but in the upcoming 5G systems this barrier will be eliminated.

Multiple-Input, Multiple-Output (MIMO) antennas also increase the spectral efficiency by adding spatial multiplexing, where different data streams are transmitted for each antenna and each stream carries different information but shares the frequency resources [8]. In LTE-

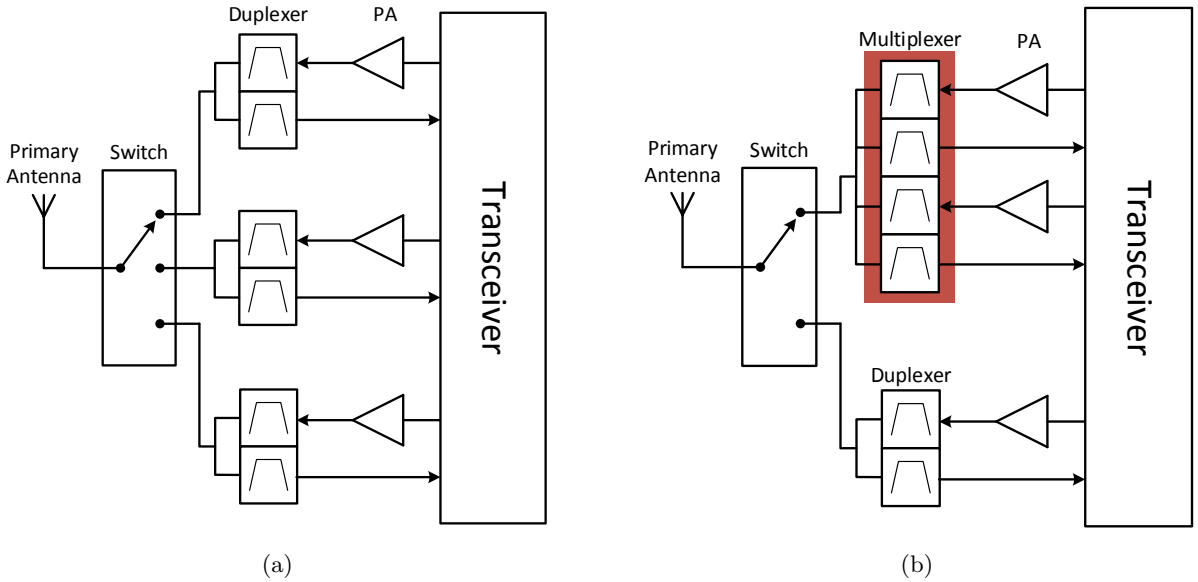

Figure 1.2: Simplified block diagram of a mobile device architecture: (a) duplexer approach and (b) multiplexer approach.

Advanced standard is introduced an 8×8 MIMO in the DL and 4×4 in the UL [3].

Historically, three new frequency bands were created each year on average. LTE-Advanced Release 12 [9] brings up to 44 independent bands for mobile communications. With that standard, there has also been an explosive growth in the number of newly defined CA combinations. Unfortunately, assigned frequency bands of operation are different in each region of the world, therefore increasing the complexity of Radio-Frequency (RF) Front-End Modules (FEMs) required in mobile devices ready to an international use. The architecture of the transceiver (TRx), including RF front-end configuration, in a handset aiming a high bandwidth global coverage should be ready to enable the full set of benefits of LTE-Advanced latest releases. For instance, the latest smartphones support more than 20 LTE bands coexisting with GSM and WCDMA standards, as well as WiFi, Bluetooth, and GPS systems.

The requirements for intraband and interband CA creates new challenges for RF-FEM designers. Interband CA requires simultaneous operation on two or more different frequency bands. The classical architecture in which different bands are selected using a switch connected to different duplexer components, as the one depicted in Figure 1.2 (a), becomes obsolete with CA. Multiplexer solutions (see Figure 1.2 (b)) simplify the design, reduce product footprint, conserve power, and improve overall system performance by covering primary band combinations. Currently, leader manufacturers in filter components and RF-FEMs are investing a lot of effort in multiplexer solutions for CA combinations [10–13]. Main challenges in multiplexer design are cross isolation between filters in a multiplexer device, given before by the switch, and linearity

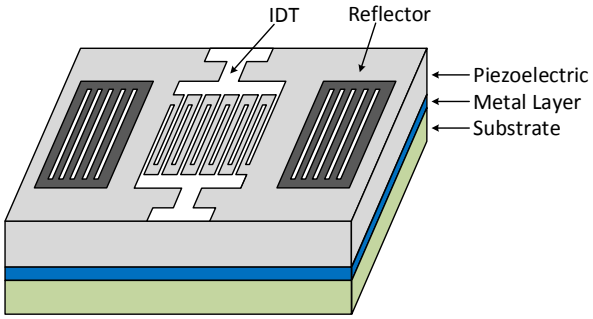

Figure 1.3: Structure of a SAW resonator.

in order to avoid nonlinear mixing products falling into one of the active bands in the device.

Acoustic devices using Surface Acoustic Waves (SAW) and Bulk Acoustic Wave (BAW) technologies are widely used for RF filters, duplexers, and multiplexers for mobile handsets. Actually, acoustic seems to be the unique filtering technology available at this moment ready to satisfy the stringent performance specifications of LTE standards. Acoustic devices fulfill the extremely low insertion loss, sharp roll-off, and high isolation characteristics required for cellular systems while occupying a small device size and compact footprint.

SAW filters dominated the markets of wireless telecommunications RF filters until approximately the end of the 90s. Since then, they coexist with BAW filters sharing the market of handset RF-FEM filters and duplexers. SAW technology is good for low cellular bands up to 2 GHz, whereas BAW presents more advantages at higher frequencies. In [14] there is a mapping of the acoustic technology that best fits the different LTE bands in terms of frequency of operation and complexity. Deciding which filter technology is better for a certain application is usually a balancing act between performance, size, and cost, and nowadays, this is well established in the industry for the actual LTE bands.

1.1 Acoustic Resonators

The difference between SAW and BAW technologies lies in how the acoustic wave propagates through the piezoelectric slab. A SAW device is made of a piezoelectric substrate with metallic structures, such as interdigital transducers (IDTs), and reflection gratings deposited on its surface, as depicted in Figure 1.3. A microwave signal applied at the input IDT stimulates a micro-acustic wave that propagates along the surface [15]. This is possible due to the piezoelectric effect that produces a deformation of the material when a voltage is applied on it. The same piezoelectric effect cause the SAW to generate an electric charge distribution at the output IDT and, therefore, a microwave output signal.

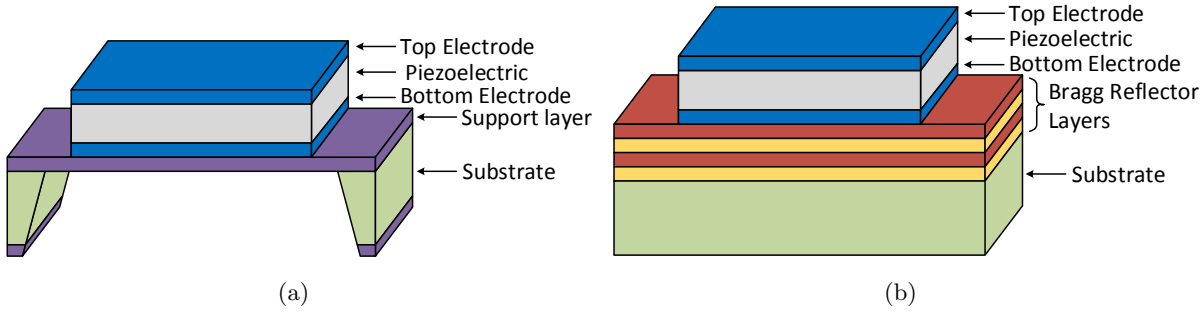

Figure 1.4: Structure of a BAW resonator: (a) Thin Film Bulk Acoustic Wave Resonator (FBAR) and (b) Solidly Mounted Resonator (SMR).

SAW resonators are limited in their achievable frequency of operation because of the separation of each finger in the IDT. Practical limitations lie at 2.5 GHz because the requirements for line width and gap dimensions in the IDTs require less than 0.25 μm lithography resolution, which requires a lot of effort for manufacturing [16]. SAW devices are generally manufactured on a Lithium Tantalate ($LiTaO_3$) or Lithium Niobate ($LiNbO_3$) crystal substrates. In fact, $LiTaO_3$ was the preferred substrate material for mobile applications because the resonator bandwidth fits perfectly with the required one for these applications. However, for temperature compensated SAW (TC-SAW) devices, in which an additional layer of silicon dioxide (SiO_2) on the top of the IDT is added to reduce the frequency shift due to temperature variation, $LiNbO_3$ is essential to increase the resonator bandwidth [17]. Although SAW technology is still growing with improved performance, it is a mature technology used almost since the emergence of mobile phones. A main advantage of SAW technology over BAW is the simplicity and low cost of the manufacturing process, in which only a few process steps are necessary.

Meanwhile, a BAW resonator is made of a piezoelectric plate sandwiched between metallic electrodes. The most used piezoelectric material for BAW devices is aluminum nitride (AlN) and molybdenum (Mo) or tungsten (W) for the electrodes [18]. When a voltage difference is applied on the electrodes the piezoelectric effect generates an acoustic wave propagating vertically in the bulk of the structure, that is, in the direction of the electric field. The resonance frequency is determined by the thickness and material properties of the piezoelectric and the electrodes. The fundamental resonance is found when the resonator plates, including the electrodes, are exactly one-half of the acoustic wavelength.

The first BAW device for CDMA-PCS duplexer was proposed by Agilent in 1999 [19] and introduced on the market in 2001 [20]. The structure they used to confine the acoustic wave in the resonator and isolate the substrate was called film bulk acoustic resonator (FBAR). The idea was to create an air-gap cavity below the bottom metal electrode, as depicted in Figure 1.4 (a). Due to the mechanical properties of this medium, the acoustic wave is reflected

on top and bottom electrode surfaces and resonance is thereby achieved. Mirror-type solidly mounted resonator (SMR) approach had entered the market somewhat later [21]. In the SMR configuration a Bragg reflector is placed below the bottom metal electrode, as shown in Figure 1.4 (b). The Bragg reflector consists of alternating metal and oxide layers, i.e., high and low acoustic impedance materials, that confines the acoustic wave under certain conditions.

FBAR devices present low loss and high quality factor compared with SMR, in which unwanted lateral modes have a direct path to the substrate through the acoustic mirror. The excitation of these parasitic modes, specially at the parallel resonance, causes energy lost because of signal leakage, with the corresponding degradation of the quality factor (Q) [22]. The most common solution to this problem is the optimization of the SMR layers for both the thickness and lateral modes [23, 24]. Maximum quality factors of about 5000 and 3000 are typical for FBAR and SMR configurations, respectively, whereas in SAW devices the quality factor is approximately of 1300 [25]. With respect to power handling, SMR devices endure higher power levels better than FBAR because the acoustic mirror actuates as a heat sink. In FBAR, the heat generated in the membrane can only leak through the anchor points. However, FBAR is still much better than SAW, in which the IDT fingers are prone to electromigration damage with high power levels [16]. An extensive comparison between SAW and BAW technologies can be found in [26].

1.1.1 Electrical Performance of Acoustic Resonators and Modeling

The electrical input impedance of an acoustic resonator is characterized by the presence of two resonances. At the resonance or series frequency f_s, the magnitude of the input impedance tends to its minimum value, ideally zero, whereas at the anti-resonance or parallel frequency f_p the input impedance tends to its maximum value, ideally infinity. The measured input impedance of a BAW resonator is shown in Figure 1.5. It can also be observed that the phase between resonant frequencies is about 90°, but outside these frequencies the phase is about -90°, behaving as a capacitor.

The electromechanical coupling coefficient k^2_{eff} of the resonator determines the amount of electrical energy converted into mechanical energy or vice versa. It is related with the separation of the resonance frequencies f_s and f_p, therefore determining the bandwidth of the resonator.

The most simple model of an acoustic resonator is given by the Butterworth-Van Dyke (BVD) equivalent circuit, widely used for conventional single crystal quartz bulk resonators [27]. The BVD model is suitable for modeling the fundamental operating mode of an acoustic resonator and, because of its simplicity, it is the preferred model to be used in system- and circuit-level designs. An improved and more realistic model, the modified Butterworth-Van Dyke (mBVD) model, was presented in [28]. In addition to the lumped inductor and capacitors, the electric,

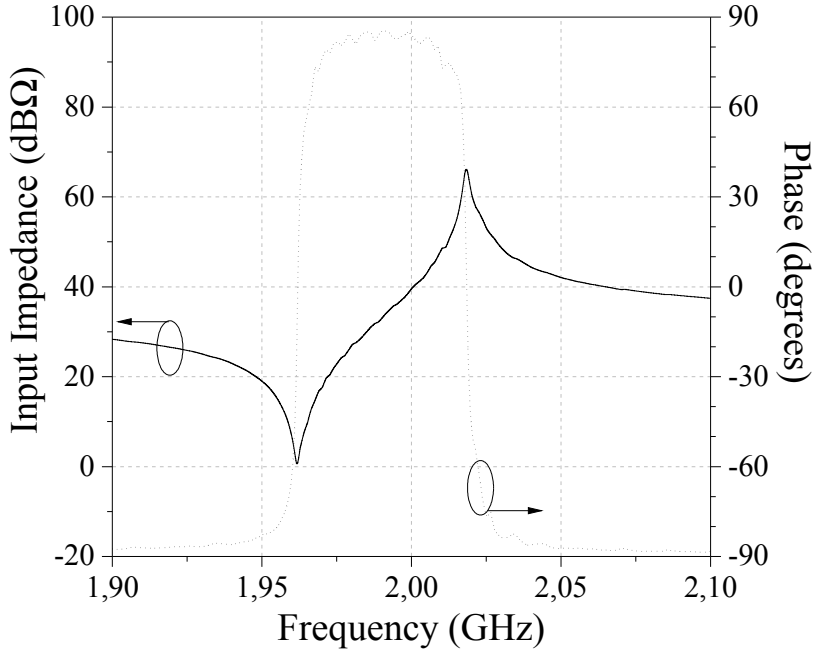

Figure 1.5: Input impedance magnitude and phase of a measured BAW resonator.

acoustic, and material losses are also modeled with resistors. Furthermore, substrate effects and electrode leads can also be included in the mBVD model [29]. The lumped components of the mBVD circuit can be easily translated into physical dimensions and properties of the resonator: area A, resonant frequency f_s, coupling coefficient k^2_{eff}, and quality factor Q. In general, k^2_{eff} and Q are given by the process of the chosen technology, and the designer only has A and f_s as variables to work with.

Other equivalent one-dimensional (1D) models commonly used for designing BAW are the Mason model [30, 31] and the transfer matrix approach [32]. These models are useful to construct the layer stack. In fact, they provide the electrical response as a function of the physical parameters and the thicknesses of the layers in the acoustic stack. In SMR-BAW, the Mason model is able to describe the effects introduced by the acoustic mirror by cascading a set of transmission lines modeling each layer in the stack. In SAW, the three-port mixed matrix approach, also known as P-matrix, describes the coupling of surface acoustic waves to electric field in an IDT in terms of Scattering and admittance matrices [33, 34]. The P-matrix of the whole device is obtained by cascading the P-matrices of the transducers and reflectors, subdivided at the same time by P-matrices of more basic cells [35]. Thus, the P-matrix is suitable for modeling resonators having several IDTs and reflectors. In general, the simulation time of these 1D models is higher compared with that of the mBVD, although they are still suitable for filter design including optimization procedures.

The finite-element method (FEM) allows the modeling of two-dimensional (2D) and three-dimensional (3D) effects of the resonator, like spurious modes and bulk leakage [36–38]. In a FEM simulation, the acoustic resonator is discretized into a finite number of elements in which the coupled-field analysis is calculated. Although these simulations require high computation costs, they provide an accurate prediction of the resonator performance, and are useful for suppression of spurious lateral modes [39]. FEM solution is also useful to analyze SAW devices such as dual mode SAW (DMS) filters, in which equivalent circuit models or P-matrices ignore relevant second-order effects [40].

1.2 Filter Topologies Based on Acoustic Resonators

In general, two main filter configurations can be classified according to the connection type between the acoustic resonators: those connected electrically and those acoustically coupled. Ladder- and lattice-type filters belong to the first approach, whereas stacked crystal filters (SCFs) and coupled resonator filters (CRFs) belongs to the second one [16]. Nowadays, the two most important topologies for mobile phone applications are ladder-type filters and CRFs in SAW, also known as DMS filters [41].

The conventional ladder-type filter is made of several consecutive series and shunt acoustic resonators, as depicted in Figure 1.6 (a). Ladder-type filters can be realized either in SAW and BAW technologies. They obtain high selectivity, because of the finite transmission zeros (TZs) below and above the passband, but poor out-of-band (OoB) rejection, mainly controlled by the number of resonators in the filter. To improve the OoB rejection, we additionally need to include external elements in series or parallel to the resonators [42], that can be externally implemented on the laminate. Matching external elements are usually required, particularly in multiplexer modules in whose several ladder-type filters are connected together in one common port. One of the major drawbacks of ladder-type filters is related to their achievable bandwidth, limited by the effective electromechanical coupling constant. To achieve larger bandwidths, additional external elements or cross-coupled topologies are some viable solutions.

DMS filters, on the other hand, are based on the transverse or longitudinal acoustic coupling between IDTs. A basic two-IDT DMS topology is shown in Figure 1.6 (b). CRF filters lead to wider bandwidths and better OoB rejection than ladder-type filters, but less selectivity because the TZs are placed in the origin and infinity. A potential topology yielding the best rejection and stopband suppression is obtained with the combination of a ladder-type stage and a CRF section. Furthermore, single-ended to balanced mode conversion is possible with CRF filters, although it is not used any more in mobile devices due to the large number of filters in the RF front end.

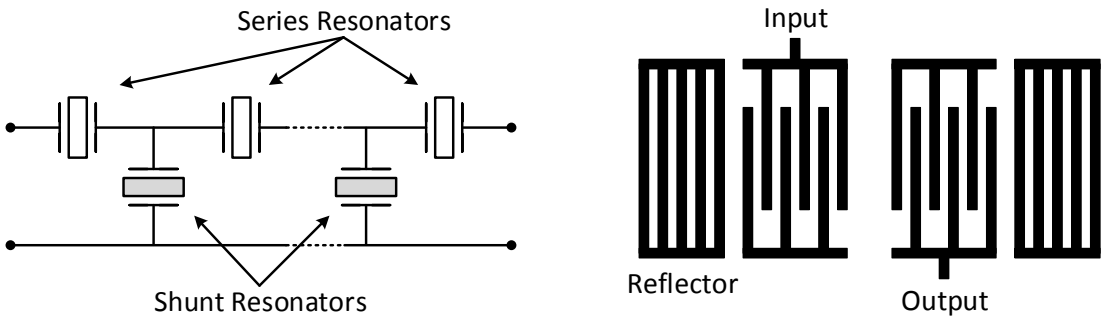

(a) (b)

Figure 1.6: Most used filter configurations: (a) ladder-type and (b) DMS-SAW.

1.3 Motivation and Purpose of the Thesis

The popularity of mobile devices worldwide has led the market for high-performance RF filters based on acoustic resonators to a huge success. The number of frequency bands keeps growing every year, and latest-generation smartphones are expected to support most of them, thus providing the full set of benefits of LTE latest releases. Nowadays, a top-tier smartphone supports more than 20 LTE bands, calling for more than 30 filters in a device. This vision justifies the steady pressure to shrink the available area for RF filters and modules whereas the compliance matrix of the spectrum mask specifications keeps increasing. The trend is now the integration of multiple filters into RF modules with switches and power amplifiers, because it yields smaller footprints and optimum performance.

RF filters based on acoustic resonators, either realized in SAW or BAW technologies, exhibit unbeatable advantages with respect to other technologies, specially for mobile applications. However, the increasingly complex specifications, with extremely high rejection of adjacent bands combined with low insertion loss, strengthen the need for advanced filter design techniques. Furthermore, the stringent technological requirements, i.e., the effective coupling constant, the maximum number of different resonant frequencies, and the quality factor, lead the design of a stand-alone filter to a more and more challenging task. With CA, the design of multiplexer modules, with isolation levels of -60 dB between multiple bands, becomes even more complicated.

The easier practice to start a design given some specifications is to modify an existing filter core and optimize the available variables in order to satisfy the new requirements. This methodology of design process may be promoted by the customer necessity or time to market pressures. However, trying to optimize a relatively large number of ill-advised variables for the current stringent requirements could not be the best procedure to acquire a good solution. Global optimization methods, which can partially solve this problem, are time consuming and do not assure the best solution for a finite number of iterations.

The designer understanding of the behavior of each component in the network is essential for the derivation of a good design. A common practice, and much better compared to the mentioned previously, is the creation of a potential topology including the arrangement of resonators, port matching, and grounding, by focusing on certain primary targets in order to obtain a good starting point for further optimization. The area, resonant frequencies, and external components are the variables for the optimization of insertion loss (IL), return loss (RL), and isolation between the filters in the multiplexer module. The overall OoB requirements are usually checked in the 3D FEM simulation, in which the layout, laminate, and mutual couplings behavior is contemplated. After each iteration of the optimization process, the result is compared with the given specifications and, in case all goals are not fulfilled, the circuit topology and values of the elements are re-adjusted to start a new optimization iteration. In [43], detailed information about the general filter design methodology can be found.

Our breadth of view is to address the design of filters based on acoustic resonators from a methodological perspective by using synthesis techniques. Nowadays, the design of RF filters with attenuation poles at finite frequencies is quite well understood and widely used for less restrictive filter technologies. The synthesis methodology is carried out according to a low-pass model based on cross-coupled schemes or by means of the well-known extracted pole technique. The recent introduction of non-resonating nodes (NRNs) has allowed these synthesis techniques to be used in the design of acoustic filters. Fully canonical inline topologies without the need of a direct source-load cross-coupling can be realized by using NRNs, and their characteristics agrees with those observed in the well-established acoustic wave based ladder-type networks.

The synthesis approach begins with the definition of a general class of Chebyshev filtering function with finite transmission zeros (TZs). The filtering function can be constructed directly from the filter degree, the position of the finite TZs, and the RL level as input variables. These input variables can be selected according to the frequency range mask specifications. The parameters of a low-pass equivalent circuit are obtained from the polynomial definition of the filtering function. An inline low-pass prototype can be transformed into a ladder-type band-pass network made of BVD resonators. Once the BVD parameters are associated with the physical properties of acoustic resonators, the synthesis is completed. Since the synthesis methodology is all based in direct numerical analysis, the computational effort is negligible.

However, not any synthesized network among the infinite possibilities is ready to be implemented with acoustic technology. Assuming that the topology and resonator models are the adequate ones, they have to account for technological feasibility in terms of resonant frequencies and effective coupling coefficients. The parameters of the BVD model are bounded by these technological constraints, and the result of the synthesis must contemplate them. Since, as already mentioned, the input variables to the synthesis methodology are the filter degree, the TZs, and the RL, the resulting BVD elements and, consequently, the technological parameters,

are subject to them. Therefore, the goal in the design is to find the set of TZs and RL for a given filter order that satisfies not only the frequency mask specifications, but the technological constraints as well. An automatic search engine based on a local optimization routine has been implemented in this work to this end. It is important to observe the difference with the design methodologies mentioned above. Using synthesis techniques, an ideal filter response is always obtained in a fast and accurate way. The optimization of the set of TZs and RL is negligible in terms of computational cost, because there are only a few input variables to optimize and the starting guess is always well-defined. The mask specifications and the technological requirements are defined as constraints during the optimization procedure. Meanwhile, different solutions can be easily obtained in terms of better RL, minimum power density distribution, or minimum size. The main advantage of using synthesis techniques in the design of acoustic based filters is that the designer is able to straightforward validate the feasibility of the design and check different filter orders or topologies, as well as obtain suitable starting points for further optimization processes, e.g., FEM analysis, packaging, etc.

Leveraged in this synthesis methodology, further research have been developed in this work for the design of cross-coupled topologies based in acoustic technology. The coupling matrix approach is a useful tool that contains most of the relevant information about the cross-coupled network. Direct synthesis techniques or optimization of the coupling matrix elements allows the design of advanced filter topologies with improved characteristics compared to those of ladder networks.

These synthesis techniques, based in low-pass prototypes that are later transformed into band-pass networks with BVD resonators, present many advantages for the design of acoustic filters, as already mentioned. However, the low-pass response is a narrowband approximation of the behavior of the band-pass network, and TZs in the origin and infinite frequencies are not contemplated. Variations on the phase parameters at frequencies far from the band may also occur, which could be a problem for multiplexer module designs. Therefore, the last objective of this work is to introduce the derivation of a proper band-pass filtering function in order to extract the network elements directly in the band-pass domain. This assures a total control of the magnitude and phase parameters in the whole range of frequencies.

The main purpose of this thesis was to develop system-level design methodologies to address the stringent specifications and challenges for 4G and the upcoming 5G filters and multiplexers. The proposed methodologies are native-oriented to accommodate the acoustic technology, either SAW and BAW, and assure feasibility by integrating synthesis, topology, and technology. Important features like the effect of the losses, the monitoring of the resonator power density, the maximum allowable values of the external elements, etc. are all investigated and introduced in the design methodology, yielding a solution closer to a real one.

1.4 Thesis Outline

In this chapter, the acoustic technology has been briefly reviewed. Acoustic resonators, either based on bulk or surface acoustic waves, as well as its basic performance and modeling have been introduced. The main filter configurations have been also presented and classified. Finally, the motivation and the main objectives for the thesis have been discussed.

Chapter 2 is dedicated to synthesis techniques for the design of ladder-type filters, duplexers, and multiplexers based on acoustic resonators. It introduces different, but equivalent, low-pass models of an acoustic resonator, based on resonating and non-resonating nodes (NRNs). These low-pass models have been derived from the well-known BVD model of an acoustic resonator. The ladder-type filter is therefore presented in the low-pass domain as an inline set of dangling resonators, a network very suitable for parameter extraction purposes. The network to be synthesized is therefore associated to a general class of Chebyshev filtering function, given an input admittance function from which the network is synthesized. The parameters are therefore linked by explicit equations to the acoustic technology constraints. The main technological requirements are also reviewed in this chapter as well as suggestions of how they can be taken into account during the synthesis procedure through an automatic search engine.

A brief review of the most important multiplexer topologies and the basic idea for the design of multiplexing systems are also discussed in Chapter 2. The control over the phase parameters during the synthesis procedure is essential for the design of multiplexers, and the proposed methodologies makes it an easy and fast exercise.

Chapter 3 includes synthesis techniques for the design of cross-coupled filters based on acoustic resonators. An analytical parameter extraction procedure is exploited for the synthesis of cross-coupled prototypes within some limitations on the achievable topologies. The study of the relationship between the characteristic frequencies and the prescribed transmission zeros has taken advantage of this synthesis technique. The understanding and management of complex TZs after the extraction of a cross-coupling are also detailed in this chapter. In addition, the technique is used to study a potential electro-magnetic feedthrough between the ports of a filter, and solutions to overcome the undesired effect are also detailed.

A general technique based on the coupling matrix optimization is presented at the end of Chapter 3 for the design of any cross-coupled topology. The coupling matrix is defined in order to best accommodate the acoustic resonators models, based on NRNs, and a smart optimization of its elements based on the characteristic frequencies is able to provide a solution that satisfies the mask specifications and the technological requirements whereas the frequency response fits into a general class of Chebyshev filtering function.

Chapter 4 introduces a synthesis technique of ladder-type filters directly in the band-pass

domain. Fundamental theory of the band-pass filtering functions necessary to accommodate the acoustic ladder-type filter behavior is presented. The number of prescribed singularities in the origin and infinity is very important for a proper formulation of the filtering function, and the realizable network depends completely on this definition. Two cases are differentiated during the chapter: one with capacitors and other with inductors as input/output matching elements. Although numerical issues might be found during the synthesis, these band-pass techniques present a big potential and may be an adequate solution to the frequency transformation inaccuracies, especially with the upcoming multiplexer systems where an accurate control of the phase is essential over a wide range of frequencies.

Finally, the conclusions are summarized in Chapter 5, as well as some future work recommendations.

The reader should note that the aim of the synthesized filters on the examples provided in this thesis is to illustrate the flexibility, suitability, and the potential of the proposed methodologies, rather than providing final designs which are limited by intellectual property.

1.5 Research Contributions

This dissertation collects the work that has been developed during the Ph.D. program and next is a list of the publications that have been submitted:

- A. Gimenez and P. de Paco, "A Dual-TZ Extraction Technique for the Synthesis of Cross-Coupled Prototype Filters," in *IEEE Microw. Wireless Comp. Lett.*, (Accepted).

- A. Gimenez and P. de Paco, "Involving Source-Load Leakage Effects to Improve Isolation in Ladder Acoustic Wave Filters," in *IEEE MTT-S Int. Microwave Symp.*, May 2016, San Francisco (USA).

- A. Gimenez, M. Jimenez, E. Corrales, and P. de Paco, "On the Design of Advanced Filtering Responses Based on Acoustic Wave Technology," in *International Workshop on Microwave Filters*, March 2015, Toulouse (France).

- M. Jimenez, A. Gimenez, E. Corrales, and P. de Paco, "Synthesis of Advanced Filters with Hybrid Topology Combinations Based on Acoustic Wave Technology,", in *International Workshop on Microwave Filters*, March 2015, Toulouse (France).

- M. Jimenez, A. Gimenez, E. Corrales, and P. de Paco, "Miniaturized Power Dividers with Integrated Bandpass Response Based on BAW Coupled Resonator Filters," in *Microwave Symposium (MMS), 14th Mediterranean*, Dec. 2014.

- A. Gimenez, M. Jimenez, E. Corrales, and P. de Paco, "Lowpass Equivalent Models of a Micro-Acoustic Resonator Based on Non-Resonant Nodes," in *Micro- and Millimeter Wave Technology and Techniques Workshop*, Nov. 2014, ESA/ESTEC (the Netherlands).

- M. Jimenez, A. Gimenez, E. Corrales, and P. de Paco, "The Role of Acoustic Wave Technology in Passive Components for User-Terminals on Satellite Telecommunications Systems," in *Micro- and Millimeter Wave Technology and Techniques Workshop*, Nov. 2014, ESA/ESTEC (the Netherlands).

- M. Jimenez, A. Gimenez, E. Corrales, and P. de Paco, "A Filtering Power Divider Based on Bulk Acoustic Wave Technology," in *MEMSWAVE*, July 2014, La Rochelle (France).

CHAPTER 2

Fundamental Theories of Low-Pass Acoustic Wave Filter Synthesis

The aim of this chapter is to provide a general methodology for the synthesis of ladder-type filter networks based on acoustic wave resonators. Leveraged on traditional low-pass synthesis techniques, a preliminary design of an acoustic filter becomes a straightforward task. Furthermore, the synthesis process is fast enough to be linked with an automatic search engine that provides an equivalent network ready to satisfy the set of attenuation mask specifications and the technological requirements established by the materials used during the fabrication.

The low-pass equivalent model of an acoustic resonator is presented during the first part of the chapter. The synthesis of a Generalized Chebyshev filtering function leads us to obtain the ladder-type prototype network parameters by means of the well-known extracted-pole technique. Finally, a frequency transformation and an impedance scaling of the network is extended to obtain the band-pass circuital parameters of an acoustic wave filter. Leveraged on the band-pass network, which is in good agreement with the acoustical simulation, the set of attenuation mask specifications, at the same time than the coupling constant, the resonant frequency, the stored energy, and other technological parameters of each resonator, can be evaluated.

The control of the phase parameters during the synthesis allows to use synthesis techniques for the design of duplexers and multiplexers, in which several filters are connected at the same port. The methodology proposed in this chapter is suitable for designing multiplexer devices with the minimum number of external matching elements. The stand-alone filters are synthesized separately with a proper phase condition derived previously. Then, all filters can be connected together creating the multiplexing device without noticeable differences in the frequency response of each filter. A brief introduction to the different multiplexing configurations is presented, and an example to validate the potential of the methodology can be found at the end of the chapter.

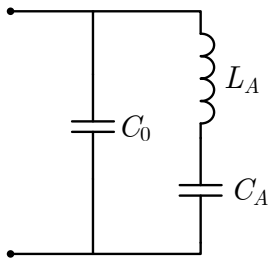

Figure 2.1: BVD equivalent electrical model of an acoustic wave resonator.

2.1 Filter Analysis and its Equivalent Circuit

The basic cell of a ladder-type filter based on acoustic wave technology is the resonator. It might be modeled by the Butterworth-Van Dyke (BVD) equivalent circuit. The model is valid either for BAW [16, 44] and for SAW [34] resonators. The BVD lumped element circuit is depicted in Figure 2.1, where C_0 corresponds to the static capacitance and the series resonator (L_A and C_A) is the motional arm. The static capacitance is due to the parallel electrode plates in BAW resonators, or to the static capacitance of the IDTs in SAW resonators. The BVD equivalent circuit is suitable for modeling the fundamental operating mode of the resonator. Generally, the higher order harmonics are neglected in the basic analysis, although they can be modeled by further motional arms in shunt configuration. The simplicity of the model makes it suitable for a parameter extraction synthesis that might be included into an optimization routine without expenses of computational time costs.

By analyzing the BVD circuit, the expression of the input impedance takes the form

$$Z_{in}(\omega) = \frac{j\left(\omega L_A - \frac{1}{\omega C_A}\right)}{1 - \omega^2 C_0 L_A + C_0/C_A}. \tag{2.1}$$

The input impedance of the BVD model describes the fundamental resonances of acoustic wave resonators, i.e. the series and parallel resonances, by requiring zero and infinite impedance values:

$$f_s = \frac{1}{2\pi\sqrt{L_A C_A}} \tag{2.2}$$

and

$$f_p = \frac{1}{2\pi}\sqrt{\frac{C_A + C_0}{L_A C_A C_0}} = f_s\sqrt{1 + \frac{C_A}{C_0}}. \tag{2.3}$$

From (2.3) it can be stated that f_p is, in normal conditions, greater than f_s because the capacitance ratio is always a positive number.

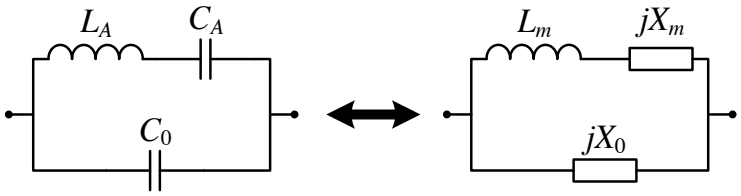

Figure 2.2: Band-pass and low-pass BVD equivalent models of an acoustic resonator.

2.1.1 Low-Pass Equivalent Model of an Acoustic Wave Resonator

In order to exploit the traditional low-pass synthesis techniques for the design of acoustic wave filters, a low-pass equivalent prototype of an acoustic wave resonator has to be established. To this end, a frequency transformation is applied to the BVD band-pass model. The result of this transformation is a low-pass equivalent circuit composed of an inductance in series with a Frequency Invariant Reactance (FIR), and both elements in parallel with a second FIR, as shown in Figure 2.2.

The foundation of the classical theory is based on networks made up of inductors and capacitors terminated in a matching resistor that exhibits symmetric responses with respect to the center of the passband. Traduced into the low-pass domain, low-pass responses are inherently symmetric with respect to the zero frequency. Consequently, the resonance frequency of each resonator is found at the center frequency of the passband [45]. However, for some applications, it is desirable to have an asymmetric response. The challenge was how to modify the classical low-pass prototype networks in such a way that when transformed into band-pass filters via frequency transformation, yields the appropriate asymmetric response.

Baum [46] was the first to introduce a hypothetical FIR element in the design of filter networks. He used the element as a mathematical tool in the formulation of the low-pass prototype filter. These hypothetical elements render the filter response to be asymmetric with respect to the zero frequency. Therefore, asymmetric band-pass responses were allowed via low-pass to band-pass frequency transformations. Over the years, this concept has been picked up by others and is now fully incorporated in the most general network synthesis techniques [47, 48].

By a simple inspection of the proposed low-pass BVD prototype in Figure 2.2, the FIR element X_m in series with the inductance tunes the resonance frequency Ω_s of the resonator. In other words, this element allows the asymmetric realization of the band-pass acoustic wave resonators and, therefore, the resonant frequency can be different than the center frequency of the passband. The other FIR X_0 is directly linked with the static capacitance, and it is responsible of the anti-resonance frequency occurrence.

The input impedance parameter of the low-pass prototype is found to be

$$Z_{in}(\Omega) = \frac{jX_0(\Omega L_m + X_m)}{\Omega L_m + X_m + X_0}. \tag{2.4}$$

The normalized frequency Ω is given by the standard low-pass to band-pass transformation

$$\Omega = \frac{\omega_0}{\omega_2 - \omega_1}\left(\frac{\omega}{\omega_0} - \frac{\omega_0}{\omega}\right), \tag{2.5}$$

where ω is the band-pass frequency variable and ω_0 is the center frequency of the passband obtained as the geometric mean of the passband edges ω_1 and ω_2.

The relationships between the low-pass and band-pass equivalent circuit parameters can be found by matching the input impedances in (2.1) and (2.4) and their derivatives. The resulting relationships evaluated at the center frequency ω_0 after the impedance scaling are found to be

$$L_A = \frac{1}{2}\left(\frac{2\alpha L_m + X_m}{\omega_0}\right) Z_0, \tag{2.6}$$

$$C_A = \frac{2}{\omega_0(2\alpha L_m - X_m)}\frac{1}{Z_0}, \tag{2.7}$$

and

$$C_0 = -\frac{1}{\omega_0 X_0}\frac{1}{Z_0}. \tag{2.8}$$

In the previous equations the parameter Z_0 is the reference impedance and α correspond to the inverse of the relative bandwidth defined as $\alpha = \omega_0/(\omega_2 - \omega_1)$.

For further understanding of the resonator behavior and for the upcoming synthesis of advanced filter configurations concerning cross-couplings in next chapters, the nodal diagram of an acoustic resonator is presented. This representation might be described by the coupling matrix, a tool commonly used for the design of microwave filters. Modeling the circuit in matricial form is particularly useful because matrix operations can then be applied. Moreover, the coupling matrix is able to include some of the real-world properties of the elements of the filter. The concept of coupling matrix was introduced by Atia and Williams for the design of dual-mode symmetric waveguide filters [49]. Since then, many works have exploited the representation for the design of several kinds of filter technologies [50–53].

Based on the low-pass BVD prototype obtained above, two equivalent low-pass configurations for the coupling matrix representation of an acoustic wave resonator are proposed: the dangling resonator and the singlet.

The Dangling Resonator

The first model consists of a unitary capacitor in parallel with a constant reactance b. Such a dangling resonator is connected through an admittance inverter J_R to a Non-Resonating Node

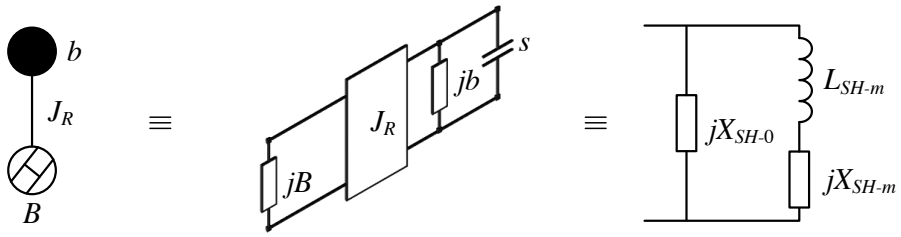

Figure 2.3: Low-pass equivalent circuit of a shunt acoustic wave resonator.

(NRN) implemented by the FIR B, as shown in Figure 2.3. The input admittance of such elementary structure is

$$Y_{in} = jB + \frac{J_R^2}{s + jb}. \tag{2.9}$$

Notice that the admittance becomes infinite when $s = -jb$, resulting in a transmission zero at normalized frequency $\Omega = -b$. This TZ might be either positive or negative, leading respectively to a series or a shunt arrangement of the band-pass resonator after the network denormalization. On the other hand, when the admittance becomes zero, an attenuation zero is produced, thus enabling the pass of the signal through the NRN. It can be noticed that the admittance characteristic of a dangling resonator is equivalent to that of the BVD prototype, as a further evidence of the equivalence of both models.

The major benefit of this model is that the FIR b of the resonant node is directly associated with the TZ of the acoustic wave resonator, i.e. the resonance frequency and the anti-resonance frequency for shunt and series positioned resonators, respectively. For the same reason, this model is particularly useful for extracted pole synthesis techniques that allows the design of inline filters [54].

By means of a simple inspection of the circuits in Figure 2.3, it can be seen that the NRN B (shunt susceptance) can be directly related with the shunt FIR X_{0-SH}, whereas the dangling resonator creates the pair L_{m-SH} and X_{m-SH}. As a result of a simple analysis the relationships between both circuits are found to be

$$X_{0-SH} = -\frac{1}{B}, \tag{2.10}$$

$$L_{m-SH} = \frac{1}{J_R^2}, \tag{2.11}$$

and

$$X_{m-SH} = \frac{b}{J_R^2}. \tag{2.12}$$

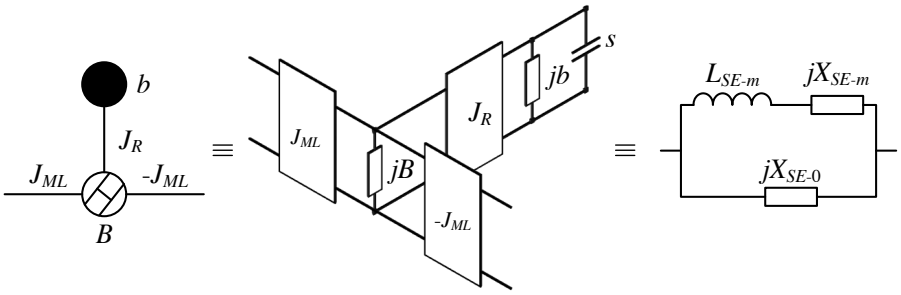

Figure 2.4: Low-pass equivalent circuit of a series acoustic wave resonator.

The relations shown above are valid for shunt acoustic wave resonators (see Figure 2.3). Therefore, it is also necessary to prepare a series resonator interpretation for the resonator synthesis. The result is a dangling resonator connected to an NRN and placed between two admittance inverters J_M, as depicted in Figure 2.4. The sign of the admittance inverters is the opposite in order to maintain the phase properties of the resonator.

The analysis of the admittance parameters of circuits in Figure 2.4 provides the following relationships:

$$X_{0-SE} = \frac{B}{J_M^2}, \tag{2.13}$$

$$L_{m-SE} = \frac{B^2}{J_R^2 J_M^2}, \tag{2.14}$$

and

$$X_{m-SE} = \frac{B}{J_M^2}\left(b\frac{B}{J_R^2} - 1\right). \tag{2.15}$$

For both the shunt and series cases, the NRN is directly related with the static capacitance of the BVD model. To assure a positive capacitor after the band-pass transformation, the susceptance B has to be negative for series resonators and positive for shunt resonators. Similarly, the value of the susceptance element of the resonant node b, which is directly related with the transmission zero as $\Omega_i = -b_i$, has to be negative for series resonators, therefore introducing a TZ above the passband, and positive for shunt resonators, introducing a TZ below the passband.

The capacitance ratio γ in terms of the low-pass elements of the dangling resonator model is found to be

$$\gamma = \frac{B}{J_R^2}\left(\frac{b}{2} - \alpha\right) - \frac{1}{2} \tag{2.16}$$

for series resonators, and

$$\gamma = \frac{B}{J_R^2}\left(\alpha - \frac{b}{2}\right) \tag{2.17}$$

for shunt resonators.

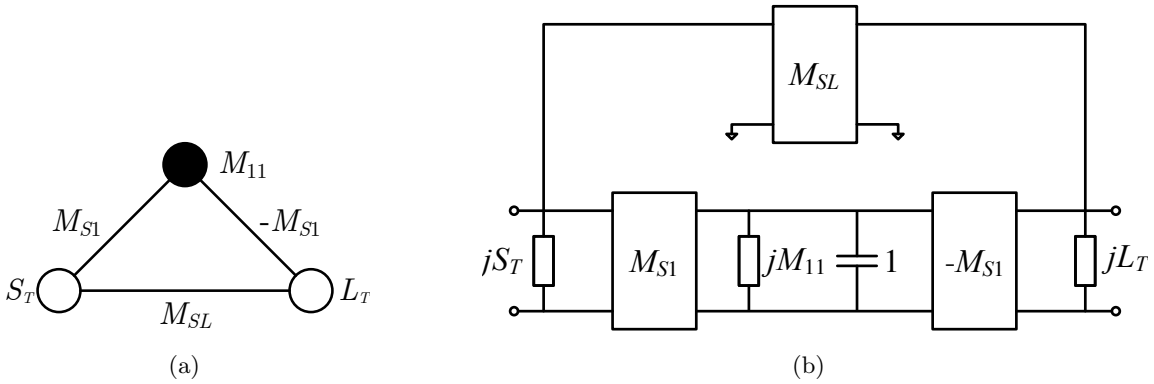

Figure 2.5: The singlet structure: (a) nodal and (b) circuital representations.

The Singlet

The second model we propose is based on the well-known trisection, that consists of a three resonant nodes coupled to each other. This scheme has been widely used for the design of advanced filter topologies [55]. However, Amari introduced a variant of the trisection by using NRNs in [56], and called it the singlet. This building block is made of one resonator coupled to two NRNs, as shown in Figure 2.5 (a). To clarify the structure, in Figure 2.5 (b) there is the circuital scheme of the singlet.

The singlet is a canonical network, and it might introduce one TZ at a finite frequency. This representation is useful because it differentiates clearly between the electrical and acoustical behavior present in a series-positioned acoustic wave resonator. In case of shunt resonators, the dangling resonator model is also valid to differentiate the behaviors.

The direct path between source and load M_{SL}, including the FIR elements on both extremes jS_T and jL_T, is directly related with the static capacitance C_0 and, therefore, it is proportional to the active area of the resonator and inversely proportional to the thickness of the piezoelectric layer. The $ABCD$ matrix of the source to load path is

$$\begin{bmatrix} 1 & 0 \\ jS_T & 1 \end{bmatrix} \begin{bmatrix} 0 & j/M_{SL} \\ jM_{SL} & 0 \end{bmatrix} \begin{bmatrix} 1 & 0 \\ jL_T & 1 \end{bmatrix} = \begin{bmatrix} -L_T/M_{SL} & j/M_{SL} \\ jM_{SL} - jL_T S_T/M_{SL} & -S_T/M_{SL} \end{bmatrix}. \tag{2.18}$$

Since the $ABCD$ matrix in (2.18) is directly related with the $ABCD$ matrix of the static arm of a series-positioned acoustic wave resonator, it might be satisfied that

$$\begin{bmatrix} -L_T/M_{SL} & j/M_{SL} \\ jM_{SL} - jL_T S_T/M_{SL} & -S_T/M_{SL} \end{bmatrix} = \begin{bmatrix} 1 & -j/\omega C_0 \\ 0 & 1 \end{bmatrix}. \tag{2.19}$$

Therefore, it is obtained that $S_T = L_T = -M_{SL}$ and, for $\omega = \omega_0$, the static capacitance to be

$$C_0 = \frac{-M_{SL}}{\omega_0}. \tag{2.20}$$

Notice from (2.20) that the source-load coupling M_{SL} has to be always negative to assure a positive static capacitance.

On the other hand, the resonating path between source and load belongs to the acoustical branch of the resonator. The resonant node between the inverters M_{S1} can be easily transformed to a series LC resonator, thus being equivalent to the motional arm of the BVD model. In order to obtain the relationships between the band-pass model and the singlet, the $ABCD$ matrices of the low-pass and the band-pass circuits are compared and evaluated at $\omega = \omega_0$, resulting in

$$L_A = \frac{2 + M_{11}W}{2M_{S1}^2\omega_0 W} \tag{2.21}$$

and

$$C_A = \frac{2M_{S1}^2 W}{\omega_0 \left(2 - M_{11}W\right)}, \tag{2.22}$$

where W corresponds to the relative bandwidth.

The capacitance ratio γ in terms of the low-pass elements of the singlet model results in

$$\gamma = \frac{M_{SL}\left(M_{11}W - 2\right)}{2M_{S1}^2 W}. \tag{2.23}$$

2.1.2 The Ladder-type Filter

In this section the classical ladder-type filter based on acoustic wave resonators is discussed. This inline network is implemented with electrically coupled resonators, and usually requires a pair of matching inductors at both ports.

Figure 2.6 shows the circuit diagram of a simple ladder filter having resonators in series and shunt branches, and a pair of inductors at input and output terminations. As it can be seen, ladder-type filters are organized alternatively connecting series and shunt resonators, although other configurations are possible. For example, by replacing a shunt resonator by a shunt capacitor, two series resonators can be coupled, therefore maintaining the number of TZs above the passband while reducing the degree of the filter.

A typical ladder filter response and the input impedance of a shunt and a series resonator is shown in Figure 2.7, for the purpose of describing the ladder-type filter principle of work. The resonance and anti-resonance frequencies (f_s and f_p respectively) are clearly identified in the input impedance curves for both series and shunt resonators. At the resonance frequency f_s^{SH} the impedance of shunt resonators tends to zero, creating a short-circuit to ground and producing a transmission zero. This TZ is always located at frequencies below the passband due to the acoustic resonator nature. Increasing the frequency causes the shunt resonator to become inductive until the anti-resonance frequency f_p^{SH} is reached. At this frequency shunt resonators

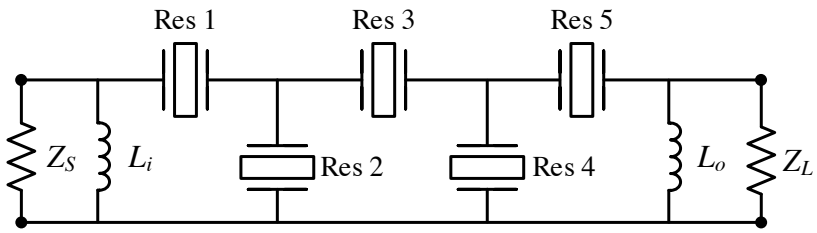

Figure 2.6: Ladder-type filter of order $N = 5$ having series and shunt resonators, and matching elements at input and output ports.

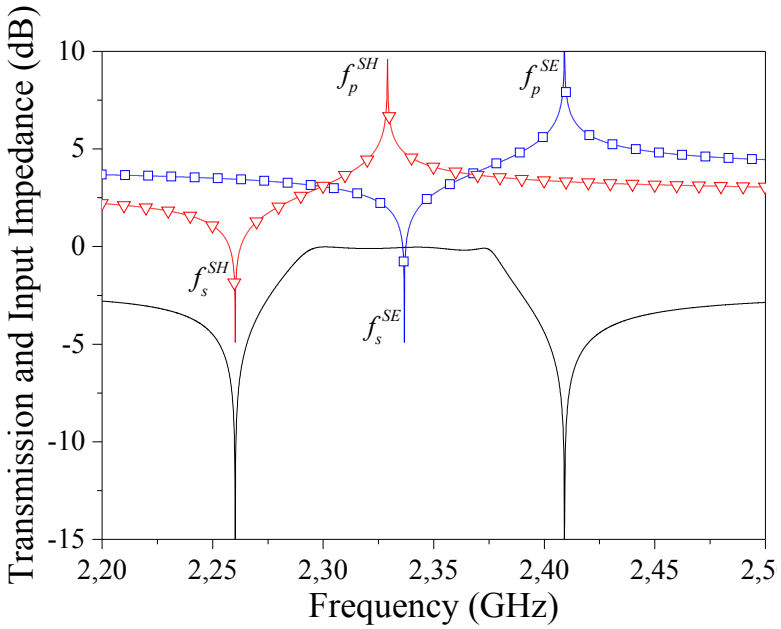

Figure 2.7: Performance principle of a ladder-type filter.

behave like open-circuits, and the signal can be transmitted between the ports. Similarly, at the resonance frequency of series resonators f_s^{SE} the signal flows through the series resonators due to its low impedance condition. Finally, further increasing the frequency, we find the anti-resonance of series resonators f_p^{SE}, where the impedance tends to infinity creating an open-circuit between terminals.

At frequencies far from the passband, the out-of-band rejection is controlled by the capacitive voltage divider nature of the ladder circuit. More ladder sections increase the ultimate rejection, but also increase the in-band insertion loss. Therefore, ladder-type filters are the perfect choice for applications that require a steep roll-off and low attenuation away from the passband. However, as it is presented in upcoming chapters, several configurations including cross-coupled resonators may overcome the ladder weaknesses.

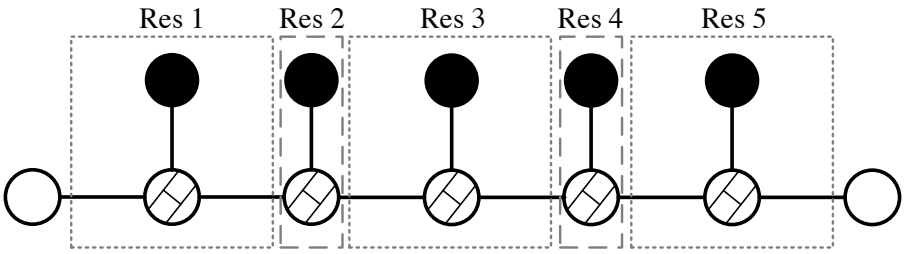

Figure 2.8: Nodal diagram of an equivalent low-pass ladder-type filter of order $N = 5$ based on the dangling resonator model. Black circles are resonant nodes, white circles are source and load terminations, dashed circles are NRNs, and lines are couplings between nodes.

The maximum achievable bandwidth of acoustic wave ladder-type filters is limited by the pole-zero distance of the acoustic wave resonators. As has been discussed previously, this distance is complementary to the electromechanical coupling coefficient k^2_{eff}, or inversely equivalent to the capacitance ratio γ, which becomes determined by materials and fabrication processes. However, the pole-zero distance can be enlarged by external reactive elements persevering the technological feasibility. In [43, 57] are given the relationships for the values of the external elements with the resonator parameters for four different combinations of technological adaptation.

Leveraged on the models presented in section 2.1.1, the low-pass nodal diagram of the filter under consideration is shown in Figure 2.8. Shunt resonators (Res 2 and Res 4) are made of an NRN and the dangling resonator, while series resonators (Res 1, Res 3, and Res 5) further include side inverters. The port matching inductors are included in source and load terminations as shunt FIRs in this case.

The ladder-type filter based on acoustic wave technology is a fully canonical network, because each resonator introduces a transmission zero at finite frequencies. Furthermore, each transmission zero is independently controlled by one resonator. That feature provides modularity in the design process, and allows the use of the extracted pole synthesis technique [54].

Meanwhile, it is well-known that a fully canonical network requires of a source-load coupling to exhibit $n_{fz} = N$ transmission zeros [50]. The use of NRNs makes possible to create fully canonical networks without the need of a direct source-load coupling. The acoustic wave ladder-type filters are one of such special cases, where the source-load coupling exists but through the reactive path of static capacitors.

2.2 The Generalized Chebyshev Function Class

The design procedure of a microwave filter is usually based on the association of a lumped-element low-pass prototype network to a given frequency response. The prescribed frequency

characteristics can be defined by a polynomial filtering function that satisfies the electrical specifications. Several filtering functions can be found in the literature, such as the maximally flat, Chebyshev, elliptic, etc. Among all of them, the generalized Chebyshev filtering function is the most appropriate one to describe the behavior of ladder-type filters based on acoustic wave resonators. This is because the general class of Chebyshev functions might include even and odd degrees, symmetric and asymmetric characteristics, and a set of prescribed transmission zeros independent from each other.

First, we shall initially consider the filter as a passive, lossless and reciprocal two-port network. Its S-parameter matrix can be expressed in a general polynomial form as [1]

$$S = \begin{bmatrix} S_{11}(s) & S_{12}(s) \\ S_{21}(s) & S_{22}(s) \end{bmatrix} = \frac{1}{E(s)} \begin{bmatrix} F(s)/\varepsilon_R & P(s)/\varepsilon \\ P(s)/\varepsilon & (-1)^N F(s)^*/\varepsilon_R \end{bmatrix}, \tag{2.24}$$

where N is the filter degree, and consequently, the number of resonators. $E(s)$ and $F(s)$ are N-th degree polynomials with complex coefficients for the complex frequency variable $s = j\Omega$. The real constant ε_R allows the normalization of $E(s)$ and $F(s)$ to be monic (highest degree coefficient unitary). $P(s)$ is a polynomial of degree n_{fz}, equal to N for ladder-type acoustic wave filters. The constant ε normalizes the highest degree coefficient of $P(s)$ to unity.

Polynomial $P(s)$ is the numerator of the transmission parameter S_{21}. Its roots are the transmission zeros, already prescribed at the beginning of the design. Similarly, polynomial $F(s)$ is the numerator of the reflection parameter S_{11}, and its roots are the reflection zeros. Both polynomials roots must be purely imaginary or appear in complex conjugate pairs. Therefore, polynomials $P(s)$ and $F(s)$ have coefficients that alternate between purely real and purely imaginary as the power of s increases.

The denominator polynomial $E(s)$ is strictly Hurwitz to assure the system stability. This implies the roots of $E(s)$ to lie on the left-hand plane of the complex frequency variable, i.e., the real part of the complex roots has to be negative. This real part appears as $e^{\alpha t}$, where α is the real part of the root, in the transient response of the filter and thereby characterizes the amplitude response as a function of time. With the real part of the roots being negative, the output voltage is stabilized after a transition period, and the steady-state condition is reached. Polynomial $E(s)$ can be derived from the conservation of energy equation if $P(s)$ and $F(s)$ are known as follows:

$$E(s)E(s)^* = \frac{F(s)F(s)^*}{\varepsilon_R^2} + \frac{P(s)P(s)^*}{\varepsilon^2}. \tag{2.25}$$

For a passive, lossless, and reciprocal network, the S-parameters yields one unique orthogonality

[1] The symbol * identifies the para-conjugate polynomial operator:

$$Q(s)^* = Q^*(-s).$$

condition

$$S_{11}(s)S_{12}(s)^* + S_{21}(s)S_{22}(s)^* = 0. \tag{2.26}$$

Rewriting the orthogonality equation in polar coordinates and applying simple mathematical considerations, an important relation between the phases of the $S_{11}(s)$, $S_{22}(s)$, and $S_{21}(s)$ polynomials are obtained:

$$-\theta_{n21}(s) + \frac{\theta_{n11}(s) + \theta_{n22}(s)}{2} = \frac{\pi}{2}(2k \pm 1), \tag{2.27}$$

where the subscript n indicates the numerator part of the S-parameter and k is an integer.

In equation (2.27), the right-hand side is an odd multiple of $\pi/2$ radians and frequency independent. Therefore, the difference between the angle of the $S_{21}(s)$ numerator and the average of phases of the $S_{11}(s)$ and $S_{22}(s)$ numerators is always orthogonal.

Further development of equation (2.27) yields [58]

$$(N - n_{fz})\frac{\pi}{2} - k_1\pi = \frac{\pi}{2}(2k \pm 1), \tag{2.28}$$

where N is the order of the filter, n_{fz} is the number of transmission zeros, and k_1 is an integer. This equation implies that the integer quantity $(N - n_{fz})$ must be odd so that its right-hand side is satisfied. For fully canonical networks, where $(N - n_{fz}) = 0$ is even, an extra $\pi/2$ radians has to be added to the left-hand side of equation (2.28) to maintain the orthogonality condition. This effect is equivalent to multiplying the polynomial $P(s)$ by j.

2.2.1 Relationship Between ε and ε_R

The real constants ε and ε_R are used to normalize the highest-degree coefficient of polynomials $P(s)$, $F(s)$, and $E(s)$. ε can be determined by evaluating the $S_{21}(s)$ parameter at a convenient frequency, where the transmission level is known. For instance, at $s = \pm j$ the equiripple return loss RL level for Chebyshev filters might be prescribed, and the real constant can be obtained as

$$\varepsilon = \frac{1}{\sqrt{1 - 10^{-RL/10}}} \left|\frac{P(\Omega)}{E(\Omega)}\right|_{\Omega=\pm 1}. \tag{2.29}$$

By further inspection of the S-parameters definition and equation (2.29), the following relation can be derived:

$$\frac{\varepsilon}{\varepsilon_R} = \frac{1}{\sqrt{10^{RL/10} - 1}} \left|\frac{P(\Omega)}{F(\Omega)}\right|_{\Omega=\pm 1}. \tag{2.30}$$

On the other hand, the constant ε_R is determined by evaluating the $S_{11}(s)$ parameter for $s = \pm j\infty$. If $n_{fz} < N$, that is, at least one transmission zero is at infinite

frequency, $|S_{21}(s = \pm j\infty) = 0|$. Then, the conservation of energy condition dictates that $|S_{11}(s = \pm j\infty) = 1|$ and, because the polynomials $F(s)$ and $E(s)$ are monic, it is found that $\varepsilon_R = 1$. However, for the fully canonical case, where $n_{fz} = N$, the attenuation at $s = \pm j\infty$ is finite, and ε_R is derived from the conservation of energy condition. As before, since all polynomials are monic, it is obtained that

$$\varepsilon_R = \frac{\varepsilon}{\sqrt{\varepsilon^2 - 1}}. \tag{2.31}$$

2.2.2 Determination of the General Chebyshev Class of Filtering Function

Low-pass prototype filters based on acoustic resonators are ready to accommodate a general class of Chebyshev filtering functions, with a set of prescribed transmission zeros and return loss level. In fact, they are suitable to produce a fully canonical response with a number of attenuation poles at finite frequencies equal to the degree of the filter. The S-parameters are related to the filtering function $C_N(\Omega)$ by

$$|S_{21}(\Omega)|^2 = \frac{1}{1 + \left|\dfrac{\varepsilon}{\varepsilon_R} k C_N(\Omega)\right|^2} = \frac{1}{1 + \left|\dfrac{\varepsilon}{\varepsilon_R}\dfrac{F(\Omega)}{P(\Omega)}\right|^2}, \tag{2.32}$$

where k is a normalizing constant. The poles and zeros of the filtering function $C_N(\Omega)$ of degree N are the roots of $P(\Omega)$ and $F(\Omega)$ respectively, that is, the transmission zeros and the reflection zeros.

For the general Chebyshev characteristic, the filtering function has the form [59]

$$C_N(\Omega) = \cosh\left[\sum_{n=1}^{N} \cosh^{-1}\left(x_n\left(\Omega\right)\right)\right], \tag{2.33}$$

where $x_n(\Omega)$ is a function of the frequency variable Ω that requires the following properties to describe a Chebyshev characteristic:

- At $\Omega = \Omega_n$, where Ω_n is either a transmission zero at finite frequency or infinity, $x_n(\Omega) = \pm\infty$.
- At the passband edges, defined at $\Omega = \pm 1$, $x_n(\Omega) = \pm 1$.
- Between $\Omega = -1$ and $\Omega = 1$, $1 \geq x_n(\Omega) \geq -1$.

By developing the conditions above the function $x_n(\Omega)$ is derived as

$$x_n(\Omega) = \frac{\Omega - 1/\Omega_n}{1 - \Omega/\Omega_n}. \tag{2.34}$$

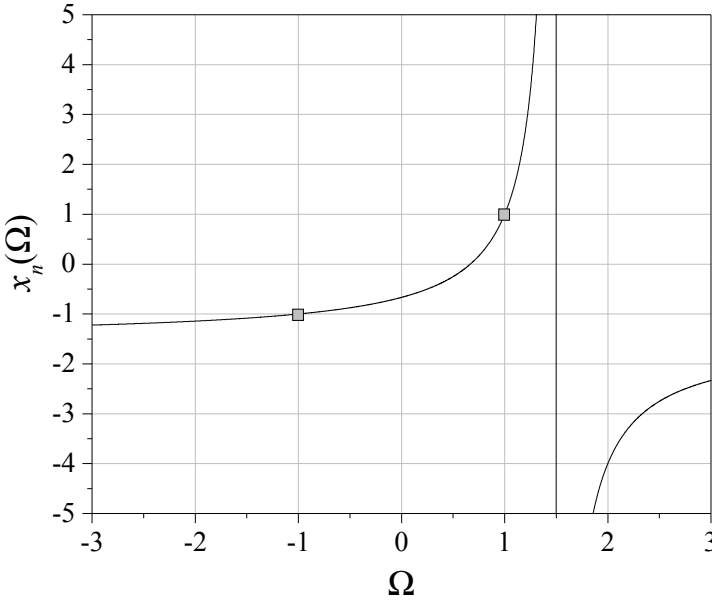

Figure 2.9: Function $x_n(\Omega)$ with a prescribed transmission zero at $\Omega_n = 1.5$. The rectangles indicates the passband frequency edges.

In Figure 2.9 it is shown the behavior of the function $x_n(\Omega)$ in the Ω plane for a prescribed transmission zero at $\Omega_n = 1.5$. All conditions specified above are satisfied, thus providing a general Chebyshev characteristic.

The next step is to expand equation (2.33) to determine the numerator and denominator polynomials $F(\Omega)$ and $P(\Omega)$, respectively. By following the technique in [58], the denominator of the cost function is derived as

$$P(\Omega) = \prod_{n=1}^{N} (1 - \Omega/\Omega_n), \tag{2.35}$$

whose zeros are the transmission zeros. The coefficients of $F(\Omega)$, also referred to as $U_N(\Omega)$, are computed by a recursive technique where the solution for the nth degree polynomial is built up from the results of the $(n-1)$th degree. $V_N(\Omega)$ is always multiplied by a transformed variable $\Omega' = \sqrt{\Omega^2 - 1}$, and is introduced here as an auxiliary polynomial.

The recursion cycle is initiated by considering the first prescribed transmission zero Ω_1 and setting $N = 1$ as

$$U_1(\Omega) = \Omega - \frac{1}{\Omega_1}, \tag{2.36a}$$

$$V_1(\Omega) = \Omega' \sqrt{\left(1 - \frac{1}{\Omega_1^2}\right)}. \tag{2.36b}$$

Having obtained the first degree polynomials, the cycle continues with the rest of the prescribed transmission zeros Ω_n until all of them, including those at $\Omega_n = \infty$, are used. The remaining $(N-1)$ cycles uses the following equations to update polynomials $U_i(\Omega)$ and $V_i(\Omega)$ for each iteration i:

$$U_i(\Omega) = \Omega U_{i-1}(\Omega) - \frac{U_{i-1}(\Omega)}{\Omega_i} + \Omega' \sqrt{\left(1 - \frac{1}{\Omega_i^2}\right)} V_{i-1}(\Omega) \tag{2.37a}$$

$$V_i(\Omega) = \Omega V_{i-1}(\Omega) - \frac{V_{i-1}(\Omega)}{\Omega_i} + \Omega' \sqrt{\left(1 - \frac{1}{\Omega_i^2}\right)} U_{i-1}(\Omega) \tag{2.37b}$$

At the end of the recursive technique, the determined $U_N(\Omega)$ polynomial has the same roots than $F(\Omega)$, the numerator of the filtering function $C_N(\Omega)$. Therefore, polynomials $P(s)$ and $F(s)$ becomes fully determined by the transmission zeros, and the constants ε and ε_R by the return loss parameter. Finally, the common denominator $E(s)$ can be constructed by using the principle of energy conservation in equation (2.25).

2.3 Realization of Ladder-type Prototype Filters

The general class of Chebyshev filtering function provides an equiripple behavior in the passband and has a limited number of transmission zeros in the stopband. The transfer and reflection parameters can be expressed as the ratio of two finite-degree polynomials and a normalization constant, that describes the general Chebyshev characteristics. The input reflection parameter $S_{11}(s)$ has the form

$$S_{11}(s) = e^{j\theta_{11}} \frac{F(s)}{\varepsilon_R E(s)}, \tag{2.38}$$

where $e^{j\theta_{11}}$ is a phase term that has no effect on the return loss magnitude because the argument θ_{11} is a real quantity. The term participates actively in the extraction of the network parameters, particularly when the first element connected to the source is a non-resonating node, as occur in micro-acoustic prototype filters. But, even more important, this phase term is used to accomplish the common port phase requirements in duplexer and multiplexer designs.

To determine the phase term, the first element that constitutes the network has to be examined. In case that the circuit presents a resonant node connected to the source, there is at least one transmission zero at infinity, and the asymptotic value $|S_{11}(\infty)|$ is equal to 1. Since $F(s)$ and $E(s)$ are considered monic polynomials and $\varepsilon_R = 1$ when $n_{fz} < N$, the angle must be $\theta_{11} = 0$.

Meanwhile, for fully canonical ladder-type networks in which the first node is an NRN of constant reactance jB, as shown in Figure 2.10, no transmission zeros are found at infinity. The

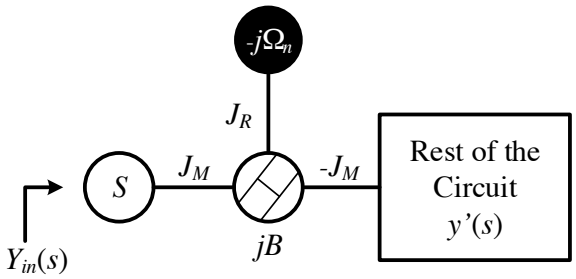

Figure 2.10: Circuit whose first node from the source is an NRN.

expression of the input admittance if no FIR is considered at source node is

$$Y_{in}(s) = \frac{J_M^2}{jB + \dfrac{J_R^2}{s - j\Omega_n} + \dfrac{J_M^2}{y\prime(s)}}. \tag{2.39}$$

This equation shows that the input admittance equals zero at the position of the transmission zero $s = j\Omega_n$ and, therefore, all the signal is reflected at the input port ($S_{11} = 1$). Using this condition in (2.38) it is obtained that

$$e^{j\theta_{11}} = \left.\frac{\varepsilon_R E(s)}{F(s)}\right|_{s=j\Omega_n}. \tag{2.40}$$

By using this phase term, the FIR element at the source node (and load in case of symmetric networks) is not necessary anymore in stand-alone filer designs. The study can also be realized for the output reflection parameter $S_{22}(s)$, resulting in exactly the same results. Notice that if the phase term is not properly considered, it is satisfied that $|S_{11}(j\Omega_n)| = 1$, although it remains a phase part that has to be implemented by a matching FIR element at input/output node. Following the same principle, we will show in later sections the benefits of a phase matching approach in duplexer designs, where phase shift sections can be avoided by adjusting the reflection coefficient phases of the individual filters.

With the reflection coefficient fully determined by equations (2.38) and (2.40) and considering a terminal admittance normalized to unity, the input admittance of the whole filter becomes

$$Y_{in}(s) = \frac{1 - S_{11}(s)}{1 + S_{11}(s)} = \frac{\varepsilon_R E(s) - e^{j\theta_{11}} F(s)}{\varepsilon_R E(s) + e^{j\theta_{11}} F(s)}. \tag{2.41}$$

The input admittance obtained from the generalized Chebyshev polynomials in (2.41) has to be equal to the input admittance of the network to be extracted. Multiple combinations regarding the position of each dangling resonator in the structure, as well as the management of the degree of freedom introduced by the NRNs, yields in different prototype networks but sharing the same response. However, at the end of the extraction, the input admittance must have been completely removed.

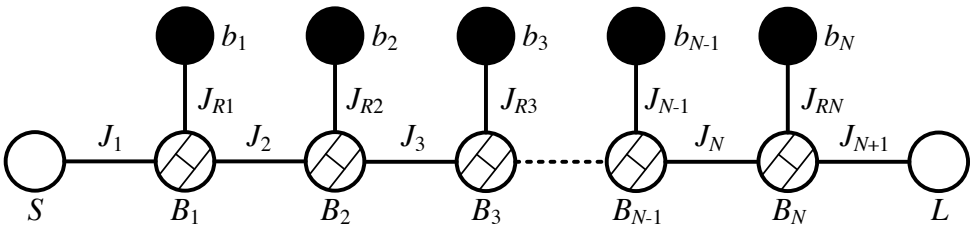

Figure 2.11: Low-pass nodal diagram of an inline prototype filter with N transmission zeros.

2.3.1 Parameter Extraction of Stand-Alone Ladder-Type Networks

This section describes the extraction procedure of an inline low-pass filter prototype. The technique is based on a Darlington approach to obtain the reactances that constitutes the network from the input admittance function $Y_{in}(s)$. The extraction of the elements is carried out successively from one port to another, and starts matching the admittance function in (2.41) with that of the network to be extracted. For the ladder-type filter shown in Figure 2.11 the admittance function might be expressed as

$$Y_{in}(s) = \cfrac{J_1^2}{jB_1 + \cfrac{J_{R1}^2}{s+jb_1} + \cfrac{J_2^2}{jB_2 + \cfrac{J_{R2}^2}{s+jb_2} + \ldots + \cfrac{J_N^2}{jB_N + \cfrac{J_{RN}^2}{s+jb_N} + \cfrac{J_{N+1}^2}{jB_L + G_L}}}}, \tag{2.42}$$

where B_L is the FIR matching element at output terminal and G_L is the load conductance, usually normalized to 1 Siemens.

It may be noticed that in equation (2.42) the input FIR jS is neglected, because it is no longer necessary if the reflection phase has been properly considered using (2.40). However, it has to be considered at the output port because, except in case of fully symmetrical networks, the matching output element is always required, as will be demonstrated later in this section.

The ladder-type filter based on acoustic resonators is made up of a concatenation of dangling resonators between inverters. Therefore, the extraction technique is a recursive procedure of dangling resonator parameters extraction. In Figure 2.12 there is the nodal diagram of the ith dangling resonator b_i with a unitary capacitor connected through an admittance inverter J_{Ri} to an NRN B_i. The input admittance $y_{in}(s)$ of such basic building block is

$$y_{in}(s) = \cfrac{J_i^2}{jB_i + \cfrac{J_{Ri}^2}{s+jb_i} + y\prime(s)}, \tag{2.43}$$

or equivalently,

$$\frac{J_i^2}{y_{in}(s)} = \frac{J_{Ri}^2}{s+jb_i} + jB_i + y\prime(s), \tag{2.44}$$

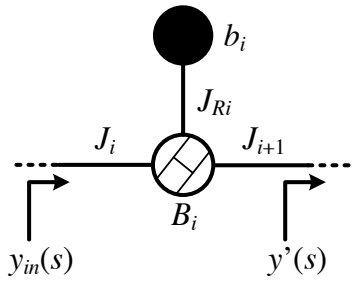

Figure 2.12: Nodal diagram of a dangling resonator connected to an NRN.

where $jb_i = -j\Omega_i$, the normalized frequency of the ith transmission zero given by the ith dangling resonator.

It is interesting to notice that the left-side of equation (2.44) presents a partial fraction form. The admittance residue evaluated at pole $j\Omega_i$ yields the coupling J_{Ri} as

$$J_{Ri}^2 = J_i^2 \text{ residue } \left(\frac{1}{y_{in}(s)}\right)\Bigg|_{s=j\Omega_i}. \tag{2.45}$$

The use of NRNs entails degrees of freedom that has to be managed by the designer to properly obtain the best design. For example, the coupling J_{Ri} in equation (2.45) depends on the coupling J_i, which can be arbitrary determined yielding different prototype networks. This technique is really useful in several filter technologies able to implement and control the couplings between resonators and NRN. However, for ladder-type filters based on acoustic wave technology, the coupling between resonators is an electrical connection. Furthermore, the main-line couplings are used to transform the low-pass dangling resonator to a low-pass BVD network, as shown in section 2.1.1. Thus, the considered degree of freedom is absorbed during the circuital transformation of the series resonators.

To simplify the extraction procedure the main-line couplings J_i are specified as the free parameters and set to $J_i^2 = 1$. For possible convenience, once the network has been completely synthesized, scaling rules might be applied to suit the elements of the circuit to a more feasible values regarding the intended realization, as detailed in [57]. The dangling resonator coupling can be further obtained as

$$J_{Ri}^2 = (s - j\Omega_i)\left.\frac{1}{y_{in}(s)}\right|_{s=j\Omega_i}. \tag{2.46}$$

The dangling resonator is now completely determined, and composed of a unitary capacitor, a FIR $jb_i = -j\Omega_i$, and a coupling J_{Ri} given by equation (2.46). To conclude the basic building block extraction, the NRN B_i has to be obtained from the admittance function. But first, the

dangling resonator has to be extracted by updating $y_{in}(s)$ as

$$y_{in}(s) \longleftarrow \frac{J_i^2}{y_{in}(s)} - \frac{J_{Ri}^2}{s + jb_i} = jB_i + y\prime(s). \tag{2.47}$$

To determine the NRN B_i the admittance function has to be evaluated at the following transmission zero Ω_{i+1}, for which the admittance term $y\prime(s)$ becomes zero. It is interesting to highlight that any of the remaining transmission zeros, prescribed when the general Chebyshev filtering function has been determined, can be used here to cancel out $y\prime(s)$. Depending on the chosen TZ the network might be more suitable in terms of technological constraints, as detailed in the following sections.

The FIR jB_i is therefore obtained as

$$jB_i = y_{in}(s)|_{s=j\Omega_{i+1}}, \quad y_{in}(s) \longleftarrow y_{in}(s) - jB_i, \tag{2.48}$$

where Ω_{i+1} is a prescribed finite transmission zero for ladder-type filters based on acoustic wave resonators. For inline filters with TZ at infinite frequencies, Ω_{i+1} becomes infinity if the following node is only a resonator instead of a dangling resonator. In equation above, the input admittance is also updated and ready to start the extraction of the basic building block using (2.46), (2.47), and (2.48).

Despite that the extraction can be done from the input and the output ports simultaneously, here we only consider the procedure starting from the input to the output terminals. For large inline networks it is preferably to perform the extraction from both ports in order to minimize the collected round-off errors. Even though, for typical filter orders of five to nine, the recursive technique from the input to the output is sufficiently accurate.

To finish the extraction of the network, once the last dangling resonator has already been extracted, the remaining elements in the network are the last NRN B_N, a FIR connected to load B_L, and the port conductance G_L. Figure 2.13 depicts the nodal diagram of the last dangling resonator of a ladder-type circuit connected to load node. The input admittance function of such network is

$$y_{in} = jB_N + \frac{J_{N+1}^2}{jB_L + G_L}. \tag{2.49}$$

Solving the equation for a coupling value of $J_{N+1} = 1$, the admittance can be separated into a real and an imaginary parts as

$$\Re\left[y_{in}\right] = \frac{G_L}{B_L^2 + G_L^2} \tag{2.50a}$$

$$\Im\left[y_{in}\right] = B_N - \frac{B_L}{B_L^2 + G_L^2} \tag{2.50b}$$

The terminal characteristic conductance G_L is determined by the component in which the filter is connected to, and it is usually normalized to unity. Nevertheless, the FIRs B_N and B_L can

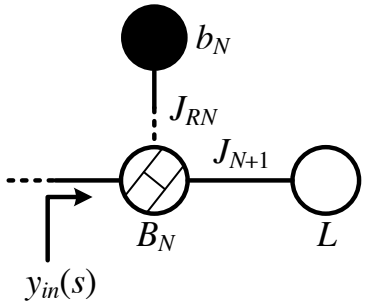

Figure 2.13: Nodal diagram of the last basic building block (dangling resonator) connected to load. Dot lines represent circuit parameters that has already been extracted of the admittance $y_{in}(s)$.

be determined by the remaining admittance function and the prescribed load conductance as follows:

$$B_L = \pm\sqrt{\frac{G_L - G_L^2\Re[y_{in}]}{\Re[y_{in}]}} \tag{2.51}$$

and

$$B_N = \Im[y_{in}] + \frac{B_L}{B_L^2 + G_L^2}. \tag{2.52}$$

By simple inspection of equation (2.51) it can be seen that there is a trade off that determines the nature of the last external reactance B_L being positive or negative and, consequently, the resulting value of the NRN B_N. This choice can be determined by the coupling coefficient constant k_{eff}^2 of the last resonator, in order to be the more feasible one. But other interests such as to have an external inductance instead of a capacitor in order to minimize the area can also be considered.

On the other hand, if $G_L = 1$ is considered, the real part of the remaining admittance $\Re[y_{in}]$ must be smaller than 1. Otherwise, B_L becomes pure imaginary, meaning a resistive element. This undesired effect can be solved by introducing an additional reactive element to the output port, or by matching the filter to a proper load conductance such that B_L becomes real in (2.51).

In case of symmetrical networks, that can be synthesized by determining a symmetric set of transmission zeros during the extraction procedure (i.e. $\Omega_1 = \Omega_N$, $\Omega_2 = \Omega_{N-1}$, and so on), the real part of the admittance function becomes $\Re[y_{in}] = 1$ if the phase has been properly considered and, therefore, the load FIR element B_L results in zero valued. For unsymmetrical networks, the source FIR is removed by the input reflection phase condition, although it is usually necessary at the output terminal in order to match the port conductance and phase parameters.

2.3.2 Duplexers Design Considerations

An important feature of any duplexer design is the isolation between the transmitter and the receiver filters. The incoming signal from the antenna at the receiver frequency band is divided between the receiver and transmitter paths. The incoming signal flows to the transmitter path, where it is rejected and routed newly to the receiver path. The interference of such reflected signal and the direct one from the antenna to the receiver must be constructive in order to assure the signal integrity. The same effect occurs with the signals transmitted from the TX to the antenna and the interference signal reflected in the receiver filter.

Our procedure to face this situation is by adjusting the input reflection phase of both transmitter and receiver filters in order to introduce zero degrees at the center frequency of the counterband, called dual frequency f_{Dual}. In this work, the dual frequency is considered either the RX center frequency for TX filter design or the TX center frequency for RX filter design. Contrary to the design of stand-alone filters, where the phase term of the input reflection coefficient is adjusted to avoid the need of lumped matching elements, during the design of duplexer devices the phase adjustment necessary to control the interference makes matching elements to be required during the extraction procedure.

The phase term is calculated by evaluating the polynomials $F(s)$ and $E(s)$ at $s = j\Omega_{Dual}$ as

$$e^{j\theta_{Dual}} = \left.\frac{\varepsilon_R E(s)}{F(s)}\right|_{s=j\Omega_{Dual}}, \tag{2.53}$$

where θ_{Dual} is the required angle to impose a zero reflection phase at the normalized counterband frequency Ω_{Dual}.

The input admittance necessary to start the extraction of the network is obtained using equation (2.41) but taking $\theta_{11} = \theta_{Dual}$. The extraction procedure of ladder-type duplexers is exactly the same as that described above, but taking into account the external FIR at source node B_S. This is calculated evaluating the input admittance at first transmission zero frequency as

$$jB_S = y_{in}(s)|_{s=j\Omega_1}\,. \tag{2.54}$$

Once the transmitter and the receiver are completely synthesized separately, their input ports can be connected to create the duplexer structure. If the phase parameters of both filters have been properly adjusted during the synthesis, no other components such as phase shifters, transmission lines, etc. are required, making the duplexer structure as simplest and functional as possible.

It is also important to state that the frequency response of the whole duplexer structure may be slightly altered because the phase is exactly zero at the center of the dual band, but not in the whole passband. Additionally, the band-pass transformation is a narrow band approximation,

and it also affects to the response of the band-pass device. However, as a positive effect of the transmitter and receiver filters connection, the counterband attenuation is improved in a few dB that might be essential in designs with stringent specifications.

2.4 Technological Considerations During the Design of Acoustic Wave Filters

The synthesis and extraction procedure themselves do not deal with any technological restriction, and it is the designer who has to take advantage of the proposed techniques but focusing on satisfying the requirements. Micro-acoustic wave technology suffers from several conditions that must be accomplished before the fabrication of the device. Differences in the requirements collection can also be found if the filter is made of BAW or SAW resonators. Although not all restrictions are forced by the technological process of manufacturing. Other considerations are relevant in terms of reliability, performance, and chip size. Requirements for RF front-end modules band-pass filters besides steep skirts and large bandwidths are low insertion loss, high out-of-band rejection, power durability, electrostatic discharge stability, and good nonlinear behavior. Nowadays, only acoustic technologies are able to meet all these requirements in packages as small as 1.5 mm^3, although the design becomes a challenging task.

In this section, we will discuss some fundamental design considerations for BAW and SAW devices, and the proper way to manage them by using the synthesis techniques described above.

2.4.1 Electromechanical Coupling Coefficient

The coupling constant K^2 is defined by the piezoelectric material properties and is a measure of conversion efficiency between electrical and acoustical domains. Certain materials are intrinsically better at making the electroacustic conversion than others. Aluminum Nitride (AlN) and Zinc Oxide (ZnO) are the most suitable piezoelectric materials for microwave filters based on BAW resonators. Meanwhile, Lithium Tantalate ($LiTaO_3$) and Lithium Niobate ($LiNbO_3$) are preferred crystal substrates for SAW based resonators.

On the other hand, the effective coupling coefficient k^2_{eff} is a property of a resonator. It is highly influenced by the material coupling constant K^2, and it is the biggest challenge in the design of acoustic devices. In part this coefficient determines the strength of coupling of the electric field in the piezoelectric material to the mechanical motion of the acoustic resonator, therefore characterizing the transducer. Additionally, it might be determined as the ratio of the energy stored in the electric field and the energy stored in the acoustic field. The main difference between K^2 and k^2_{eff} is that the former is fully determined by the piezoelectric material properties, and the latter comprises the metallization layers or electrodes and the manufacturing

processes. Material, orientation, and thickness of the electrodes, the process of the crystal growing, the smoothness of bottom-electrode surface, and the chemical surface condition are some of the parameters that have significant influence in k^2_{eff}. The state-of-the-art coupling coefficient for an SMR-BAW at 2 GHz is $k^2_{eff} = 6.7\%$. [60].

Different definitions of k^2_{eff} can be found in the literature, e.g. the IEEE standard definition

$$k^2_{eff} = \frac{\pi}{2}\frac{f_s}{f_p}\cot\left(\frac{\pi}{2}\frac{f_s}{f_p}\right), \tag{2.55}$$

which is in complete agreement with the results derived for a BAW resonator with infinitely thin electrodes [31]. However, the 2$^{\text{nd}}$ order Taylor series of the IEEE standard definition of the electromechanical coupling coefficient is a really good approximation easier to use for modeling purposes:

$$k^2_{eff} = \frac{\pi^2}{4}\left(\frac{f_p - f_s}{f_p}\right)\left(\frac{f_s}{f_p}\right). \tag{2.56}$$

For characterizing SAW resonators the capacitance ratio γ is mostly used [34]. It is inversely proportional to the electromechanical coupling coefficient and, definitely, much more manageable. It is given in terms of static and motional capacitors and the frequencies of resonance as

$$\gamma = \frac{C_0}{C_A} = \frac{1}{(f_p/f_s)^2 - 1}. \tag{2.57}$$

The relationship between k^2_{eff} and γ is

$$k^2_{eff} = \frac{\pi^2}{8}\left(\frac{1}{\gamma}\right)\left(1 - \frac{1}{\gamma}\right). \tag{2.58}$$

From equations (2.55) and (2.56) it is evident that the coupling coefficient can be related to the pole-zero distance of an acoustic resonator. For that reason, high coupling coefficients are required for the design of wide bandwidth filters. To improve the filter performance characteristics, external reactive elements might be included either in series or in shunt with the acoustic resonator (see [43]). The use of external reactances entails a tuning in the frequencies of resonance, and the effective coupling coefficient is modified accordingly. Furthermore, the use of external inductors grounding shunt resonators introduces notches outside of the passband. However, if the overall number of external inductors with low quality factor Q is high, the insertion loss may increase, deteriorating the performance in the passband.

The electromechanical coupling coefficient is therefore a restriction during a design, given by the process of the chosen technology in the relevant frequency range. The challenge is to have all the acoustic resonators bounded by the electromechanical coupling coefficient during a filter design. After the synthesis of a low-pass prototype and the frequency transformation, the resulting band-pass resonators have an arbitrary value of k^2_{eff}, which can be between the

technological feasible values or not. In the worst case, if k^2_{eff} is not between the required margin, the designed filter is not viable to be implemented with the specified technology, and a new design is indispensable.

By simple inspection of the input variables of the proposed synthesis methodology, only the transmission zeros and return loss values can be rearranged to satisfy the required k^2_{eff} or, equivalently, the capacitance ratio γ. Small deviations of the input parameters result in a different Chebyshev filtering function, with a different set of transmission poles. In consequence, the resonance frequencies of series resonators f_s^{SE} and anti-resonance frequencies of shunt resonators f_p^{SH} will be differently arranged. The anti-resonance frequencies of series resonators f_p^{SE} and resonance frequencies of shunt resonators f_s^{SH} are the transmission zeros (see section 2.1.2), prescribed at the beginning of the synthesis, and manually controlled by the designer. This re-organization of the resonance frequencies affects the values of k^2_{eff}, and it is only needed to find the set of TZs and RL that satisfies the required value for the physical implementation of the resonators.

2.4.2 Quality Factor

The second but not less important parameter needed to meet the stringent requirements of current and future filters is the quality factor Q of the resonator. The unloaded Q is the ratio of the stored energy in a network divided by the power dissipated in that network over one cycle. High Q-values are the main advantage of FBAR over SAW resonators in the frequency range up to 2 GHz. Q-values higher than 3000 and around 2500 for FBAR and SMR technologies respectively, against Q-values around 1000 for SAW have been reported [18, 61]. Duplexers with extremely small gaps between TX and RX bands, thus requiring steep skirts, needs of high Q resonators to satisfy both insertion loss and out-of-band requirements.

The main loss mechanisms are due to electrical losses in electrodes and interconnects, acoustic leakage both in vertical and lateral directions, substrate losses, viscous losses, and scattering losses due to imperfections on layer surfaces [16]. The effect of all these losses cannot be considered in the basic BVD circuit because it does not have any resistive element. A more realistic representation of an acoustic wave resonator is the modified BVD (mBVD) circuit given in Figure 2.14 [28]. The series resistance R_S is associated with the electrical resistance of the metal electrodes, which are always present to connect the resonator. The motional resistance R_A and the static resistor R_0 are related to the acoustic and material losses, respectively.

The quality factor is a function of frequency $Q(f)$ and hence, different Q-values can be defined at series resonance f_s, denoted Q_s, and at parallel resonance f_p, denoted Q_p. At the

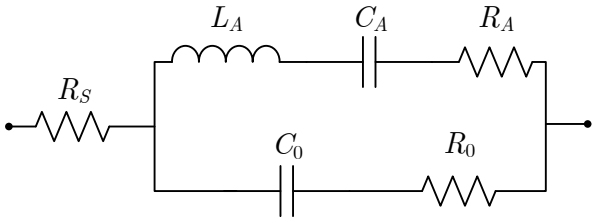

Figure 2.14: Modified Butterworth-Van Dyke equivalent circuit of an acoustic wave resonator considering losses mechanisms.

series resonance, the quality factor is defined as

$$Q_s = -\frac{1}{2} f_s \left.\frac{\partial \varphi}{\partial f}\right|_{f=f_s} \approx \frac{2\pi f_s L_A}{R_A + R_S}, \tag{2.59}$$

where φ is the phase angle of the impedance. At anti-resonance frequency, the quality factor is defined as

$$Q_p = \frac{1}{2} f_p \left.\frac{\partial \varphi}{\partial f}\right|_{f=f_p} \approx \frac{2\pi f_p L_A}{R_A + R_0}. \tag{2.60}$$

In equations (2.59) and (2.60) the quality factor is related to the impedance-phase-slope of the resonator, or group delay. This is a common way to measure the Q-values of a fabricated resonator, although it becomes difficult in some cases due to the spurious modes present in the surrounding of the resonance frequencies. Fitting the measured Q-circle to a mBVD model simplifies the task of ascertaining Q if lateral modes are less enough.

Low quality factors mean larger power dissipation, and it is translated into larger insertion loss and stronger round-edges in the passband limits. The proposed synthesis procedure is a lossless methodology with infinite Q assumption. Therefore, the transfer function under consideration must be different for networks with lossy resonators. Its poles and zeros must be displaced along the real axis in the complex frequency plane. This effect, known as dissipation factor or loss tangent ($\tan\delta$), is obtained by modifying the complex frequency variable $s \longleftarrow s + \tan\delta$. The unloaded quality factor is related to the loss tangent by

$$Q = \frac{1}{\tan\delta}. \tag{2.61}$$

In terms of the low-pass frequency domain, the response of the prototype network including losses can be obtained by modifying the low-pass frequency variable as

$$\Omega \longleftarrow \Omega - \frac{j}{Q_{LP}}, \tag{2.62}$$

where Q_{LP} is the low-pass quality factor, related with Q by

$$Q_{LP} = Q\frac{\Delta\omega}{\omega_0}. \tag{2.63}$$

This is a good approximation of the prototype filter response including losses in the low-pass domain. However, it considers uniform Q for all frequencies, and small deviations compared with real values might be essential to fail or satisfy insertion loss specifications. A more accurate manner to include losses at the end of the synthesis is by calculating the mBVD parameters for the required Q_s, Q_p, and R_S, which are usually estimated given the technology and fabrication processes. The frequency response of the band-pass network based on mBVD resonators takes into account the losses, and more realistic insertion loss and OoB rejection levels can be checked.

Designs with several external inductors may suffer from high loss effects, because inductors exhibit low Q-values in the range of 20 to 50. For this reason, the quality factor of external elements must be also considered during the design of a filter with stringent specifications.

The position of the TZs and the RL level affects the network parameters and the way the losses damage the response. However, when low Q-values are specified, it could become impossible to meet the mask requirements. A common practice to overcome this issue is to enlarge the filter bandwidth reducing the low passband edge f_1 and increasing the high one f_2. It is important to realize that modifying the filter bandwidth will affect the low-pass to band-pass transformation of the resonator parameters and hence, the frequencies of resonance and coupling coefficients. A meticulous control of the input variables, i.e. the transmission zeros and return loss, as well as the bandwidth and edge frequencies is essential to satisfy feasibility and specifications.

2.4.3 Power Handling

Acoustic filters have been consolidated in modern mobile transceivers due to high electrical performance and the small area occupied. However, power densities increase with the miniaturization of the resonators. High power densities lead to self-heating, undesired nonlinear effects, and could alter, or even destroy, the AW device. BAW resonators can withstand higher power levels than SAWs, because there are no narrow IDT fingers which tends to experience electromigration damage.

Other research has focused attention on how the temperature is distributed in a BAW resonator, isolated from the rest of the structure, depending on its layer stack composition [62, 63]. Self-heating may be a consequence of an aggressive environment, with an homogeneous distribution of the temperature leading to a frequency shift in the transmission response, or due to the presence of high power signals. The latter generates a heterogeneous distribution of the temperature, which leads to a distortion of the filter response. A comparison of these different distributions is presented in Figure 2.15. By means of the methodology proposed in this work and a proper modeling of the temperature behavior, these heat distributions and their effects on the response can be easily considered and corrected during the procedure.

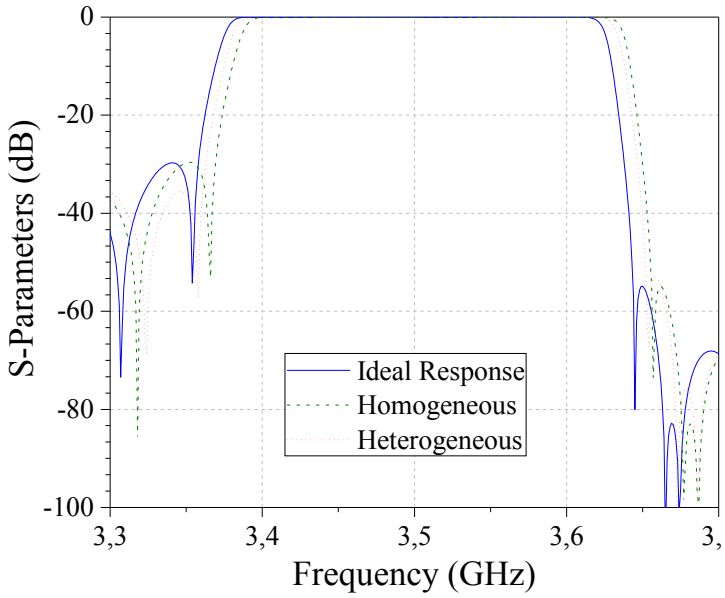

Figure 2.15: Transmission response comparison for the ideal case and for homogeneous and heterogeneous distributions of the temperature.

Different works have focused on improving the power handling in SAW devices. Enhancing the electro- and stress-migration properties of the weakest material in a resonator leads to better power handling. Multi-layered electrodes have been reported in [64, 65] to improve power durability. In [66], epitaxial aluminum electrodes and their growth mechanism increase the lifetime of the resonators for high power situations.

For both BAW and SAW devices it is a common practice to double in series (cascade) an AW resonator because of better power handling. Nevertheless, the effect of cascading an AW resonator is similar to that of cascading a capacitor, resulting in a static capacitance of value $C_0' = 2C_0$. In terms of die size, this is equivalent to having two resonators with double area occupancy. For a parallel plate BAW resonator, the active area A is given by

$$A = \frac{C_0 t_p}{\varepsilon_0 \varepsilon_r}, \tag{2.64}$$

where t_p is the thickness of the piezoelectric layer, ε_0 is the free-space permittivity, and ε_r is the piezoelectric material relative permittivity. For SAW resonators, the static capacitance is determined by the aperture width W and the number of transducer pairs N_t as [67]

$$C_0 = \varepsilon_0 \varepsilon_r N_t W. \tag{2.65}$$

The trade-off between power handling and chip size depends on the synthesis results. How the energy is distributed along the resonators in a ladder-type filter is subject to the resulting network parameters and hence, to the TZs and RL. The difference between a good design and

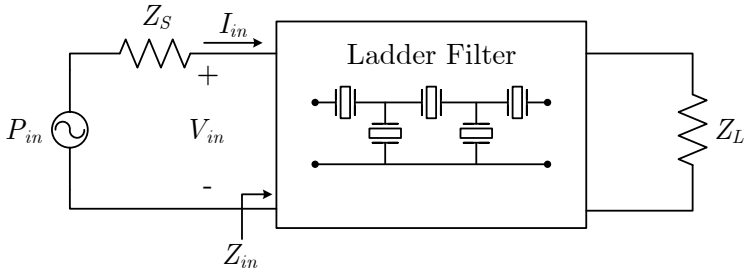

Figure 2.16: Scheme of the filter for power calculations.

the best design may be given by an accurate control of the power density along the resonators, traduced into smaller area and better efficiency.

The power density calculation can be realized by using the mBVD models for a specified input power P_{in}. In Figure 2.16 there is the scheme used for stored energy and power density calculations. Once the synthesis of the band-pass network is completed, the input impedance Z_{in} can be calculated cascading the $ABCD$ matrices of each mBVD resonator. The input voltage V_{in} can be derived as

$$V_{in} = \frac{Z_{in}}{Z_S + Z_{in}} V_S, \tag{2.66}$$

where Z_S is the source or port impedance and V_S the source voltage, derived from the input power as

$$V_S = \sqrt{8 P_{in} Z_S}. \tag{2.67}$$

The input current I_{in} is obtained from the Ohm's law $I_{in} = V_{in}/Z_{in}$. Figure 2.17 depicts the mBVD models of a series and a shunt resonator, including external elements in case the coupling coefficient or the capacitance ratio γ has to be adjusted to a required value. A series inductor L_{ext} is necessary to increase γ, whereas C_{ext} reduces it. Each resonator in a filter might be considered as a black box described by an $ABCD$ matrix of the form

$$[ABCD]_{SE} = \begin{bmatrix} 1 & Z_R(s) \\ 0 & 1 \end{bmatrix} \tag{2.68}$$

for series resonators and

$$[ABCD]_{SH} = \begin{bmatrix} 1 & 0 \\ Y_R(s) & 1 \end{bmatrix} \tag{2.69}$$

for shunt resonators.

The admittance $Y_R(s)$ is the inverse of the impedance $Z_R(s)$ describing the resonator input impedance as

$$Z_R(s) = R_S + sL_{ext} + \frac{1}{sC_{ext} + \dfrac{1}{R_0 + \dfrac{1}{sC_0}} + \dfrac{1}{R_A + sL_A + \dfrac{1}{sC_A}}}. \tag{2.70}$$

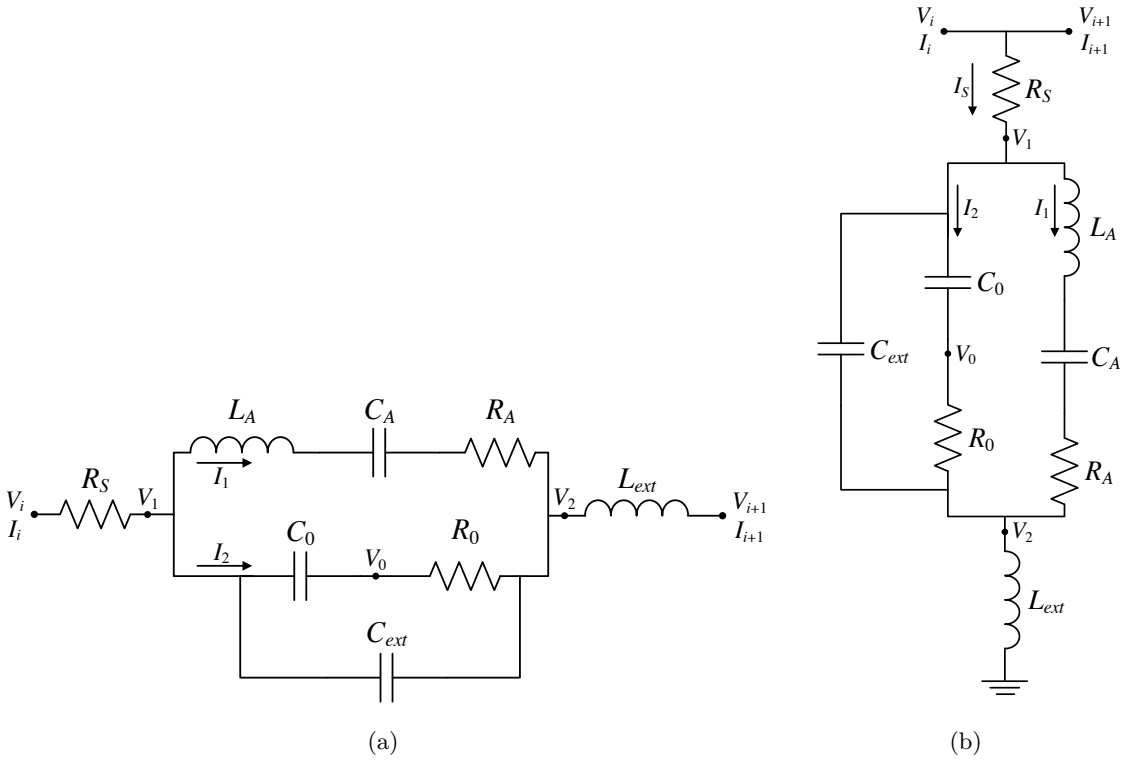

Figure 2.17: Modified BVD of resonators for voltages and currents calculation, including external elements for k_{eff}^2 adjustments: (a) Series resonator and (b) shunt resonator.

The voltage and current at each node of the filter can be calculated by using the definition of the $ABCD$ parameters:

$$\begin{bmatrix} V_i \\ I_i \end{bmatrix} = [ABCD] \begin{bmatrix} V_{i+1} \\ I_{i+1} \end{bmatrix}, \tag{2.71}$$

where the $ABCD$ matrix is given by (2.68) and (2.69). Internal voltages V_1 and V_2 are given by

$$V_1 = V_i - R_S I_i \tag{2.72a}$$
$$V_2 = V_{i+1} + sL_{ext} I_{i+1} \tag{2.72b}$$

for series resonators, and

$$V_1 = V_i - R_S I_s = V_i - R_S(I_i - I_{i+1}) \tag{2.73a}$$
$$V_2 = sL_{ext} I_s = sL_{ext}(I_i - I_{i+1}) \tag{2.73b}$$

for shunt resonators. The currents I_1 and I_2 for both series and shunt resonators are therefore

obtained as

$$I_1 = \frac{V_2 - V_1}{R_A + sL_A + \dfrac{1}{sC_A}} \tag{2.74a}$$

$$I_2 = \frac{V_2 - V_1}{R_0 + \dfrac{1}{sC_0}}. \tag{2.74b}$$

Finally, the voltage V_0 is given by

$$V_0 = V_2 - I_2 R_0. \tag{2.75}$$

With the voltages and currents of the resonators properly defined, the stored energy in the motional and static branches, i.e., the stored energy in the acoustic resonator, can be calculated. For the resonant tank made of L_A and C_A, the stored energy is divided into the magnetic and electric average energies W_m and W_e respectively, calculated as

$$W_m = \frac{1}{4}|I_1|^2 L_A \tag{2.76a}$$

$$W_e = \frac{1}{4}|V_c|^2 C_A = \frac{1}{4}|I_1|^2 \frac{1}{\omega C_A}, \tag{2.76b}$$

where V_c is the voltage in the motional capacitance C_A. Similarly, the stored energy in the static capacitor C_0 is given by

$$W_{e0} = \frac{1}{4}|V_2 - V_1|^2 C_0. \tag{2.77}$$

The stored energy in a resonator is $W_T = W_m + W_e + W_{e0}$, although the major influence is produced in the motional branch. Ernst et al. demonstrated in [68] that there is a direct relation between the total stored energy, the incident power, and the group delay in passive, lossless and reciprocal network given by

$$W_S = P_{in}\tau_g. \tag{2.78}$$

We are considering lossy networks to derive more accurate results of stored energies in the resonators and properly decide which resonators are susceptible to damage. Therefore, equation (2.78) becomes an approximation of our case of interest when $W_S = \sum_{i=1}^{N} W_{Ti}$, where W_{Ti} is the stored energy in the i-th resonator. Furthermore, in W_T we only consider the stored energy in the acoustic resonators, but not the energy in the external elements, which is usually low compared to the energy of the resonators. In any case, the relationship in (2.78) states that for a given incident power, the group delay is proportional to the total stored energy. Therefore, an appropriate management of the network parameters yielding less stored energy results in better group delay characteristics.

For the power density calculation of each resonator, the reactive power P_q has to be divided by the area of the resonator. An approximate method to calculate it is using the static capacitance,

Table 2.1: Band-25 Duplexer Specifications

Requirement	*Freq. Band (MHz)*	*Value (dB)*
Insertion Loss	1850 - 1915 (TX)	> -2
	1930 - 1995 (RX)	> -2.5
Isolation	1930 - 1995 (TX)	< -50
	1850 - 1915 (RX)	< -50
Out-of-Band Rejection	1710 - 1755 (B4-RX)	< -45
	2110 - 2155 (B4-TX)	< -45

which is related to the size of the resonator, resulting in

$$P_d(\omega) = \frac{P_q}{C_0} = \frac{2\omega W_T}{C_0}. \tag{2.79}$$

The power density is a function of frequency, and it is usually determined at the right filter passband edge, because it represents the worst scenario in terms of power levels. For a synthesized network, resonators exhibiting a power density that exceed a maximum value of breakthrough have to be cascaded, with the consequences that it entails. Sometimes it is required to cascade a resonator more than two times, because of the high power density it involves, thus increasing the size of the component.

2.5 Example of a Ladder-type Filter Design

In this section an example of a duplexer design is developed to demonstrate the proposed design methodology. The technological requirements and mask specifications are treated as the main goals to validate a design. However, among several designs that already satisfy these conditions, the designer has to manage other requirements such as good power handling, minimum die size, or minimum number of external elements, depending on customer demands.

The example focuses on the design of an E-PCS (Band-25) duplexer, with the specifications shown in Table 2.1. The gap between transmission TX and reception RX bands is only 15 MHz with a required attenuation of -50 dB. If temperature margins and fabrication tolerances are considered, this gap might reduce to 5 to 10 MHz, thus increasing the complexity of the design. In this example a state-of-art coupling coefficient of 6.7% for AlN piezoelectric material is considered. It is important to remark that the values contemplated during the example are basically to demonstrate the capabilities of the methodology, and they might be not merely realistic.

The design of both TX and RX filters begins with the study of the effective coupling coefficient k^2_{eff} and the resonant frequencies f_s according to the transmission zeros and return loss input (to the synthesis procedure) variables. There are different possibilities to ascertain the

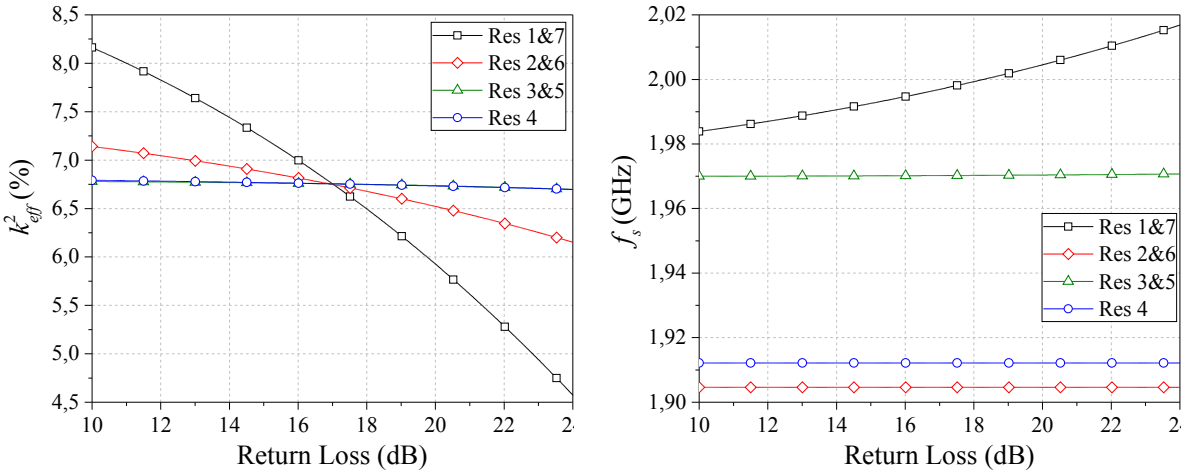

(a) (b)

Figure 2.18: (a) Electromechanical coupling coefficient k^2_{eff} and (b) resonant frequencies f_s of each resonator for a predefined set of transmission zeros and different values of return loss.

most adequate set of TZs and RL for each design. Establishing a frequency set of TZs, a variation on the RL yields different resonators with different k^2_{eff}, although the transmission zeros remain static. On the other hand, for a predefined RL level, a variation of each TZ might help to study a large number of designs and to decide on the most appropriate one. All these studies are very useful for the design of acoustic wave filters and let the designer compare solutions that satisfy the maximum number of requirements with the minimum number of external elements.

For example, Figure 2.18 (a) displays the effective coupling coefficient for a sweep of the return loss. The filter is of degree $N = 7$ with low-pass transmission zeros $\{\Omega_1, \Omega_7\} = 2.12$, $\{\Omega_2, \Omega_6\} = -1.61$, $\{\Omega_3, \Omega_5\} = 1.45$, and $\Omega_4 = -1.42$. It can be observed that the set of TZs is symmetrical from the beginning to the end. For this reason, the extracted inline network is also symmetrical, making the technological requirements easier to satisfy because only four different resonators are necessary to construct the network. The figure shows that the optimum value of return loss, for which all resonators satisfy the material system definition $k^2_{eff} = 6.7\%$ without the need of external elements, is RL = 17 dB. Any attempt to synthesize this filter with the prescribed TZs above and a different value of RL will result in a different network requiring four external elements; in particular, resonators 1, 2, 6, and 7, since their k^2_{eff} differ from the required one, while resonators 3, 4, and 5 are almost constant at the specified value. Thus, that particular knowledge is essential to design acoustic filters with a minimum number of external elements while satisfying the technological restrictions.

A similar study can be performed for the resonant frequencies f_s, as depicted in Figure 2.18 (b). However, these parameters do not depend completely on the results of the synthesis,

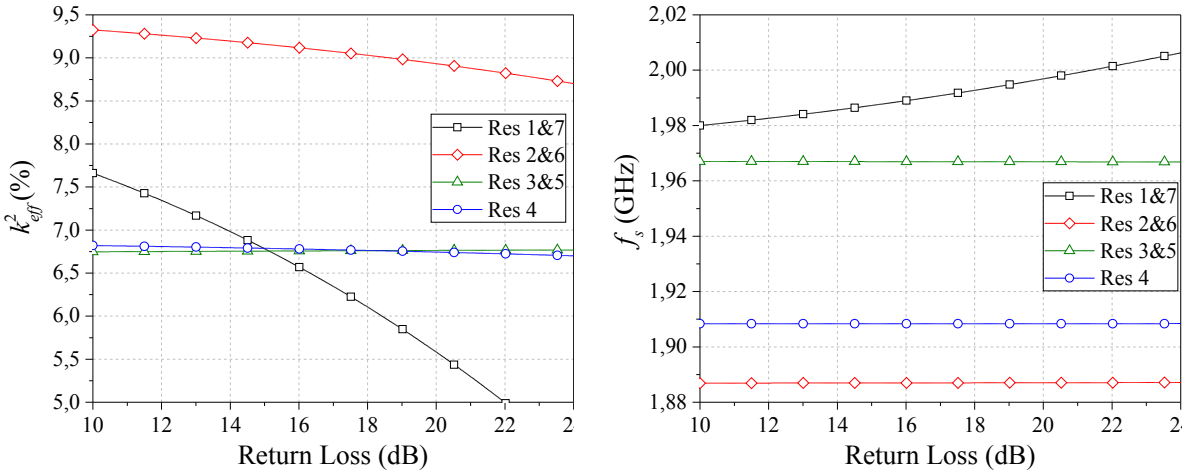

Figure 2.19: (a) Electromechanical coupling coefficient k^2_{eff} and (b) resonant frequencies f_s of each resonator for a predefined set of transmission zeros and different values of return loss.

because the resonance frequencies of shunt resonators are prescribed with the transmission zeros. Typically only the two discrete frequencies of series and shunt resonators are available in BAW technology, although more frequency shifts are possible by adjusting the thickness of the top metal electrode. The consequence is that a frequency shift of an individual resonator generally requires another masking step in an already complex process, making the fabrication more complicated. The number of resonant frequencies for the proposed TZs is always four for any value of RL. It could be possible to modify the TZ of resonator 4 to match the resonance frequency with that of resonators 2 and 6. However, the coupling coefficient will be affected, and probably external elements will be required.

Receiver Filter Design

For the design of the RX filter, we decided to completely modify the set of TZs mentioned above and thus, the whole network. Figure 2.19 shows the coupling coefficients and resonant frequencies of each resonator in the filter for the following transmission zeros set, $\{\Omega_1, \Omega_7\} = 2.26$, $\{\Omega_2, \Omega_6\} = -2.26$, $\{\Omega_3, \Omega_5\} = 1.63$, and $\Omega_4 = -1.61$, and different values of return loss. For a RL value of approximately 15 dB, resonators 1, 3, 4, 5, and 7 present a coupling coefficient of 6.76%, while resonators 2 and 6 require $k^2_{eff} = 9.15\%$. Looking at the resonance frequencies, 4 different resonators are necessary. However, external elements might be introduced to resonators 2 and 6, in order to modify their k^2_{eff} and f_s. In order to reduce k^2_{eff} to 6.76%, series inductors connected to ground can be used, and easily implemented physically by wire-bounds or externally on the laminate.

Table 2.2: Synthesized BVD band-pass elements of the Band-25 receiver filter.

Parameters	**Res 1&7**	**Res 2&6**	**Res 3&5**	**Res 4**
L_A (nH)	111.35	21.04	102.59	21.03
C_A (pF)	0.0576	0.331	0.0638	0.331
C_0 (pF)	0.9791	5.625	1.0850	5.595
L_{ext} (nH)	-	0.31	-	-
$L_{in/out}$ (nH)	4.393			
k^2_{eff}	6.76	6.76	6.76	6.76
f_s (GHz)	1.9875	1.9074	1.9670	1.9084

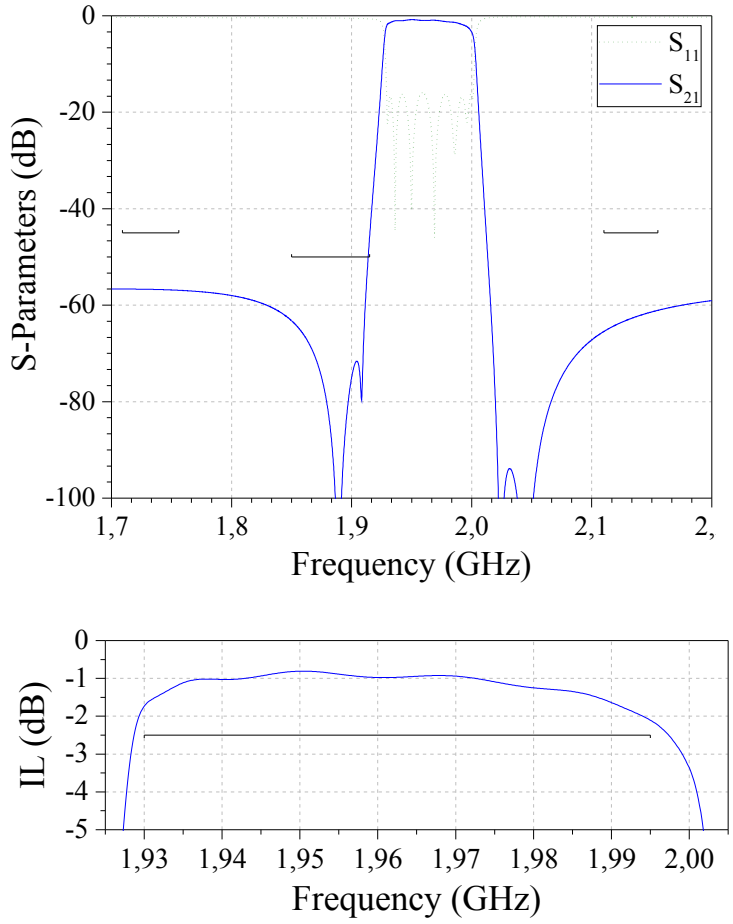

Figure 2.20: Magnitude simulation and insertion loss details of the B25-RX filter. The quality factor used on the circuit simulations are $Q = 1500$ for acoustic resonators and $Q = 25$ for external coils. An electrode resistance of $R_S = 0.15\ \Omega$ as well as fabrication and temperature margins of 500 ppm are considered.

With two external inductors of $L_{ext} = 0.31$ nH, resonators 2 and 6 yield in the required coupling coefficient value of 6.7%, and a resonance frequency of 1.9074 GHz, very similar to that of resonator 4. Thus, only 3 different resonators are necessary. Table 2.2 shows the band-pass BVD elements obtained for the above mentioned TZs and RL, as well as the coupling coefficient and resonance frequencies of each resonator. We can observe that the technological requirements are satisfied due to the external ground inductors in resonators 2 and 6. Also a pair of inductors in parallel at the input and output are necessary to assure a phase of 0 degrees at the TX center frequency.

The magnitude response of the synthesized filter is shown in Figure 2.20. For the simulation, a quality factor of $Q = 1500$ is considered at both resonance and anti-resonance frequencies, and a $Q = 25$ for external coils. An electrodes resistance of $R_S = 0.15\ \Omega$ is also contemplated, to make the simulation more realistic. It can be observed that the mask specifications are completely satisfied for a fabrication tolerance and temperature margins of 500 ppm. To accomplish the insertion loss specification, the filter bandwidth has been enlarged 0.417 MHz and 6.151 MHz for the left and the right passband edge frequencies, respectively.

Transmitter Filter Design

A similar procedure has to be executed for the design of the Band-25 transmitter filter. An adequate set of TZs and return loss have to be found in order to satisfy both the technological requirements and the frequency mask specifications, shown in Table 2.1. The following low-pass TZs have been chosen for the synthesis of the TX filter: $\Omega_1 = 1.44$, $\Omega_2 = -2.50$, $\Omega_3 = 1.60$, $\Omega_4 = -1.65$, $\Omega_5 = 1.60$, $\Omega_6 = -2.50$, and $\Omega_7 = 1.74$, for a return loss of 17.3 dB. Because of the stringent requirements, notice that the transmission zeros set is not symmetrical and $\Omega_1 \neq \Omega_7$.

Table 2.3 shows the parameters of the band-pass BVD circuit of each resonator resulting from the synthesis, as well as the coupling coefficients and resonance frequencies. It is interesting to observe that, in general, smaller static capacitors yields from this design, compared to that of the RX filter. This is favorable in order to reduce the area, although dealing with larger power densities will require several resonator cascadings. Another observation of the resulting values is that this design requires 4 different resonance frequencies, with the complexity that it entails. In further design processes, such as layout generation, electromagnetic simulations, packaging, etc., the network might be re-optimized to require only 3 different resonance frequencies, but starting from a really good seed design. Finally, 3 external ground inductors are also necessary to assure technological feasibility.

The S-parameters simulation of the synthesized B25-TX network is shown in Figure 2.21. All OoB and IL specifications are satisfied considering a $Q = 1500$ for acoustic resonators, a $Q = 25$ for external coils, and an electrode resistance of $R_S = 0.15\ \Omega$. Likewise in the RX design,

Table 2.3: Synthesized BVD band-pass elements of the Band-25 transmitter filter.

Parameters	**Res 1**	**Res 2**	**Res 3**	**Res 4**	**Res 5**	**Res 6**	**Res 7**
L_A (nH)	56.57	41.12	170.2	37.61	170.4	39.36	99.58
C_A (pF)	0.127	0.184	0.042	0.201	0.042	0.192	0.071
C_0 (pF)	2.150	3.129	0.711	3.418	0.710	3.268	1.209
L_{ext} (nH)	-	0.800	-	0.110	-	0.773	-
L_{out} (nH)	19.67						
k^2_{eff}	6.76	6.76	6.76	6.76	6.76	6.76	6.76
f_s (GHz)	1.881	1.829	1.886	1.830	1.886	1.829	1.891

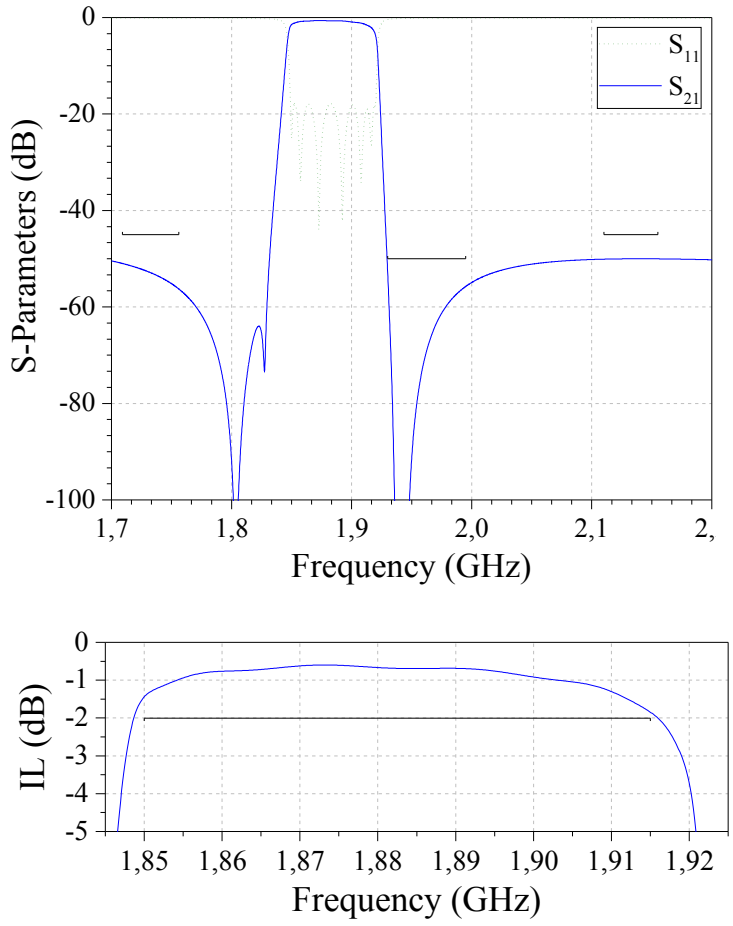

Figure 2.21: Magnitude simulation and insertion loss details of the B25-TX filter. The quality factor used on the circuit simulations are $Q = 1500$ for acoustic resonators and $Q = 25$ for external coils. An electrode resistance of $R_S = 0.15\ \Omega$ as well as fabrication and temperature margins of 500 ppm are considered.

the bandwidth of the transmitter filter has had to be enlarged in 0.478 MHz and 5.105 MHz for

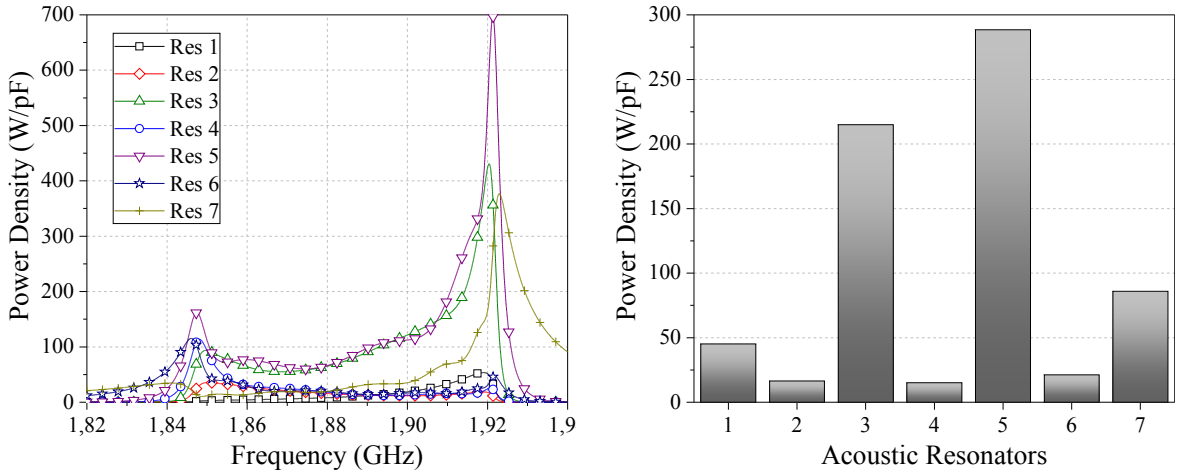

(a) (b)

Figure 2.22: Power density of each resonator of the synthesized TX filter for an input power of 29 dBm for (a) the whole TX passband range, and (b) at 1915 MHz, the right edge of the passband.

both passband edges to satisfy IL specification.

As opposed to receivers, transmitter filters have to be ready to deal with high power signals. A minimum resonators lifetime is required without breakdown. An approximation of the energetic problem is considered. For an input power of 29 dBm to the transmitter filter, power densities of each resonators are derived to study how the energy is distributed along the filter and how to deal with most energetic resonators. Figure 2.22 (a) shows the power density of each resonator for the whole passband range of frequencies. It can be seen that the most critical point is at the upper passband skirt. Therefore, it is a common practice to calculate the power density at f_2, the upper passband frequency, as shown in Figure 2.22 (b). For the B25-Tx, the power density has been calculated at $f_2 = 1915$ MHz. It can be observed that resonators 3 and 5 concentrate much more power density than the others, mainly because their static capacitance is small, yielding small resonators. Therefore, these are the resonators that has to be definitely cascaded to assure a minimum device lifetime. Furthermore, by cascading some resonators the linearity is also improved, although this is not dealt with in this thesis.

Band-25 Duplexer

The final step on the design of the Band-25 duplexer is to connect both the synthesized RX and TX filters to form the duplexer network. Since the input phases of both designs has been properly considered during the synthesis, the filters can be connected without much interference on the response. Obviously, the phase is only corrected at center frequency of the passbands, and

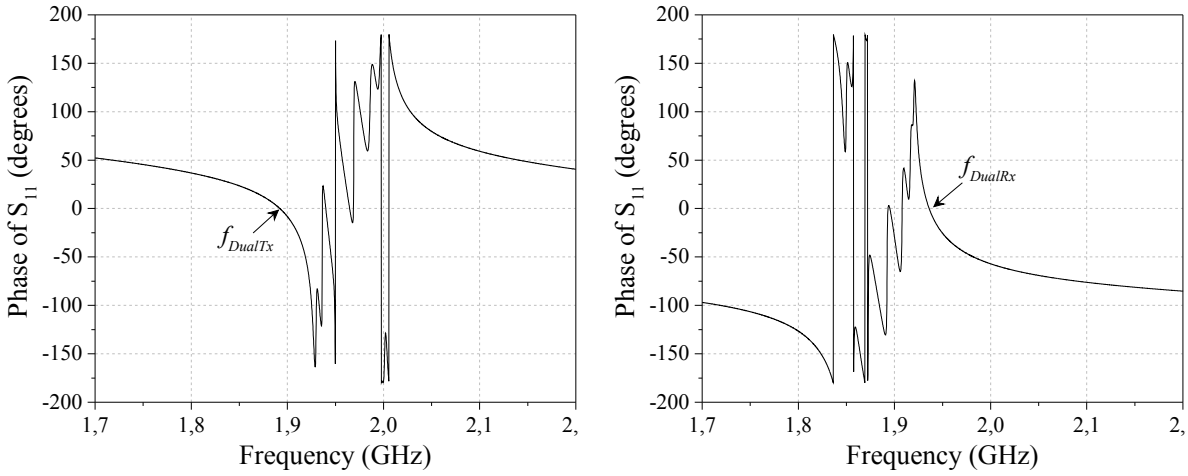

Figure 2.23: Input phase simulation of the synthesized Band-25 duplexer: (a) RX filter, with a phase of 0 degrees at f_{DualTx}, and (b) TX filter, with a phase of 0 degrees at f_{DualRx}.

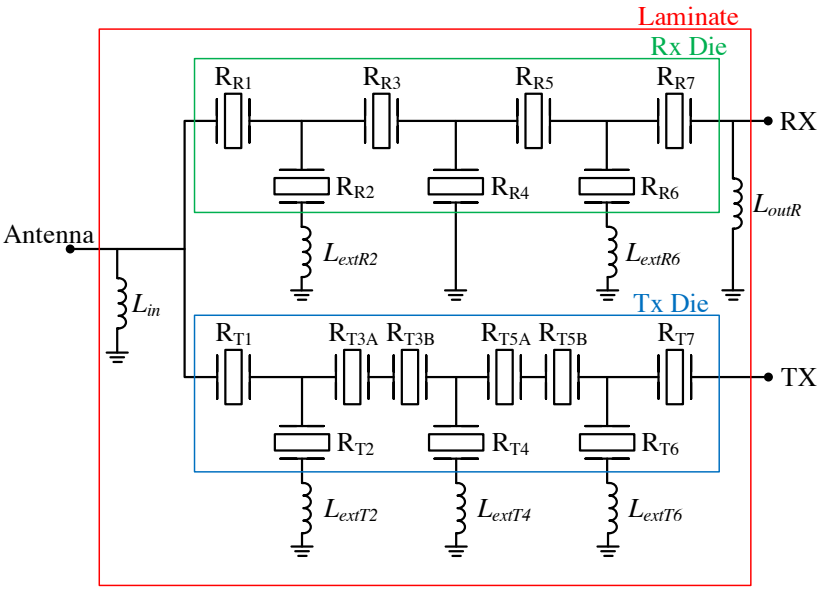

Figure 2.24: Network of the synthesized Band-25 duplexer.

load effects may occur far from the bands. Figure 2.23 shows the phases of the S_{11} parameter for (a) the receiver and (b) the transmitter filters. It can be observed in the figures that the phase is exactly 0 degrees at dual frequency in both cases.

The full designed network for the Band-25 duplexer is depicted in Figure 2.24. The RX die includes the acoustic resonators of the RX filter, while the TX die includes the acoustic resonators of the TX filter, contemplating the cascading of resonators 3 and 5 for better power

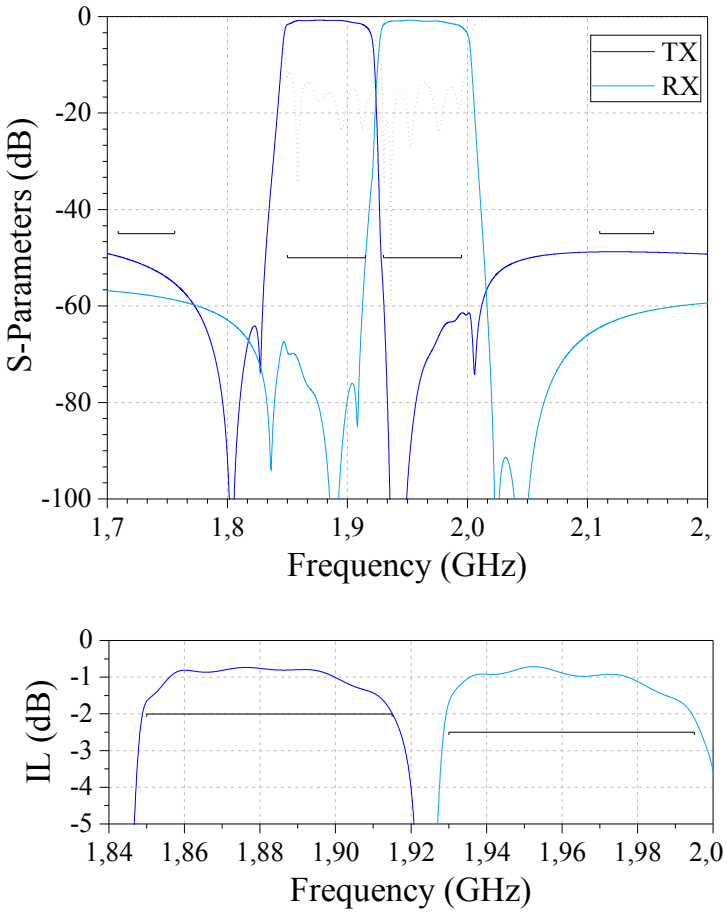

Figure 2.25: Magnitude simulation and insertion loss details of the Band-25 duplexer. The quality factor used on the circuit simulations are $Q = 1500$ for acoustic resonators and $Q = 25$ for external coils. An electrode resistance of $R_S = 0.15\ \Omega$ as well as fabrication and temperature margins of 500 ppm are considered.

handling. The external ground inductors are implemented on the laminate, as well as the input and output matching elements. The input inductor at the antenna port L_{in} can be calculated as the parallel of both input elements of RX and TX filters. In this case, since the synthesized TX filter has a negligible input inductor, L_{in} becomes directly the input element of the RX filter. It may also be observed that the output inductor of the transmitter has been also neglected due to its large impedance value.

Finally, the magnitude simulation of the whole duplexer is shown in Figure 2.25. The mask specifications remain all satisfied once the duplexer has been created, as expected. Insertion loss levels have been slightly increased, specially at the passband edges, due to a load effect between the filters. However, the specifications remain fulfilled.

2.6 Multiplexers Approach

Limited spectrum allocations and non-contiguous spectrum blocks are ultimate barriers for network capacity, and draw a simplified vision of the great challenge that mobile operators are facing to support large data traffic across their networks. Carrier Aggregation (CA) is a technique used to combine multiple LTE component carriers across the available spectrum to increase data rates by supporting wider bandwidth signals, thus achieving network performance improvements without increasing radio resources. The requirements posed by CA includes to maintain low insertion loss, good out-of-band rejection, good power handling, and small areas, as well as loading effect minimization, low levels of cross-isolation, and good management of nonlinear mixing products (IMDx).

By using single carrier in frequency-division duplexing (FDD), a RF duplexer ensures that transmissions on the uplink do not interference with reception on the downlink. With LTE-CA it is required to connect multiple Rx, Tx, and/or time-division duplexing (TDD) filters to a common antenna port.

In the last decade a great effort has pushed up RF-filters based on micro-acoustic technology, either SAW or BAW, at forefront of RF-FEM industry while figuring out the higher growth rates. Their common configurations are based on duplexer structures or as stand-alone filters.

Currently, the market approach with singly function packaged RF-filter is being replaced by the same technology embedded into integrated RF modules. Miniaturization continues being essential considering the limited space available while the bands counts rise. The integration of multiple RF filters into modules is the only progress vector, while new additional requirements have to be considered with this multiplexing configuration.

Multiplexers are used to separate a wideband signal into a number of narrowband signals. Multiplexers are also employed to provide the opposite function combining different narrowband channels into a single wideband composite signal for transmission through a common antenna, therefore referred to as combiners or channelizers.

In this section we propose a general description of the most commonly used configurations of multiplexer modules and the role that each one can play within the mobile RF-FEM arena. A taxonomy classification is given in two main families, the directional and manifold configurations. A general methodology for the design of multiplexing devices, based on the filter synthesis proposed above, is also presented. With this procedure, the filter designer is allowed to find out the appropriate condition in such a way that the individual filters implement intrinsically the necessary phase correction. Finally, for validation purposes, an example of a quadplexer with Band 25 Tx/Rx and Band 4 Tx/Rx in the medium frequency spectrum band allocation is shown.

2.6.1 Multiplexing Topologies

The most commonly used multiplexing configurations can be classified into two general families. The first one, directional configurations, includes hybrid-coupled multiplexers, circulator-coupled multiplexers and directional-coupled multiplexers. Meanwhile, the second configuration called manifold-coupled multiplexers includes comb and herringbone configurations. The star topology can be understood as a particular case of the herringbone configuration.

Directional Configurations

In the hybrid-coupled multiplexer configuration each channel includes two paired filters and two identical quadrature couplers. Figure 2.26 shows the schematic of a hybrid-coupled multiplexer. The main advantage of this approach is the modularity it offers. The directional coupler minimizes the interaction among the channel filters. Moreover, in case that a new frequency band is planned to be introduced, hybrid-coupled multiplexers allow the reconfiguration with new additional channels and without disrupting the existing multiplexer design afterwards. From the performance point of view, it is also advantageous that only half of the input power flows through each filter. Therefore, for high power applications the filter design can be simplified saving area of individual filters. However, its overall large size is a weakness, specially for the user segment, because two filters and two hybrid couplers per channel are necessary. For this configuration, the phase deviation between the two paired filter paths is another design concern. The two signals must flow through balanced paths to sum constructively at the channel output.

A circulator-coupled approach is conceptually quite similar. The unidirectional property of the circulator makes amenable to modular integration and easy design. Despite its size is reduced because only one filter per channel is necessary, the circulator size continues being a major limitation, particularly in the user segment. Moreover, successive channels exhibit higher loss because the insertion loss increase with each step through the channel sequence.

Finally, directional-coupled multiplexers are four-port devices in which one port is terminated with a load and the other three ports work fundamentally as a circulator connected to the band-pass filter. The incident power at one port flows to the port connected to the band-pass filter, while the reflected power from the filter return to the third port. The advantage in directional-coupled multiplexers is that they do not require the use of ferrite circulators.

Manifold Configurations

In regards to miniaturization and best absolute insertion loss, the manifold-coupled configuration is considered the optimum choice. The design of a manifold-coupled multiplexer requires the consideration of all the channel filters at the same time. Then, the effect of channel interactions

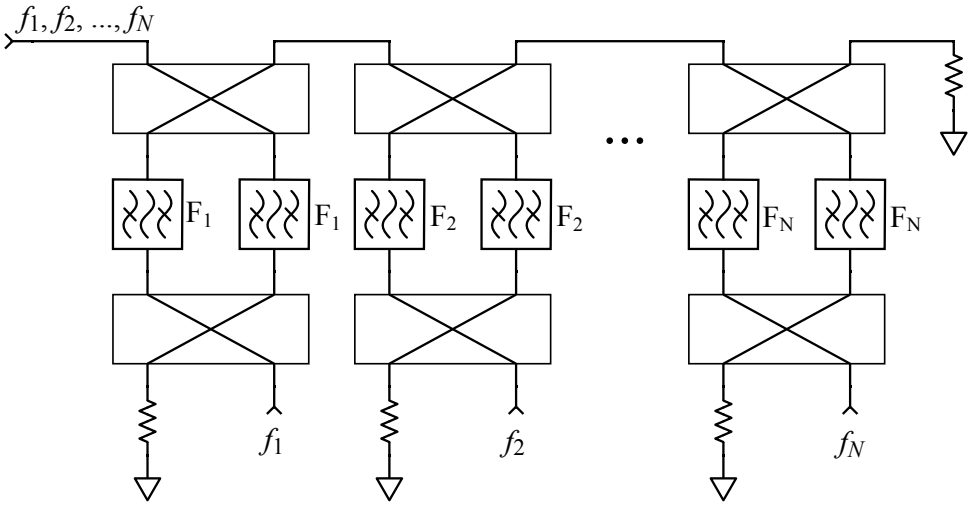

Figure 2.26: Schematic of a hybrid-coupler multiplexer.

can be corrected during the design process of each individual filter. As a consequence, manifold-coupled multiplexers are not pleasant for a flexible frequency plan, and any modification in the allocation band or in the overall number of bands requires a new multiplexer design. Furthermore, this approach becomes more difficult to design as the number of channels increase.

Several common manifold multiplexer configurations can be found in the literature. A manifold multiplexer is given by channel filters connected to a common output port. The most relevant are comb and herringbone configurations. In the former, the filters are connected to one side of the manifold, whereas in the latter they are connected to both sides, as shown in Figure 2.27 (a) and (b), respectively. The star configuration, also considered a manifold configuration, has a common junction as shown in Figure 2.27 (c). These three configurations are quite similar in concept and design procedure. The main difference is the presence of manifold phase shifters between channels that separate the antenna port with the starting node in the manifold section. This provides to the manifold extra degrees of freedom to optimize the design.

It is important to observe that in the star configuration the power of all the channels gather at the common junction. This may cause higher voltages and a hot spot. Meanwhile, the power in the manifold tends to be more evenly distributed. The star-junction configuration is the most popular for a relatively small number of channels.

Any of the manifold-coupled configurations makes feasible to combine an arbitrary number of channels, regardless of their bandwidths and channel separations. The most valued feature is that it is achievable a channel performance closer to that obtained from a stand-alone filter by itself. No other multiplexer configurations are able to match this performance. The manifold itself is a low loss transmission path. All the channel filters are electrically connected to each

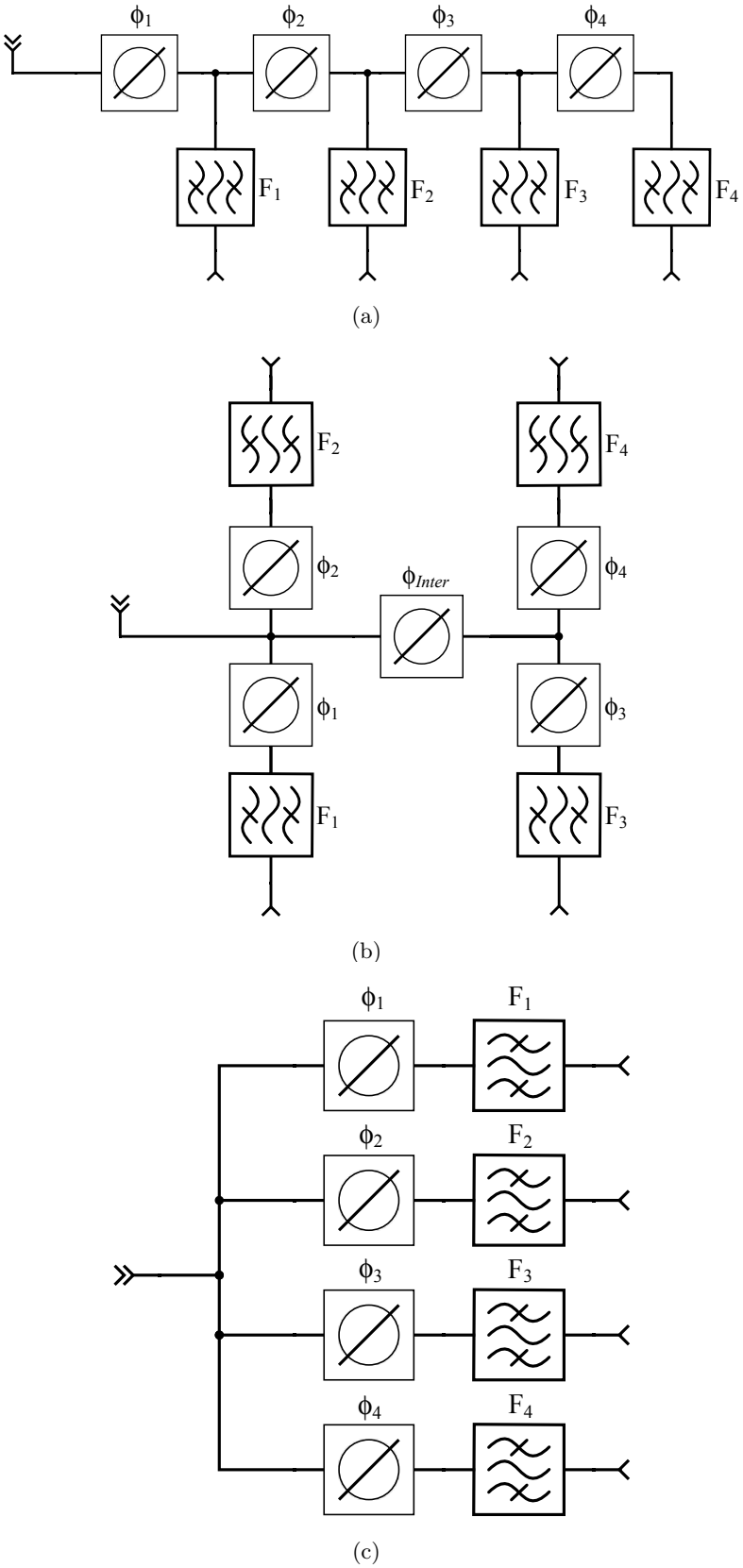

Figure 2.27: Schematic of manifold-coupled multiplexers with (a) comb, (b) herringbone, and (c) star-junction configurations.

other through the near-lossless manifold, and its design has to consider all filters as a whole, not as individuals, since there are no directional or isolating elements in between.

2.6.2 Synthesis of Multiplexers with Manifold Configuration

In a multiplexer, each filter sees the others filters as reactive loads. Classical methods for the synthesis of multiplexer devices are based on the compensation of this reactive load by adding compensating impedances or by modifying the phase of the reflection coefficient. With a general filter synthesis methodology, like that described above for stand alone filters and duplexer devices, an efficient approach is to synthesize each filter in such a way that the equivalent reactive loads of the other filters are seen as aggregated structures, attaining a null input admittance at each frequency band considered simultaneously.

In a multiplexer with M bands there are $M+1$ ports. Considering the input to output path for one band through its respective filter, there are $M-1$ isolated filters loading all together the main path. It is therefore necessary to find out the M phase shifters simultaneously, by solving the corresponding M equations.

Given that the synthesis methodology presented above has been natively created to satisfy technological feasibility, each filter design variables are tuned to their corresponding transmission zeros and return loss in order to fulfill the technological constraints and the specified set of spectrum masks. Meanwhile, the reflection phases of all stand-alone filters are properly adjusted according the set of equations. The overall synthesis methodology for multiplexer devices may be summarized as follows:

1. Derivation of the M transmission responses that satisfy the spectrum mask specifications by optimization of the TZs and return loss. Each response is characterized by the polynomials $P(s)$, $F(s)$, and $E(s)$.
2. Solve the equations for the M phase shifters, resulting in a required phase for each filter.
3. Calculate the input admittance of the M filters.
4. Network synthesis of each filter.
5. Frequency transformation and impedance scaling.
6. Validation of the technological feasibility. Start an automatic search engine from 1 up to the material system constraints are satisfied. Then, the procedure is over.

Errors in the phase parameters after the frequency transformation may be found for high frequency and large bandwidth filters. Then, it is preferred to solve the phase equations in the band-pass domain, or use band-pass synthesis techniques, like those presented in Chapter 4.

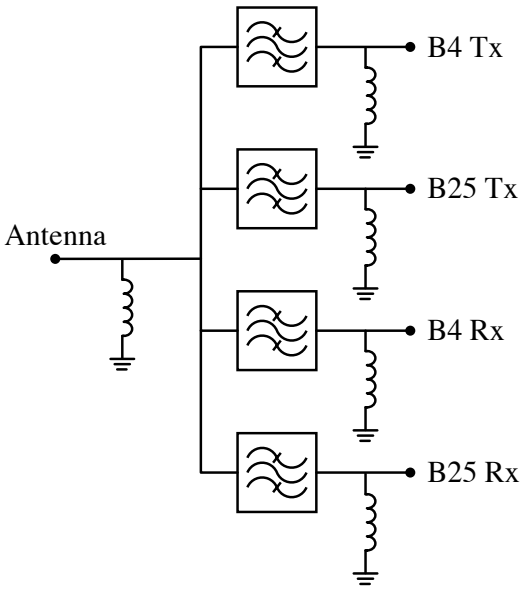

(a)

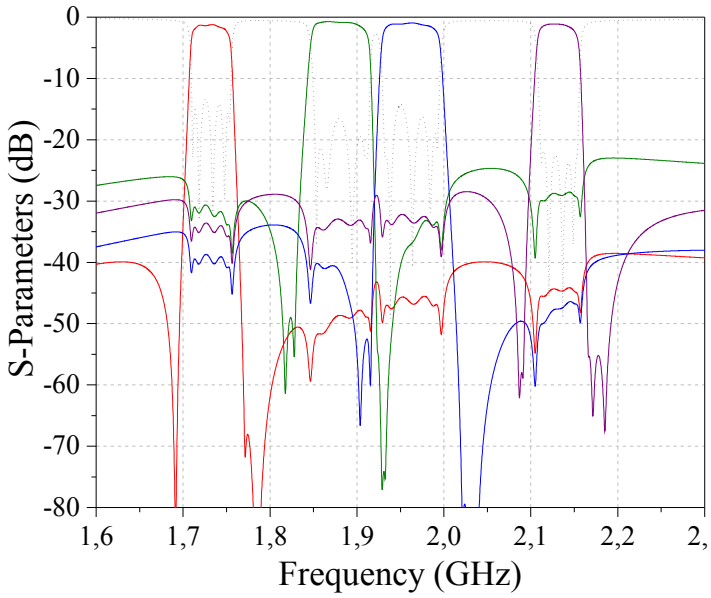

(b)

Figure 2.28: Four filter multiplexer including Band 4 and Band 25: (a) schematic of the synthesized quadplexer and (b) frequency response.

2.6.3 Example of a 4 Channel Multiplexer

In this section, a 4 filter multiplexer including Band 4 and Band 25 is designed in order to show the potential of the methodology. Each channel has been decided to be a 5th degree ladder-type filter with different sets of transmission zeros and return loss. This means that the response of

each filter is completely different than that of the others. Although the filters are fully canonical networks considering they will be implemented with acoustic resonators, the material system and other technological constraints are not relevant for the example.

Figure 2.28 (a) shows the schematic resulting from the synthesis. Each filter has input and output inductors, whose value depend on the required phase. Since all filters start in series resonator, all input inductors are in shunt configuration. This allows to join all shunt inductors on the antenna node. On the output side, however, they are still required on each path.

The simulated frequency response of the synthesized multiplexer is shown in Figure 2.28 (b). It can be observed that, after synthesize each filter separately, the multiplexer response has been successfully achieved. Differences between the stand-alone filter responses and the behavior once the filters are connected are almost negligible. The most critical ones are found on the edges of the passbands, although, to our experience, these are not larger than 0.2 dB.

2.7 Chapter Summary

In this chapter a synthesis methodology for the design of ladder-type filters based on acoustic wave resonators has been presented. The synthesis is realized on the low-pass domain, and thus, an equivalent low-pass model of an acoustic resonator has been derived, named dangling resonator. The ladder-type network is assembled by cascading N dangling resonators, yielding a fully canonical network of degree N with N transmission zeros.

A general-class of Chebyshev polynomials are introduced to describe the filter transfer function, that can be accommodated by acoustic wave filters. The input variables to the synthesis of the network procedure are the transmission zeros and the return loss, from which the transfer function polynomials can be derived by using a recursive technique. From the polynomials describing the characteristic frequencies, i.e. transmission zeros and reflection zeros, the input impedance can be determined. Then, the whole low-pass network parameters are easily obtained by means of the extracted pole technique. A frequency transformation of the low-pass prototype yields a band-pass network based on BVD resonators.

During the design of acoustic wave filters, some considerations have to be contemplated from the very beginning in order to succeed without much optimization iterations in further processes such as electromagnetic simulations. Technological feasibility, among other factors, can be treated as goals during the design. In this chapter, the most important ones and the proper manner to manage them during the synthesis have been also presented.

An example of a Band-25 duplexer has been used to demonstrate how the challenging exercise of design a filter based on acoustic wave technology becomes simple, fast, and accurate. Obviously more steps are required until the fabrication of the device, including multi-physics

FEM simulations, physical layout and package development, electromagnetic simulations, etc., and the filter parameters must be re-optimized several times. However, the starting guess for all these further processes is, probably, one of the best possible options. Furthermore, the methodology presented in this chapter is so fast, if well programmed, that let the designer to check different combinations of resonators, external elements, and filtering responses in a few minutes, and chose the best one in terms of performance, area, feasibility, and power handling.

The methodology has also been exploited for the design of multiplexer devices. Since the phase parameters are easily manageable with this techniques, a set of equations can be solved to obtain the required phase of each stand-alone filter making the multiplexer. With this phase, each filter can be synthesized separately and then connected all together at the antenna port. As verified, the frequency response of the multiplexer device remains essentially unaffected compared with that of each stand-alone filter. The main advantage of using this techniques is that the matching at the antenna port can be realized with only a shunt inductor, without the need of additional phase shifters.

CHAPTER 3

Synthesis of Cross-Coupled Filters Based on Acoustic Resonators

In the previous chapter a synthesis methodology for the design of ladder-type filters based on acoustic resonators has been presented. To this end, two low-pass equivalent circuits has been derived from the BVD band-pass circuit, widely accepted as an accurate model of the fundamental mode of operation of an acoustic resonator. By cascading several low-pass equivalent models of an acoustic resonator an inline topology is constructed, which becomes a ladder-type filter after an adequate band-pass transformation.

In this chapter we are moving one step further. Using the same low-pass equivalent models, a procedure for the synthesis of prototypes having a cross-coupled configuration is given. Similar to the procedure presented in Chapter 2, the synthesis is based on a recursive extraction of a basic sub-network, which can be either a resonant node or a dangling resonator plus a cross inverter between the ports of the sub-network. This definition of the basic sub-network imposes some limitations to the methodology. In particular, the number of distinct topologies that can be realized is $2^{(N-2)}$, with N the order of the filter, and are characterized by an inline network and up to N cross-couplings between non-adjacent nodes.

The proposed technique is not only valid for the design of cross-coupled prototype networks, but it might be useful to synthesize ladder-type filters given that parasitic cross-couplings will be present in further design steps. Moreover, leakage effects due to electromagnetic feedthrough can also be taken into account, thus improving typical attenuation limitations once the filter is physically mounted into the package. These considerations are all covered in this chapter, and some examples are presented as a proof of concept to validate the methodology.

Finally, an optimization technique based on the coupling matrix approach is also introduced

in this chapter. It is suitable for the design of cross-coupled structures that can not be synthesized by the above-mentioned techniques. The parameters of the coupling matrix are optimized for a cost function minimization based on the characteristic frequencies, i.e. the poles and zeros of the transfer function.

3.1 Introduction to Cross-Coupled Synthesis Techniques

In general, microwave filters can be designed in many different ways. However, the increasingly stringent requirements enforce the use of filtering functions exhibiting transmission zeros (TZs) at finite frequencies. Ladder-type acoustic wave filters are fully canonical networks, introducing as many TZs as resonators. Alternative approaches based on acoustically coupled resonators might accommodate TZs at infinity, improving the attenuation at frequencies far from the pass-band. The most employed acoustically coupled topologies are the Dual Mode SAW (DMS) and Multi-Mode SAW (MMS) for SAW technology, and Stacked Crystal Filter (SCF) and Coupled Resonator Filter (CRF) for BAW. Hybrid filters combines ladder and acoustically coupled structures to merge the corresponding valuable features in a unique device.

Cross-coupled topologies exhibiting TZs at finite frequencies are commonly designed with cross-coupled resonators or extracted-pole configurations. The latter was introduced by Rhodes and Cameron in [69], where the resonant node (RN) was considered as the fundamental element in filtering structures. However, more recent attention has focused on the synthesis of prototypes combining RNs and non-resonant nodes (NRNs). Filters employing NRNs are particularly useful because the NRNs provide degrees of modularity and flexibility to the whole network. For example, structures with singlets as the main building block have the capacity to control each TZ independently [56].

In Chapter 2, the singlet has been introduced as a low-pass equivalent model of an acoustic wave resonator positioned in series. An alternative model, the dangling resonator, has been also detailed. Since each acoustic resonator in a ladder network introduces one TZ independently of the rest of the structure, an NRN is indispensable in both low-pass equivalent models to procure the above-mentioned features without the need of cross-couplings. Thereby, the extracted-pole technique presented in Chapter 2 only applies for inline topologies or, equivalently, ladder-type filters.

Further studies have been carried out on the synthesis of mixed topologies made of cascaded inline extracted-pole blocks (dangling resonators connected to NRNs or NRN-RN pair) and cross-coupled segments with only RNs [70]. However, the most recent work by Tamiazzo and Machiarella describes a general procedure for the synthesis of low-pass coupled prototypes including both RNs and NRN-RN pairs [71]. The realizable topologies are characterized by an inline set of resonators and dangling resonators cross-coupled from the outside to inside, and

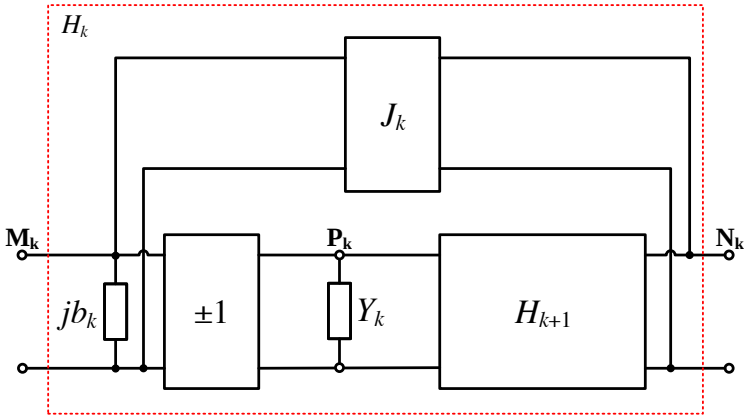

Figure 3.1: Sub-network k to be extracted recursively.

are up to $2^{(N-2)}$ distinct configurations.

Cameron introduced in [50] several filter realizations obtainable by coupling matrix rotations. The transversal coupling matrix can be straightforward synthesized comparing the admittance matrix associated to the polynomials, with that of the transversal network. Although the technique enables the possibility to find a world of distinct cross-coupled topologies, it can not be applied when NRNs are considered. To date, smart optimization techniques of the coupling matrix parameters are the only alternative to design complex cross-coupled topologies including NRNs.

3.2 General Synthesis Technique of Cross-Coupled Prototype Filters

In this section the general procedure allowing the synthesis of prototype filters having a cross-coupled configuration proposed by Tamiazzo and Machiarella in [71] is detailed. An extended case based on a double transmission zero extraction is proposed to provide additional configurations, which contribute in the design of feasible solutions for hybrid configurations based on acoustic resonators.

3.2.1 Sub-Network Definition and Realizable Topologies

The procedure of synthesis requires N recursive steps. At step k, a sub-network as the one shown in Figure 3.1 is considered for extraction. It is made of an input frequency invariant susceptance jb_k cascaded with a unitary inverter, an admittance Y_k, and the rest of the network H_{k+1}, plus a cross-inverter J_k between input and output ports. The susceptance jb_k is necessary to prepare the extraction of the admittance Y_k, which can be either a RN or an NRN-RN pair, as it is

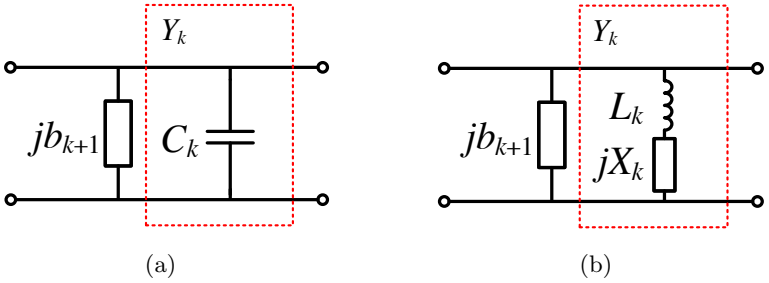

(a) (b)

Figure 3.2: Sub-network admittance Y_k scheme of (a) a resonant node and (b) an NRN-RN pair.

shown in Figure 3.2. The block H_{k+1} contains the following sub-networks to be extracted after the kth step.

In Figure 3.1, it can be observed that some nodes have been designated: M_k and N_k are the input and output nodes of the kth sub-network, respectively, and P_k is the node of the admittance Y_k to be extracted. These definitions are used to distinguish the nodes during the extraction procedure, because distinct topologies can be derived interchanging the outer nodes of the sub-network M_k and N_k. In order to identify the nodes for each step, and define if the extraction is done from the left to the right or from the right to the left in an inline view of the network, the binary word W is introduced and initially specified by the designer. It is defined here as $W_k = 0$ to carry the extraction from the left to the right (natural mode of extraction), and as $W_k = 1$ to interchange the network and extract the parameters from the right to the left. Because in both cases the node M_k indicates the input port of the sub-network, P_k is defined as $P_k = M_k + 1$ if $W_k = 0$ and $P_k = M_k - 1$ if $W_k = 1$.

The outer nodes of the block H_{k+1} once the kth extraction has been realized are defined as

$$M_{k+1} = \min(P_k, N_k) \tag{3.1a}$$
$$N_{k+1} = \max(P_k, N_k) \tag{3.1b}$$

if $W_{k+1} = 0$, and

$$M_{k+1} = \max(P_k, N_k) \tag{3.2a}$$
$$N_{k+1} = \min(P_k, N_k) \tag{3.2b}$$

if $W_{k+1} = 1$.

At the beginning of the procedure, the source is defined with $M_1 = 0$ and the load with $N_1 = N + 1$, where N is the order of the filter. In this work, W_1 has no effect in the definition of the network nodes because interchanging source and load yields in the same network with opposite ports. Thereby, we always define $W_1 = 0$.

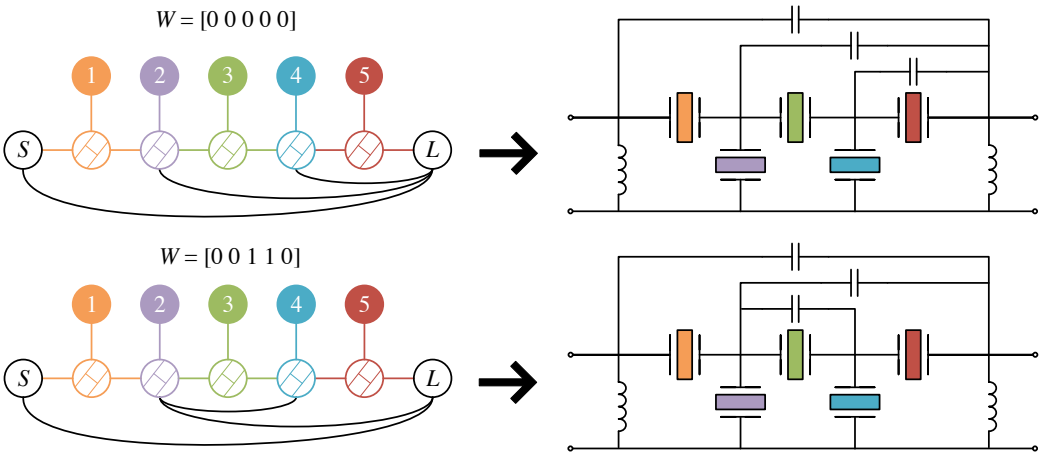

Figure 3.3: All the distinct topologies based on acoustic resonators realizable with $N = 5$ and their corresponding band-pass networks.

It can be observed that all topologies obtained by this method contain all the couplings between adjacent nodes, generating an inline structure. Distinct topologies are only achieved with different placement of the cross-couplings J_k, whose maximum number is N because the filter is made only of N sub-networks. Thereby, it can be observed that only $2^{(N-2)}$ topologies are structurally different.

In case of ladder-type filters based on acoustic resonators, the distinct cross-coupled topologies achievable with this technique decreases drastically to $2^{(N-2-np)}$, where np is the number of shunt resonators. The reason is that no cross-couplings are allowed to be connected to the NRN of series resonators, because it is physically impossible to implement them. In Figure 3.3 there are depicted all the distinct topologies realizable with a filter of order $N = 5$ based on acoustic resonators. Since the number of shunt resonators is $np = 2$, the number of different topologies is up to $2^{(5-2-2)} = 2$.

A limitation of this synthesis procedure is that the cross-couplings cannot cross each other. Moreover, in acoustic wave based technology, the cross-couplings can only be connected to source, load, and between series resonators. However, hybrid topologies combining electrically connected and acoustically coupled resonators can be easily synthesized with and without cross-couplings by using the proposed technique. Novel structures coupling series resonators with parallel capacitors or inductors can also be synthesized by this procedure, providing additional realizations but within the same cross-coupled family of topologies.

3.2.2 Synthesis Procedure

The synthesis of the low-pass prototype network is realized by means of successive extractions from the $ABCD$ polynomial matrix. This matrix is related to the characteristic polynomials of a generalized Chebyshev class of filtering function $P(s)$, $F(s)$, and $E(s)$, associated to the scattering parameters as

$$S_{11}(s) = \frac{F(s)}{\varepsilon_R E(s)} \quad \text{and} \quad S_{22}(s) = \frac{P(s)}{\varepsilon E(s)}. \tag{3.3}$$

The evaluation of the characteristic polynomials have been detailed in Chapter 2. Observe that, although the topologies to be realized in this chapter are quite different to those presented previously, they are still ready to accommodate the same transfer functions, but with TZs at infinite frequencies in some cases.

For a two-port network having the terminals normalized to unity, the $ABCD$ matrix representing the network has the following form:

$$[ABCD] = \frac{1}{jP(s)/\varepsilon} \begin{bmatrix} A(s) & B(s) \\ C(s) & D(s) \end{bmatrix}, \tag{3.4}$$

where the coefficients $A(s)$, $B(s)$, $C(s)$, and $D(s)$ may be directly expressed in terms of the coefficients of $F(s)/\varepsilon_R$ and $E(s)$ following the procedure in [58] as

$$A(s) = j\mathrm{Im}(e_0 + f_0) + \mathrm{Re}(e_1 + f_1)s + j\mathrm{Im}(e_2 + f_2)s^2 + \cdots + j\mathrm{Im}(e_N + f_N)s^N \tag{3.5a}$$
$$B(s) = \mathrm{Re}(e_0 + f_0) + j\mathrm{Im}(e_1 + f_1)s + \mathrm{Re}(e_2 + f_2)s^2 + \cdots + \mathrm{Re}(e_N + f_N)s^N \tag{3.5b}$$
$$C(s) = \mathrm{Re}(e_0 - f_0) + j\mathrm{Im}(e_1 - f_1)s + \mathrm{Re}(e_2 - f_2)s^2 + \cdots + \mathrm{Re}(e_N - f_N)s^N \tag{3.5c}$$
$$D(s) = j\mathrm{Im}(e_0 - f_0) + \mathrm{Re}(e_1 - f_1)s + j\mathrm{Im}(e_2 - f_2)s^2 + \cdots + j\mathrm{Im}(e_N - f_N)s^N \tag{3.5d}$$

for the filter degree N even, and

$$A(s) = \mathrm{Re}(e_0 + f_0) + j\mathrm{Im}(e_1 + f_1)s + \mathrm{Re}(e_2 + f_2)s^2 + \cdots + \mathrm{Re}(e_N + f_N)s^N \tag{3.6a}$$
$$B(s) = j\mathrm{Im}(e_0 + f_0) + \mathrm{Re}(e_1 + f_1)s + j\mathrm{Im}(e_2 + f_2)s^2 + \cdots + j\mathrm{Im}(e_N + f_N)s^N \tag{3.6b}$$
$$C(s) = j\mathrm{Im}(e_0 - f_0) + \mathrm{Re}(e_1 - f_1)s + j\mathrm{Im}(e_2 - f_2)s^2 + \cdots + j\mathrm{Im}(e_N - f_N)s^N \tag{3.6c}$$
$$D(s) = \mathrm{Re}(e_0 - f_0) + j\mathrm{Im}(e_1 - f_1)s + \mathrm{Re}(e_2 - f_2)s^2 + \cdots + \mathrm{Re}(e_N - f_N)s^N \tag{3.6d}$$

for N odd.

The extraction of the elements of the kth sub-network can be realized at infinity, at an arbitrary finite frequency $j\Omega_k$, or at a root of $P_k(s)$ polynomial. An additional type of extraction of two TZs simultaneously is also proposed, only valid when the filtering function accommodates at least one TZ at infinity. A vector Λ is introduced here to manage the type of extraction at each step, whose entries are defined as follows:

- $\Lambda_k = -1$ $\rightarrow$ Extraction of an NRN-RN pair at a root of $P_k(s)$.
- $\Lambda_k = j\Omega_k$ $\rightarrow$ Extraction of an NRN-RN pair at an arbitrary finite frequency $j\Omega_k$.
- $\Lambda_k = 0$ $\rightarrow$ Extraction of a RN at infinity.
- $\Lambda_k = 1$ $\rightarrow$ Dual-TZ extraction.

The vector Λ is used in the following sections to specify the type of extraction and simplify the explanations. However, it is also useful in the software tool that has been created for the synthesis of cross-coupled prototype filters.

Regardless the type of extraction, the first element of the sub-network H_k to be extracted is the cross inverter J_k, in order to leave the remaining network H'_k with the corresponding TZ. Next, the input FIR b_k is extracted to prepare the following removal of the TZ after the unitary inverter extraction. In the following, all types of extractions are detailed and analytically developed.

Extraction of a Root of $P_k(s)$ ($\Lambda_k = -1$)

At the beginning of the extraction procedure, the roots of $P_0(s)$ correspond to the prescribed TZs at finite frequencies. During the synthesis, in case that a cross inverter has been required during a previous step, the roots of $P_k(s)$ at kth step differ from the imposed TZs, and are unknown at the beginning of the process. Furthermore, it may happen that some of these zeros become complex and then cannot be properly extracted with an NRN-RN pair, as will be presented in the following sections.

In this section, we assume that the sub-network H_k has at least one finite TZ to be annihilated, i.e. at least one root of $P_k(s)$ is purely imaginary. The extraction of the TZ $j\Omega_k$, being a root of $P_k(s)$, do not require a cross-inverter J_k, which is therefore zero, and $[ABCD]'_k = [ABCD]_k$. The first element to be extracted is then the FIR b_k, in order to prepare the following removal of the root of $P_k(s)$. It can be obtained by

$$b_k = \frac{D'_k(j\Omega_k)}{B'_k(j\Omega_k)}. \tag{3.7}$$

Once b_k has been calculated, it has to be extracted from the $ABCD$ matrix by

$$[ABCD]''_k = \frac{1}{jP''_k}\begin{bmatrix} A''_k & B''_k \\ C''_k & D''_k \end{bmatrix} = \frac{1}{jP'_k}\begin{bmatrix} A'_k & B'_k \\ C'_k - b_k A'_k & D'_k - b_k B'_k \end{bmatrix}, \tag{3.8}$$

where the independent variable (s) has been omitted from the polynomials for reasons of clarity, and so $A \equiv A(s)$, $B \equiv B(s)$, etc. and $P \equiv P(s)/\varepsilon$ is assumed to have absorbed the constant ε.

The following element in the H_k sub-network is the unitary inverter, which is extracted by interchanging the $ABCD$ polynomials as follows:

$$[ABCD]'''_k = \frac{1}{jP'''_k}\begin{bmatrix} A'''_k & B'''_k \\ C'''_k & D'''_k \end{bmatrix} = \frac{1}{jP''_k}\begin{bmatrix} -jC''_k & -jD''_k \\ -jA''_k & -jB''_k \end{bmatrix}. \tag{3.9}$$

Finally, the admittance Y_k made of an inductance L_k in series with a FIR jX_k, i.e., the dangling resonator, has to be extracted. Since the network has a pole at $s_k = j\Omega_k$, which correspond to the root of $P_k(s)$ to be annihilated, the input admittance parameter results in

$$y_{11} = \frac{D_k'''(s)}{B_k'''(s)} = \left.\frac{b_{0,k}}{(s-s_k)}\right|_{s=s_k} = \left.\frac{1}{sL_k + jX_k}\right|_{s=s_k}, \tag{3.10}$$

where the resonant pair can be related with the residue $b_{0,k}$ and the pole Ω_k as $L_k = 1/b_{0,k}$ and $X_k = -\Omega_k/b_{0,k}$. The parameter $b_{0,k}$ can be found from (3.10) as

$$b_{0,k} = \left.\frac{D_k'''(s)(s-s_k)}{B_k'''(s)}\right|_{s=s_k} = \frac{D_k'''(s_k)}{B_{k+1}(s_k)}. \tag{3.11}$$

The parameter B_{k+1} is part of the $ABCD$ matrix of the sub-network H_{k+1}, given by

$$[ABCD]_{k+1} = \frac{1}{jP_{k+1}}\begin{bmatrix} A_{k+1} & B_{k+1} \\ C_{k+1} & D_{k+1} \end{bmatrix} = \frac{(s-j\Omega_k)}{jP_k'''}\begin{bmatrix} \dfrac{A_k'''}{(s-j\Omega_k)} & \dfrac{B_k'''}{(s-j\Omega_k)} \\ \dfrac{C_k''' - b_{0,k}A_{k+1}}{(s-j\Omega_k)} & \dfrac{D_k''' - b_{0,k}B_{k+1}}{(s-j\Omega_k)} \end{bmatrix}. \tag{3.12}$$

In (3.12), all polynomials have been reduced one degree. All elements of the network H_k have been completely extracted, and the recursive sequence must continue by assigning $H_{k+1} \rightarrow H_k$. However, in case that $W_{k+1} = 1$, polynomials A_{k+1} and D_{k+1} has to be exchanged in order to turn the network and continue the extraction from the other side.

It is important to remember that, when we are designing a ladder-type filter with cross-couplings, the cross inverters can only be connected to the NRNs of shunt resonators, as detailed in section 3.2.1. Thus, a cross-coupling is allowed during the extraction of a series resonator, but not during the extraction of a shunt resonator. The case presented in this section is always necessary for the extraction of all the shunt resonators in order to avoid cross inverters connected to the NRNs of the series ones and, therefore, assure a proper circuital transformation based on BVD resonators.

It might also be noticed that, by assigning $\Lambda = [-1\ -1\ \ldots\ -1]$, a classical ladder-type filter without cross-couplings, as the ones obtained by the methodology presented in Chapter 2, is obtained.

Extraction at an Arbitrary Finite Frequency $j\Omega_k$ ($\Lambda_k = j\Omega_k$)

The removal of a finite TZ requires the extraction of an extracted-pole configuration or NRN-RN pair. If the TZ to be extracted is not a root of $P_k(s)$, a cross inverter is required in order to have the remaining network with a pole at $j\Omega_k$. The cross inverter can be obtained by evaluating $P_k(s)$ and $B_k(s)$ at the TZ as follows:

$$J_k = -\frac{P_k(j\Omega_k)}{B_k(j\Omega_k)}. \tag{3.13}$$

Once the value of the required cross inverter is calculated, the $[ABCD]'_k$ matrix of the remaining sub-network H'_k is updated by

$$[ABCD]'_k = \frac{1}{jP'_k}\begin{bmatrix} A'_k & B'_k \\ C'_k & D'_k \end{bmatrix} = \frac{1}{j(P_k + J_k B_k)}\begin{bmatrix} A_k & B_k \\ C_k + 2J_k P_k + J_k^2 B_k & D_k \end{bmatrix}. \tag{3.14}$$

At this point, $P'_k(s)$ must have a root at $j\Omega_k$, the TZ to be annihilated. The following set of extractions is the same detailed above for the annihilation of a root of $P_k(s)$. First, the FIR b_k is extracted by using (3.7) and (3.25). Then, after the extraction of the unitary inverter with (3.9), the dangling resonator is obtained using (3.10) and (3.11). Finally, the $ABCD$ matrix of the following sub-network H_{k+1} is calculated by (3.12). Again, to continue the synthesis procedure, polynomials A_{k+1} and D_{k+1} have to be exchanged if $W_{k+1} = 1$. The sequence of extractions continues iteratively by assigning $H_{k+1} \rightarrow H_k$.

It is important to observe that, in (3.14), $P_k(s)$ polynomial is affected by the extraction of the cross inverter J_k. An important consequence of $P_k(s)$ alteration is that its singularities becomes different than the previous ones, i.e. the roots of $P'_k(s)$ are not the same than those of $P_k(s)$. The effect of this mismatching makes the following dangling resonators to resonate at a frequency that do not correspond with a filtering function TZ, although it is a TZ of the sub-network H_{k+1}. Furthermore, the new singularities of $P'_k(s)$ might not be only pure imaginary values, but complex conjugate pairs instead. A complex TZ cannot be annihilated by means of a dangling resonator, and additional cross-couplings have to be extracted in following steps to modify another time the singularities of $P_k(s)$ polynomial and make them purely imaginary again.

Extraction at Infinity ($\Lambda_k = 0$)

This type of extraction is performed by extracting a RN of admittance $Y_k = sC_k$. In case that, at this step, there are the same number of TZs at finite frequencies than the remaining sub-networks to be removed, i.e. H_k is fully canonical, a cross inverter J_k will be necessary. Its required value can be calculated as

$$J_k = -\lim_{s\to\infty} \frac{P_k(s)}{B_k(s)}, \tag{3.15}$$

and it has to be completely removed from the $ABCD$ matrix by using (3.14).

It can be observed in (3.15) that only when the degree of $P_k(s)$ and $B_k(s)$ are the same, the cross inverter J_k takes a value different than zero. Otherwise, when H_k has some TZ at infinity, the extracted inverter becomes zero ($J_k = 0$). Polynomial $B_k(s)$ is always fully canonical, and its roots are the global eigen-modes of the complete filter [72], whereas the degree of $P_k(s)$ indicates the remaining number of TZs at finite frequencies ready to be annihilated. Therefore, the cross inverter is only necessary in this case for fully canonical networks.

The next element of the kth sub-network to extract is the frequency invariant susceptance b_k. The extraction of this element is necessary to prepare the following removal of the TZ at infinity. The value of b_k is obtained by evaluating the polynomials $B'_k(s)$ and $D'_k(s)$ at the TZ as follows:

$$b_k = \lim_{s\to\infty} \frac{D'_k(s)}{B'_k(s)}, \tag{3.16}$$

and the $ABCD$ matrix must be updated as

$$[ABCD]''_k = \frac{1}{jP''_k}\begin{bmatrix} A''_k & B''_k \\ C''_k & D''_k \end{bmatrix} = \frac{1}{jP'_k}\begin{bmatrix} A'_k & B'_k \\ C'_k - b_k A'_k & D'_k - b_k B'_k \end{bmatrix}. \tag{3.17}$$

The unitary inverter is extracted by interchanging the $ABCD$ polynomials as follows:

$$[ABCD]'''_k = \frac{1}{jP'''_k}\begin{bmatrix} A'''_k & B'''_k \\ C'''_k & D'''_k \end{bmatrix} = \frac{1}{jP''_k}\begin{bmatrix} -jC''_k & -jD''_k \\ -jA''_k & -jB''_k \end{bmatrix}. \tag{3.18}$$

Finally, the last extraction of the admittance block Y_k requires a removal of a shunt capacitance C_k at infinity. The input admittance at this point is found to be

$$y_{11} = \frac{D'''_k(s)}{B'''_k(s)} = sC_k + Y_{k+1}, \tag{3.19}$$

where Y_{k+1} is the input admittance of the remaining network H_{k+1}. Dividing all sides of equation (3.19) by s and evaluating at $s \to \infty$, the value of the capacitance C_k can be obtained:

$$C_k = \lim_{s\to\infty} \frac{D'''_k(s)}{sB'''_k(s)}. \tag{3.20}$$

The $ABCD$ matrix of the remaining network H_{k+1} is given by

$$[ABCD]_{k+1} = \frac{1}{jP_{k+1}}\begin{bmatrix} A_{k+1} & B_{k+1} \\ C_{k+1} & D_{k+1} \end{bmatrix} = \frac{1}{jP'''_k}\begin{bmatrix} A'''_k & B'''_k \\ C'''_k - sC_k A'''_k & D'''_k - sC_k B'''_k \end{bmatrix}. \tag{3.21}$$

In (3.21), polynomials $C_{k+1}(s)$ and $D_{k+1}(s)$ have to be reduced one degree, because a TZ at infinity has been annihilated. All elements of network H_k have been completely extracted, and the recursive sequence must continue by assigning $H_{k+1} \to H_k$.

Dual-TZ Extraction ($\Lambda_k = 1$)

The Dual-TZ extraction technique is a proposed extension upon the results in [71]. To differentiate this case from the others during the iterative extraction procedure, we have defined $\Lambda_k = 1$. By using this technique, two finite transmission zeros are annihilated during one iteration and one sub-network. In general, the procedure involves the removal of a TZ by means of a cross inverter, followed by a second removal by means of an NRN-RN pair evaluated at a root of $P_k(s)$.

In the extraction techniques described above, the cross inverter is only required if a finite TZ has to be implemented with a RN or if the TZ to be extracted is not a root of $P_k(s)$. The dual-TZ technique combines both cases: a cross-inverter is extracted likewise the admittance Y_k was a RN, thus annihilating one TZ and yielding different roots of $P'_k(s)$, one of which will be removed by a dangling resonator.

The cross inverter is given by

$$J_k = -\lim_{s\to\infty} \frac{P_k(s)}{B_k(s)}, \tag{3.22}$$

and the updated $ABCD$ parameters by

$$[ABCD]'_k = \frac{1}{jP'_k}\begin{bmatrix} A'_k & B'_k \\ C'_k & D'_k \end{bmatrix} = \frac{1}{j(P_k + J_k B_k)}\begin{bmatrix} A_k & B_k \\ C_k + 2J_k P_k + J_k^2 B_k & D_k \end{bmatrix}. \tag{3.23}$$

It may be noticed that $P'_k(s)$ polynomial is reduced one degree because a TZ has been annihilated, and that its roots differs from those of $P_k(s)$. Next, in contrast to the extraction at infinity technique ($\Lambda = 0$) where the following node to be extracted is a RN after the evaluation of a cross inverter J_k at infinity, an NRN-RN pair has to be prepared for extraction. To this end, a frequency invariant susceptance b_k is obtained by

$$b_k = \frac{D'_k(j\Omega_k)}{B'_k(j\Omega_k)}, \tag{3.24}$$

and extracted from the $ABCD$ matrix as

$$[ABCD]''_k = \frac{1}{jP''_k}\begin{bmatrix} A''_k & B''_k \\ C''_k & D''_k \end{bmatrix} = \frac{1}{jP'_k}\begin{bmatrix} A'_k & B'_k \\ C'_k - b_k A'_k & D'_k - b_k B'_k \end{bmatrix}. \tag{3.25}$$

Finally, after the extraction of the unitary inverter by using

$$[ABCD]'''_k = \frac{1}{jP'''_k}\begin{bmatrix} A'''_k & B'''_k \\ C'''_k & D'''_k \end{bmatrix} = \frac{1}{jP''_k}\begin{bmatrix} -jC''_k & -jD''_k \\ -jA''_k & -jB''_k \end{bmatrix}, \tag{3.26}$$

the dangling resonator with an imaginary root of $P'_k(s)$ as the resonance frequency has to be removed by

$$b_{0,k} = \left.\frac{D'''_k(s)(s - s_k)}{B'''_k(s)}\right|_{s=s_k} = \frac{D'''_k(s_k)}{B_{k+1}(s_k)} \tag{3.27}$$

and

$$[ABCD]_{k+1} = \frac{1}{jP_{k+1}}\begin{bmatrix} A_{k+1} & B_{k+1} \\ C_{k+1} & D_{k+1} \end{bmatrix} = \frac{(s - j\Omega_k)}{jP'''_k}\begin{bmatrix} \dfrac{A'''_k}{(s - j\Omega_k)} & \dfrac{B'''_k}{(s - j\Omega_k)} \\ \dfrac{C'''_k - b_{0,k}A_{k+1}}{(s - j\Omega_k)} & \dfrac{D'''_k - b_{0,k}B_{k+1}}{(s - j\Omega_k)} \end{bmatrix}. \tag{3.28}$$

It is interesting to observe that two finite TZs has been annihilated during the kth iteration, or equivalently, the degree of $P_k(s)$ has been reduced by two. Because of this, some limitations

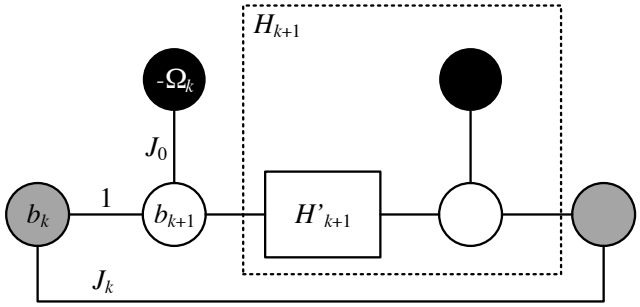

Figure 3.4: Nodal diagram of the kth sub-network ready to be extracted, in which the following configurations from the input and output nodes (grey circles) are NRN-RN pairs.

can be observed. First, the degrees of $P_k(s)$ and $B_k(s)$ have to be the same at the beginning of the dual-TZ extraction procedure, in order to extract a cross inverter J_k different than 0. This implies that at kth step, the number of the remaining finite TZs (degree of $P_k(s)$) has to be equal to the number of remaining resonators to be extracted. Otherwise, the proposed technique will eventually be the same than an extraction at a root of $P_k(s)$ ($\Lambda_k = -1$) detailed above.

On the other hand, the remaining network H_{k+1} has to be comprised of at least one RN. After the dual-TZ extraction during kth step, there are one more resonant node pending to be removed than the number of TZs. Thus, it has to be evaluated at infinity ($\Lambda = 0$). In other words, the degree of $P_{k+1}(s)$ is two times lower than that of $P_k(s)$, but the degree of $B_{k+1}(s)$ is only one time lower than that of $B_k(s)$, i.e. sub-network H_{k+1} is not fully canonical. Executing an extraction at infinity in such conditions results in a RN without cross inverter, thus equating again the degrees of the polynomials and causing sub-network H_{k+2} to be fully canonical.

It is important to notice that some of the results obtained with this extraction technique can also be obtained with the other extraction cases, but turning the network in specific points during the procedure. Results that can only be achieved with the dual-TZ technique are found when, looking from the both sides of the kth sub-network, the following configuration is an NRN-RN pair, as depicted in Figure 3.4.

The main motivation of this proposed technique was the synthesis of filters based on acoustic resonators with hybrid topologies. They are made of electrically connected inline blocks and acoustically coupled resonators. Notice that RN are required to succeed with the dual-TZ technique, but some cross-couplings cannot be implemented physically. Thus, this technique provides technological feasibility in some cases, and may help the designer to synthesize cross-coupled networks with hybrid configurations.

3.2.3 Conclusion of the Synthesis Process

At the end of the Nth step of the synthesis procedure, the network H_{N+1} that remains is constituted by the main path inverter J_{N+1} and two susceptances b_{P_N} and b_{N_N} in parallel at the contiguous nodes P_N and N_N. The $ABCD$ matrix of this sub-network is given by

$$[ABCD]_{N+1} = \frac{1}{J_{N+1}} \begin{bmatrix} -b_{N_N} & j \\ j\left(J_{N+1}^2 - b_{P_N} b_{N_N}\right) & -b_{P_N} \end{bmatrix}. \tag{3.29}$$

Meanwhile, the remaining $ABCD$ matrix at the Nth step is

$$[ABCD]_{N+1} = \frac{1}{jP_{N+1}} \begin{bmatrix} A_{N+1} & B_{N+1} \\ C_{N+1} & D_{N+1} \end{bmatrix}. \tag{3.30}$$

Therefore, the elements to conclude the synthesis process can be obtained by

$$J_{N+1} = -\frac{P_{N+1}}{B_{N+1}}, \tag{3.31}$$

$$b_{P_N} = jJ_{N+1}\frac{D_{N+1}}{P_{N+1}}, \tag{3.32}$$

and

$$b_{N_N} = jJ_{N+1}\frac{A_{N+1}}{P_{N+1}}. \tag{3.33}$$

In contrast with the synthesis of ladder-type filters, in cross-coupled topologies the phase plays an important role to generate the TZs, and the cross inverter J_{N+1} is occasionally required to be different than 1. In particular, it occurs for asymmetrical networks. In those cases, a phase modification of the polynomials $F(s)$ or $E(s)$ at the beginning of the synthesis might yield $J_{N+1} = 1$.

3.3 Existence of Complex TZs

During the synthesis, when a cross inverter J_k is extracted either to annihilate a finite TZ by a RN or a TZ at a frequency that it is not a root of $P_k(s)$, the polynomial $P'_k(s)$ is updated as $P'_k(s) = P_k(s) + J_k B_k(s)$. Therefore, the roots of this updated polynomial are not the prescribed TZs anymore. All resonators embraced by J_k resonates at different resonance frequencies in order to maintain the position of the original TZs.

The new singularities of $P'_k(s)$ may remain pure imaginary or appear in complex conjugate pairs. Pure imaginary TZs can be annihilated by means of dangling resonators, but complex TZs require further cross-couplings to be implemented. A second cross inverter extracted in the proper position modifies again $P_k(s)$ polynomial in such a way that some complex roots becomes pure imaginary, therefore allowing their annihilation by means of dangling resonators.

Table 3.1: Low-pass resonant frequencies of each NRN-RN pair or TZs.

	Ω_1	Ω_2	Ω_3	Ω_4	Ω_5
Ω_k^1	2.3	-1.8	1.6	-1.8	2.3
Ω_k^2	2	-1.73	1.62	-1.89	2.67
Ω_k^3	4	-2.14	1.63+0.25j	-1.63	1.63-0.25j

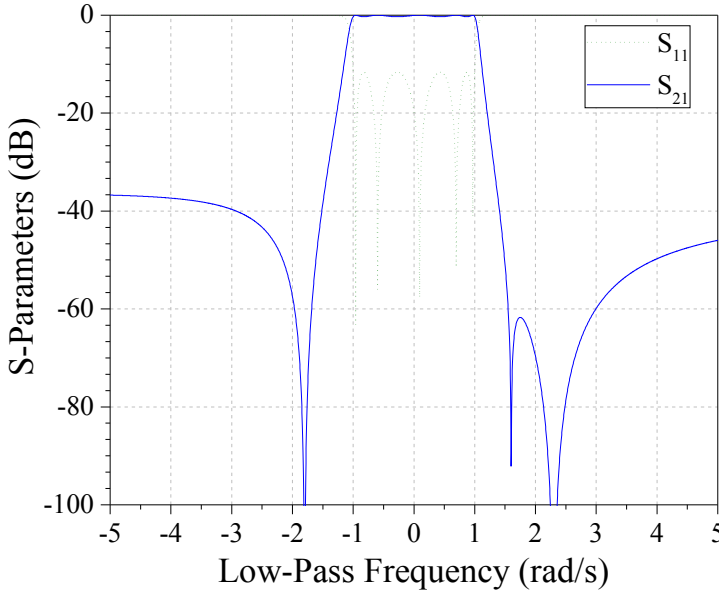

Figure 3.5: Low-pass response of the 5th order filter with TZs Ω_k^1.

In order to differentiate the cases when pure imaginary or complex TZs arise once a cross inverter is extracted, an example is presented next. A 5th order low-pass filter with TZs Ω_k^1 established in Table 3.1 and return loss 11.63 dB is synthesized. The result for $W = \begin{bmatrix} 0 & 0 & 0 & 0 & 0 \end{bmatrix}$ and $\Lambda = j\Omega_k^1$ is an inline network of NRN-RN pairs with the response shown in Figure 3.5.

Now, let us suppose that we are required to have the resonance frequency of the first resonator Ω_1 at low-pass frequency 2, by keeping the same transmission response. Because $\Omega = 2$ is not a root of $P_1(\Omega)$ polynomial at the beginning of the synthesis procedure, a cross inverter J_1 is extracted using (3.13), so the updated polynomial $P_1'(\Omega)$ has a root at the required frequency $\Omega = 2$. However, all roots of $P_1'(\Omega)$ have changed, and are different than the TZs of the original response. In Table 3.1, Ω_k^2 are the roots of $P_1'(\Omega)$. It can be observed that they are slightly different than Ω_k^1, the original roots of $P_1(\Omega)$, and all of them remain pure imaginary in $s = j\Omega$.

By analyzing the extracted cross inverter, that has been found to be $J_1 = 0.00018813$, its S_{21} transmission parameter is approximately of -70 dB. At the resonance frequency of the first resonator Ω_1^2, the main signal path through the resonators behaves like an open circuit, and the

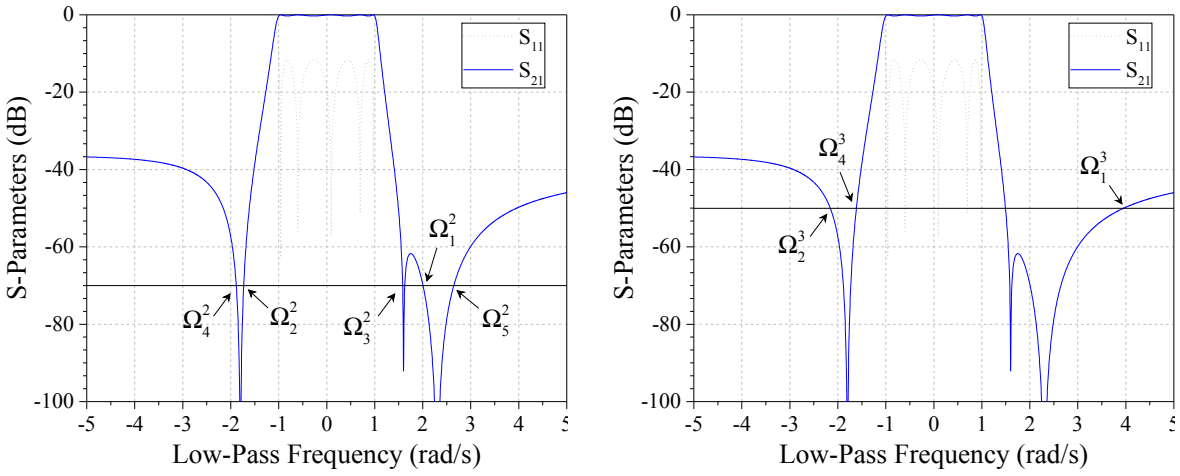

(a) (b)

Figure 3.6: Low-pass response of the filter with TZs Ω_k^1. The horizontal black line indicates the transmission level between source and load through the cross inverter J_1, of (a) -70 dB and (b) -50 dB. The updated TZs of $P_1'(s)$ are also depicted at the corresponding frequency cuts.

unique path between source and load is through the cross inverter J_1. Therefore, at $\Omega_1^2 = 2$, the transmission response of the whole network has to be of -70 dB, as can be checked in Figure 3.6 (a). Moreover, the transmission at all resonance frequencies Ω_k^2 has to be about -70 dB, since all signal at those frequencies flows through the cross inverter.

It can be observed that, to have a tuning on the resonance frequencies and maintain the roots purely imaginary, there are required at least $(N - k + 1)$ intersections of the transmission function and the signal level through the cross-coupling, where N is the filter order and k the step of extraction during the procedure.

But, what happen if there are less crossing points than the number of remaining roots to be annihilated? Following the example above, lets suppose now that we are required to have the first resonator with a resonance frequency of $\Omega_1^3 = 4$. Same than before, a cross inverter between source and load is extracted, now with value $J_1 = 0.0017$. This cross inverter presents a transmission level of -50 dB approximately, and only 4 intersection are found between this transmission level and the filter response, as it can be observed in Figure 3.6 (b). Consideration of the orthogonality unitary condition provides an important relation between the phases of the $S_{11}(s)$, $S_{22}(s)$, and $S_{21}(s)$ polynomials (see Chapter 2), from which can be derived that the zeros of the numerator polynomial of $S_{21}(s)$ parameter, i.e. $P(s)$, must lie either on the imaginary axis of the complex s plane or in mirror-image pairs symmetrically arranged about the imaginary axis, that is, complex conjugate pairs in Ω frequency variable. Therefore, since five NRN-RN pairs remain to be extracted but only four intersections exist for a transmission level of -50 dB, three pure imaginary and a pair of complex conjugate roots are the result of updating $P_1(s)$

Table 3.2: Low-pass Elements of the Synthesized 5th Order Inline Filter with Source-Load Coupling.

Parameters	**Res 1**	**Res 2**	**Res 3**	**Res 4**	**Res 5**
b_k	-4	2.14	-1.63	1.63	-1.63
B_k	-5.50	2.47	-3.03	1.62	-2.08
J_{Rk}	4.69	2.25	2.19	1.52	1.62
J_k	0.0017				

once the cross inverter J_k is fully extracted. These roots are shown in Table 3.1 as Ω_k^3.

Through this example, we have observed that complex roots are originated when the transmission level of the cross-coupling path intersects the transmission response less times than the number of remaining roots to be annihilated at kth step. In the example the cross inverter has been extracted between source and load, although the same effect occurs at any point of the network.

Even though in the example we have forced a resonance frequency different than a root of $P_k(s)$ in order to have a cross inverter between source and load, the same theory is valid for other purposes, e.g. parasitic couplings, electro-magnetic feedthrough (see Section 3.5), etc.

3.4 Complex TZs Realization

An NRN-RN pair, or dangling resonator, is not able to introduce a complex TZ by itself. The input admittance of a dangling resonator is given by (see Chapter 2)

$$Y_{in} = jB + \frac{J_R^2}{s + jb}. \tag{3.34}$$

The admittance becomes infinite when $s = -jb$, thus generating a transmission zero. Notice that b is real, and therefore, the TZ must be pure imaginary in s. Any attempt of annihilate complex TZs by means of dangling resonators will result in a distortion of the response, more noticeable in the OoB frequencies.

Next, an inline low-pass prototype with complex roots is synthesized in order to visualize the effects of extracting complex roots by means of dangling resonators. The transmission zeros of the transfer function are $\Omega_k = \big[2.3,\ -1.8,\ 1.6,\ -1.8,\ 2.3\big]$ and the Return Loss = 11.63 dB. The resonators are extracted from the left to the right, $W = \big[0,\ 0,\ 0,\ 0,\ 0\big]$, and the types of extraction are defined as $\Lambda = \big[4j,\ -1,\ -1,\ -1,\ -1\big]$. Notice that the resonance frequency of the first resonator, defined in $\Lambda_1 = 4j$, is not a TZ and therefore, it is not a root of $P_1(s)$.

A cross inverter has to be extracted first between source and load nodes, and $P_1'(\Omega)$ yields the roots $\Omega_k' = \big[4,\ -2.14,\ 1.63 + 0.25j,\ -1.63,\ 1.63 - 0.25j\big]$, with a pair of complex conjugate

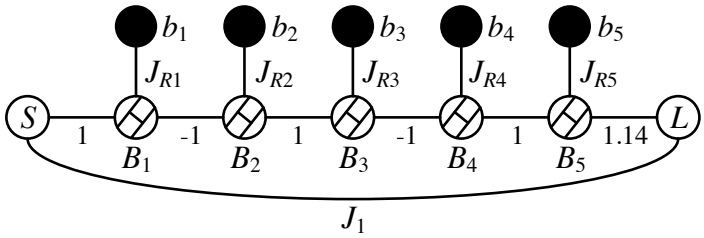

(a)

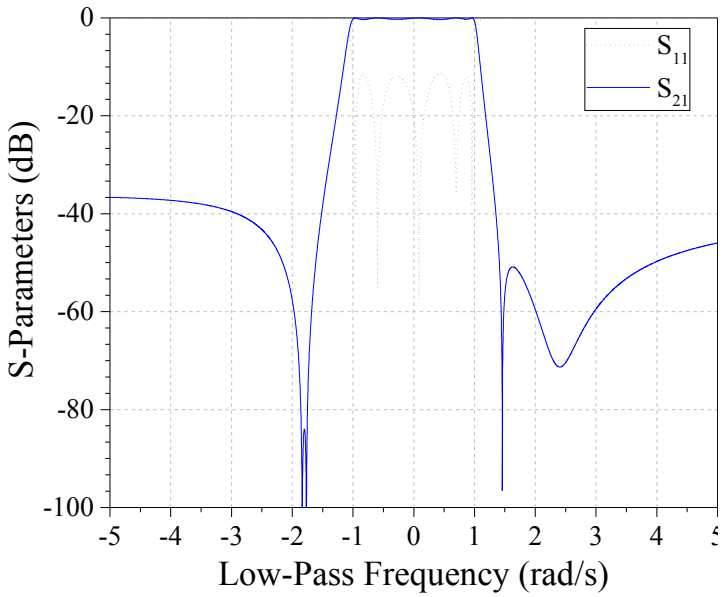

(b)

Figure 3.7: Synthesized low-pass filter with one cross-coupling and complex TZs: (a) prototype and (b) magnitude response.

singularities. In spite of the complex values, all roots are annihilated by means of NRN-RN pairs, and the low-pass prototype at the end of the process results in an inline network of dangling resonators with a cross-coupling between source and load, as depicted in Figure 3.7 (a). The extracted values of all NRN-RN pairs and the cross inverter can be found in Table 3.2. It can be noticed that resonance frequencies of resonators 3 and 5 are the real part of the complex TZs, being as the imaginary part of Ω_3' and Ω_5' cannot be implemented by a dangling resonator.

The low-pass response of the synthesized filter is shown in Figure 3.7 (b). The passband is almost maintained, despite a few deviation on the return loss levels, as well as the OoB on the lower side of the passband. However, upper side TZs, in particular those at $\Omega_k = 2$, are distorted, and the notch is not as deep as in the original response (see Figure 3.5).

This behavior, caused by the complex TZs, may be seen in EM simulations or measures of filters due to undesired parasitic couplings that can require a tuning on the resonance frequencies

Table 3.3: Low-pass Elements of the Synthesized 5th Order Inline Filter with Two Cross-Couplings.

Parameters	**Res 1**	**Res 2**	**Res 3**	**Res 4**	**Res 5**
b_k	-4	2.14	-2	1.67	-1.49
B_k	-5.50	2.52	-3.96	1.65	-2.05
J_{Rk}	4.69	2.25	2.83	1.54	1.42
J_k	0.0017		0.0092		

or even the implementation of complex singularities.

In order to overcome this issue, further cross-couplings can be forced in such a way that the complex roots become pure imaginary again. For example, the resonance frequency of the third resonator can be chosen arbitrarily and different than a root of $P_3(s)$. Accordingly, a cross inverter J_3 will be necessarily extracted, and the updated roots of $P_3'(s)$ may become all pure imaginary.

Using the example above, now the type of extraction is defined as $\Lambda = \left[4j,\ -1,\ 2j,\ -1,\ -1\right]$, thus forcing the resonance frequencies of resonators 1 and 3 to be at $\Omega_1 = 4$ and $\Omega_3 = 2$, respectively. The topology resulting from the synthesis procedure is depicted in Figure 3.8 (a), and the values of the parameters are shown in Table 3.3. The magnitude response agrees with the desired transfer function, as can be observed in Figure 3.8 (b).

In Section 3.2.1 it has been described the realizable topologies, and that cross-couplings cannot be connected to the NRNs of series resonators to assure the physical implementation of the resonators. Therefore, the resonance frequencies of shunt resonators must be always roots of $P_k(s)$, and only those of series resonators can be prescribed to force the cross-couplings to be connected to shunt resonators. This is valid for an extraction from the left to the right of the network, i.e. all Λ_k equal to 0, and may not be correct for other extraction sequences. However, by simple inspection of $P_k\prime(s)$ roots, the designer is capable to know the position of the required cross-couplings and decide their value. This is clearly a redundant configuration that can be useful to acquire the technological feasibility given by the constrained electro-mechanical coupling coefficient in AW technologies.

3.5 Design Considerations with Respect to Parasitic Electro-Magnetic Feedthrough

The general methodology for the synthesis of cross-coupled networks presented above only allows a few distinct topologies for filters based on acoustic resonators. Actually, only $2^{(N-2-np)}$ distinct possibilities are feasible, with N the filter degree and np the number of shunt resonators. For

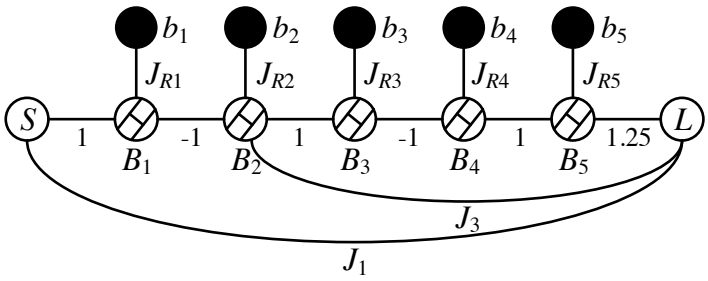

(a)

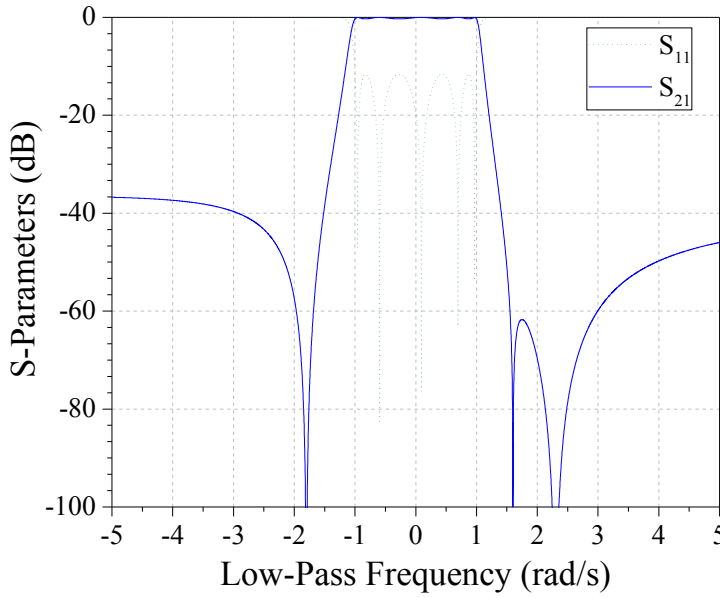

(b)

Figure 3.8: Synthesized low-pass filter with two cross-coupling (between source and load nodes, and between resonator two and load nodes: (a) prototype and (b) magnitude response.

a typical filter of degree $N = 7$ with 4 series resonators and 3 shunt resonators, only 4 distinct cross-coupled topologies can be synthesized. Moreover, all cross-couplings can only be connected to source, load, or between series resonators. Therefore, well-known cross-couplings such as a common ground inductor or a capacitive coupling between a port and a ground inductor of a shunt resonator are not possible to be synthesized with this technique.

Despite the limitation of the methodology, enormous benefits can also be collected in terms of understanding. For example, during the synthesis development, it has been detected that complex TZs can arise when a cross inverter is extracted. The apparition of complex TZs may cause degradation of the filter frequency characteristics if they are not properly treated. By means of the general synthesis methodology, these complex TZs can be re-converted to pure imaginary TZs with additional cross-couplings between the proper nodes.

In this section, a potential electro-magnetic feedthrough (EMF) between a package ports is considered from the very beginning, thus improving the filter characteristics when it is assembled. This signal leakage does not pass through the main filter path and causes attenuation limitations in the OoB frequencies. Furthermore, in certain instances, the notches caused by the TZs seems to disappear. Similar interpretations can be conducted in duplexer devices, where isolation between the transmitter and the receiver can be degraded due to undesired leakage paths.

The factors that introduce limitations on the attenuation and isolation levels of conventional miniaturized filters and duplexers has been considered in [73–75]. They can be classified into two types of signal leakage. The first one occurs via the main signal path, and it is due to the finite impedance of the RX filter in the TX band in a duplexer. The second one is the case of study in this section, and it is, for instance, due to EMF, electro-magnetic couplings, imperfect grounding, and so on. Because of the existence of these leakages, the isolation of conventional duplexers is limited to about 50 to 55 dB [73].

Further studies demonstrated that by means of an amplitude and phase adjusting block properly connected to the RX port, part of the leakage is canceled out leading to a significant improvement in the TX band isolation of the duplexer device [76]. Other techniques, such the one described in [77], eliminates the main path leakage by means of an additional and intentionally well-designed path with appropriate phase and amplitude properties. High attenuation is also achieved at an arbitrary frequency because of a notch in the transmission response.

In general, the design of filters based on acoustic resonators taking all leakages paths into account requires lots of time consuming optimization processes, using three-dimensional electro-magnetic simulations of the package combined with the equivalent circuital simulation of the resonators. These techniques force the optimizer to modify the acoustic resonator parameters in order to mitigate the undesired feedthrough effects. However, the stringent technological requirements of acoustic wave devices confines the solution map to a very small region of feasible alternatives, leading the design to an even more challenging task.

Better solutions for further optimization processes might be achieved by using the described-above synthesis methodology, but taking the leakage path between source and load into account. Effects such as attenuation limitations, TZs that vanish in determined cases, and isolation degradation, can be clearly improved during the synthesis approach, as illustrated in the following sections.

3.5.1 Electro-Magnetic Feedthrough Modeling

The EMF is a disturbing signal that can be found in many acoustic devices influencing the output signal in an undesired manner. An electrical signal applied to the input might appear as a parasitic electrical signal at the output because of EMF. The influence of packaging the devices,

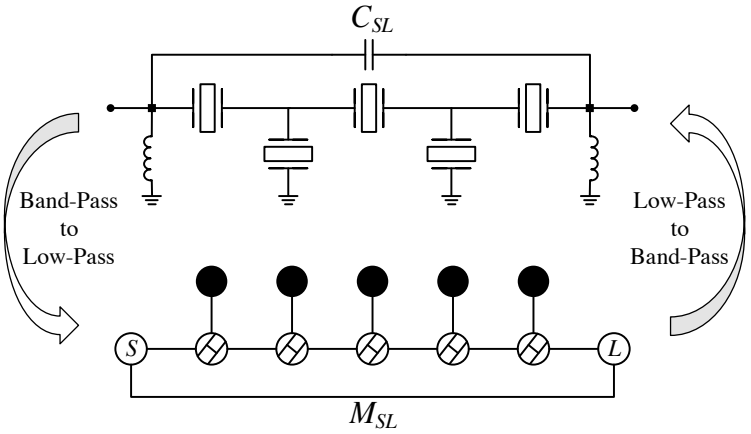

Figure 3.9: Band-pass circuital scheme of a 5th order filter based on acoustic resonators and its equivalent low-pass prototype. The electro-magnetic feedthrough trough the package is considered as an external capacitor C_{SL} connecting the input and output ports. In the low-pass prototype it is contemplated as a coupling M_{SL} connecting source and load nodes.

of bonding wires, and contact resistances has an important impact on the filter attenuation because of these parasitics. Leakage currents through the silicon substrate can create a coupling between the input and output of the device, also contributing to EMF.

Many authors have published circuital models to take parasitic elements into account [78–84], including EMF, packaging, bond wires, etc. Complex models arise when all parasitic effects are considered, which are not really useful for synthesis purposes. However, it is interesting to notice that all models present a series capacitor between input and output ports. In general, electrostatic coupling is found to be the dominant parasitic leakage due to EMF [73].

In Figure 3.9 it is depicted the band-pass circuit of a 5th order filter with a parasitic capacitor C_{SL} that models the EMF between the ports of the device. Using the admittance inverter realization shown in Figure 3.10, the EMF might be also modeled as a cross inverter $J_{SL} = -\omega C_{SL}$ between input and output ports. In the low-pass domain, the acoustic resonators are NRN-RN pairs or dangling resonators, and the EMF a cross inverter $M_{SL} = Z_0 J_{SL}$ between source and load nodes, where Z_0 is the characteristic impedance used to normalize the low-pass network. It is important to notice that the admittance inverter has to be negative in order to

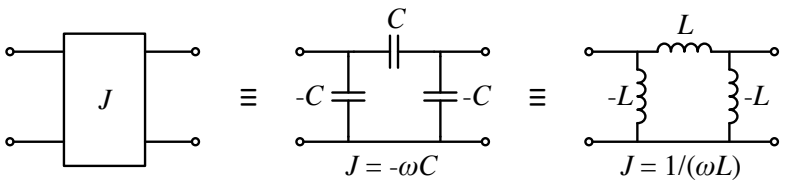

Figure 3.10: Realization of an ideal admittance inverter.

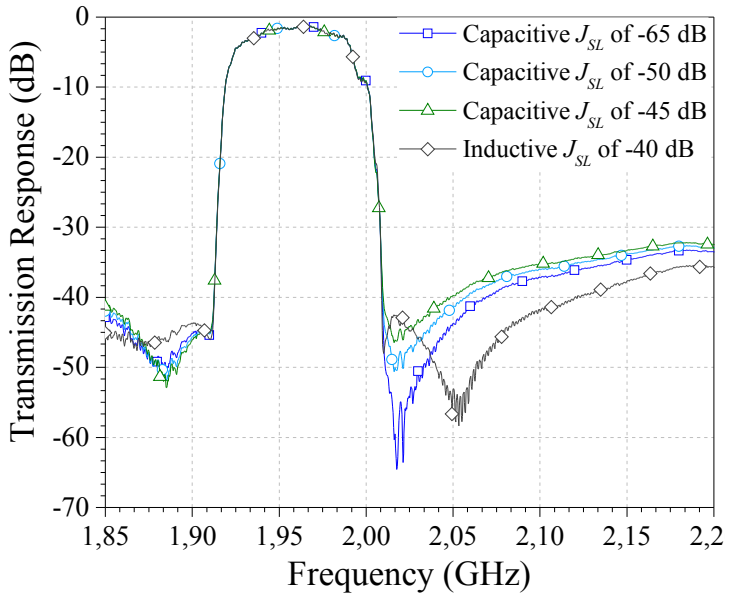

Figure 3.11: Co-simulation of a measured transmission response with different electro-magnetic feedthrough levels and nature.

result in a capacitive coupling. Otherwise, the behavior of the modeled EMF will be inductive, thus affecting the response in a different way.

A co-simulation of a measured filter with different levels of EMF is shown in Figure 3.11. For capacitive couplings, the maximum OoB attenuation is of the same level than the modeled EMF, and it occurs at the TZ frequencies. No better attenuation levels are achieved at any other frequency. With respect to the passband, it remains almost unaffected regardless the level. On the other hand, an inductive coupling also degenerates the filter response but in such a way that may improve the OoB characteristics by introducing an additional TZ at an arbitrary frequency.

3.5.2 Design Procedure

The synthesis of a filter taking into account the EMF is based in the theory detailed above in this chapter. The only difference may be found in the extraction of the cross inverter. When a parasitic coupling is considered, the cross inverter is not evaluated at any frequency, but is given by the parasitic. Therefore, M_{SL} is determined by the EMF, and the $P_1'(s)$ and $C_1'(s)$ parameters has to be updated as (3.14)

$$P_1'(s) = P_1(s) + M_{SL}B(s) \tag{3.35a}$$

$$C_1'(s) = C_1(s) + 2M_{SL}P(s) + M_{SL}^2B(s). \tag{3.35b}$$

Table 3.4: Resonator Parameters for the Different Filtering Network Solutions.

	Parameters	**Res 1**	**Res 2**	**Res 3**	**Res 4**	**Res 5**
Case 1	f_s (GHz)	1.9607	1.8901	1.9544	1.8901	1.9607
	C_0 (pF)	0.7810	3.2986	0.5717	3.2986	0.7810
	r			16		
	k^2_{eff} (%)			7.15		
Case 2	f_s (GHz)	1.9536	1.8806	1.9563	1.8955	1.9648
	C_0 (pF)	0.4276	3.6081	0.5875	2.5370	0.9124
	r	9.20	13.14	18.46	18.05	22.38
	k^2_{eff} (%)	11.77	8.56	6.26	6.39	5.22
Case 3	f_s (GHz)	1.9343	1.8856	1.9526	1.8919	1.9529
	C_0 (pF)	0.6335	4.0851	0.4939	3.2659	1.7705
	r	7.88	14.99	13.15	17.17	19.03
	k^2_{eff} (%)	13.48	7.59	8.56	6.69	6.08

Provided the level of EMF coupling, the roots of $P_1'(s)$ may be all pure imaginary or appear in complex conjugate pairs, as detailed in Section 3.3. The best case is found with all roots being pure imaginary, because only a tuning on the resonance frequencies is required. However, differences in the original roots yields different resonator parameters. Therefore, the acoustic restrictions such as the coupling coefficient or capacitance ratio parameter results in a different ones compared with the original ladder network without the parasitic coupling consideration. On the other hand, if complex roots are originated with the extraction of M_{SL}, extra cross-couplings are necessary to be extracted in further steps during the synthesis procedure, which make the filter implementation more complicated.

A design procedure of a filter based on acoustic resonators is presented next. First, a conventional ladder-type filter that satisfies the technological requirements is designed. Then, the response is distorted assuming an EMF between the ports, and different ways to improve it but preserving the same transfer function are provided.

The low-pass TZs of the filter to be synthesized are $\Omega_k = \left[1.88,\ -1.83,\ 1.69,\ -1.83,\ 1.88\right]$ for a Return Loss = 11.6 dB. In order to get an inline topology without cross-couplings, the sequence of extraction is defined as $W = \left[0,\ 0,\ 0,\ 0,\ 0\right]$ and the type of extraction as $\Lambda = j\Omega_k$. In Table 3.4 Case 1, there are the band-pass resonator parameters of the synthesized ladder-type filter of order $N = 5$ that agrees with a technological feasibility of $k^2_{eff} = 7.15\%$, typical in AlN piezoelectric materials. In Figure 3.12 there are depicted the band-pass network and the filter response. The input and output matching inductors are $L_{in} = L_{out} = 15.64$ nH.

Lets suppose that an EMF between the ports of the filter is present, that may be through the substrate or the package in which the device is assembled. The band-pass network of the

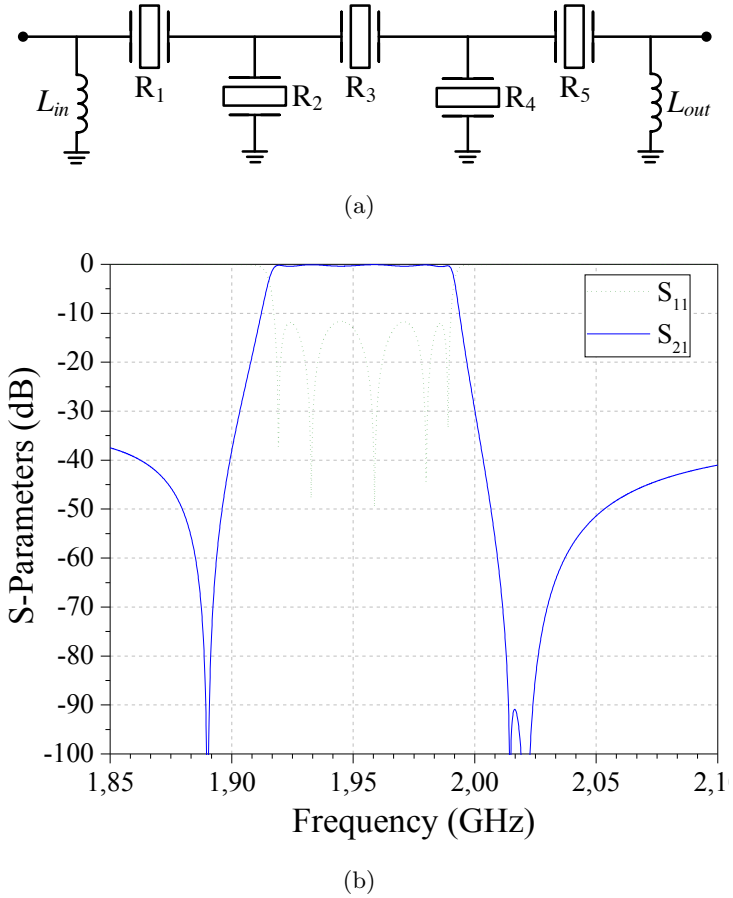

Figure 3.12: Ladder-type design with parameters shown in Table 3.4 Case 1: (a) band-pass scheme and (b) response simulation.

ladder filter in Case 1 with a capacitive EMF is depicted in Figure 3.13 (a). Due to this signal leakage, considered of -50 dB (C_{SL} = 2.607 fF), the response of the filter is distorted, as can be observed in Figure 3.14. In particular, the OoB rejection is not much better than the EMF level of -50 dB, which can be exactly found at TZ frequencies (see Section 3.3). This effect of distortion involves around 40 dB of attenuation deterioration at the TZ frequencies, only given by a simple capacitor of a few fF.

In a real design, the filtering function, i.e. the TZs and return loss, has to be modified and re-synthesized in such a way that both the technological requirements and the frequency mask specifications are most satisfied for the given EMF level. However, we will maintain the transfer function in order to properly compare the results and the improvement in the OoB frequencies.

Under the theory presented in Section 3.4, the cross inverter M_{SL} due to the EMF can be extracted at the beginning of the synthesis procedure. For an EMF level of -50 dB, that is $M_{SL} = 0.0016$, a pair of complex roots are generated after the cross inverter extraction. It has

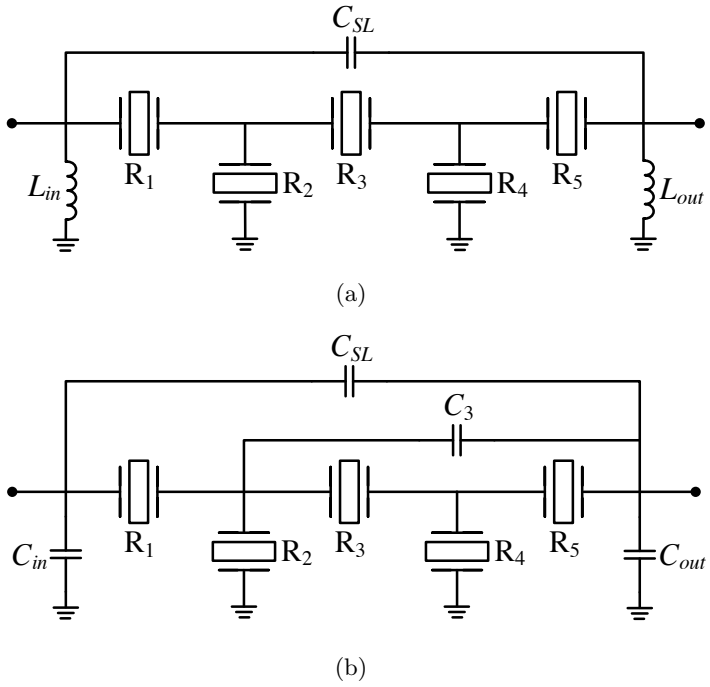

Figure 3.13: Band-pass schemes of (a) designs in Table 3.4 Case 1 and Case 2, and (b) Case 3.

been described above that complex singularities cannot be annihilated by means of dangling resonators (or acoustic resonators in the band-pass domain). But nevertheless, the synthesis can be executed anyway by defining a type of extraction $\Lambda = \left[-1,\ -1,\ -1,\ -1,\ -1\right]$, but not achieving the expected response. In Table 3.4 Case 2 there are the resonator parameters of a synthesis where the complex TZs have been omitted. An improvement in the OoB rejection is attained, although it is not optimum, as can be observed in Figure 3.14.

The appropriate way to proceed is introducing further cross-couplings in order to annihilate the complex singularities. A second cross inverter between resonator R_2 and load can be forced by setting $\Lambda = \left[-1,\ -1,\ 2j,\ -1,\ -1\right]$. The synthesis results in a cross inverter $M_3 = 0.0174$, that is $C_3 = 28.35$ fF, a matching elements of $C_{in} = 0.75$ pF and $C_{out} = 0.11$ pF, and the resonator parameters shown in Table 3.4 Case 3. The band-pass network is depicted in Figure 3.13 (b), where C_{SL} is given by the EMF.

The band-pass response, shown in Figure 3.14, significantly improves the OoB attenuation, but it no matches the original transmission response perfectly at frequencies around the upper TZs. The reason can be found both in the circuital and frequency transformations, detailed in the following section.

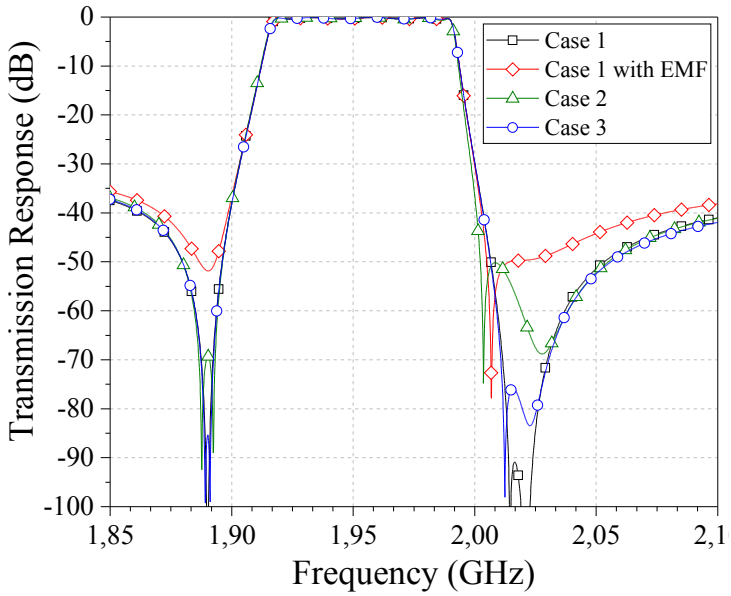

Figure 3.14: Comparison of the transmission responses of filters in Table 3.4. In Case 1 with EMF, the ladder-type filter with an EMF transmission level between terminals of -50 dB is considered.

3.6 Transformation of Cross-Coupled Low-Pass Prototypes

In this section, two issues associated with the transformation of an NRN-RN pair to a band-pass acoustic resonator and potential solutions to improve them are presented. Particularly, the first problem is given by the circuital equivalence between the dangling resonator and the low-pass equivalent BVD model of a series resonator. The second one is due to the narrowband limitations of the band-pass transformation.

In Chapter 2, the low-pass equivalence between the dangling resonator and the BVD model, depicted in Figure 3.15, was reported. The couplings J_{ML} on both sides of the dangling resonator must be, imperatively, of the same value and opposite sign. For convenience, during the iterative extraction procedure, it is usually chosen as $|J_{ML}| = 1$. However, the last inline inverter to be extracted is given by the $[ABCD]_{N+1}$ matrix (see section 3.2.3), and it is occasionally required to be different than 1. It has been observed that an adequate phase consideration of the low-pass polynomials $E(s)$ and $F(s)$ before the extraction procedure yields the last inline coupling to be $J_{N+1} = 1$. However, this effect is not only stringed to the response, but also to the topology and assignation of the TZs. Then, the required phase terms becomes hard to estimate at the beginning of the procedure, and no systematic solution has been found yet.

Even though the last inline inverter is found to be unitary by a proper phase management, the narrowband approximation used in the low- to band-pass transformation might cause mis-

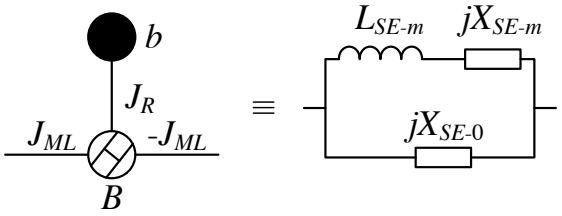

Figure 3.15: Low-pass equivalence between the NRN-RN pair a the BVD model.

matching between the responses mainly around the TZs frequencies, as it has been observed in Figure 3.14. In a cross-coupled structure, the TZs can be generated by opposite phases through the different paths, and differences between the amplitudes or the phases may cause the TZs to be not as deep as expected. As farther the resonances of a resonator from the center frequency of the passband, worsen the frequency transformation and larger the amplitude and phase differences between the signal paths.

In order to solve this, more accurate frequency transformations are necessary. Another alternative is to extract the circuital elements directly in the band-pass domain by using band-pass polynomials. These are introduced in Chapter 4.

3.7 Synthesis of Cross-Coupled Low-Pass Prototypes by Coupling Matrix Optimization

The synthesis techniques introduced above are very useful for the design of a limited set of cross-coupled topologies based on acoustic resonators. Particularly, only $2^{(N-2-np)}$, where N is the filter degree and np the number of shunt resonators, distinct topologies are feasible by using this technique. It is also a valuable methodology for the understanding of the effects caused by a cross-coupling, e.g. the complex transmission zeros. Several undesired parasitics, such as the electromagnetic feedthrough or leakage path between the ports of a filter, can be included in the procedure, thus improving the overall filter characteristics.

However, it might be interesting to synthesize complex topologies that cannot be obtained by the techniques presented above due to the cross-couplings configuration. The general theory of cross-coupled band-pass filters presented in the 1970s by Atia and Williams [85] is still widely used. It leads to a transversal coupling matrix which reproduces the system function to be synthesized. It usually includes unwanted or unrealizable couplings that can be canceled by similarity transformations [47], [85]. Unfortunately, the process is not applicable when NRNs are part of the structure, which requires novel transformation techniques.

One possible general solution to the design of filters with arbitrary topology is to apply di-

rect local optimization over the coupling matrix with successive starting points. An interesting approach in which the entries of the coupling matrix were used as independent variables was presented in [86]. A simple cost function along with a standard unconstrained gradient optimization technique was used with excellent results. In [87], Amari introduced analytical expressions for the gradient of the scattering parameters. In both works, the starting point vector is set to arbitrary values. This makes the local optimization very unstable for cost function minimization, and does not assure convergence. A solution could be global optimization methods to find the coupling matrix of a certain filter topology. They perform robust optimization, no matter about the starting point. However, global optimizers such as genetic or stochastic are very time consuming methods.

For the synthesis of filters based in acoustic resonators, the local optimization of a cost function based on the location of the transfer function poles, zeros, and an additional scaling constant for a predefined topology is preferred. The advantages of this technique are:

1. Design of a filter with symmetric or asymmetric response.
2. Design of a filter with arbitrary topology, even or odd order.
3. Possibility of constraint the magnitude and sign of the coupling coefficients if a given realization is intended.
4. Elimination of the round off errors given by similarity transformations.

On the other hand, the main disadvantages of local optimization methods are:

1. Exact solution is not guaranteed, and the larger the number of variables, the more difficult to achieve it.
2. The predefined topology must be able to accommodate the desired filter response. Then, a local minimum is reached by the optimization process.
3. The initial guess is preferred to be close to the target coupling matrix in order to assure fast convergence.
4. To obtain a realizable solution, the elements of the coupling matrix has to be constrained in some particular cases. For very unconstrained elements, a feasible solution might be difficult to be achieved by local optimizers.

In the following, the coupling matrix of filters based in acoustic resonators is presented. It has been arranged in a manner that the nodes are grouped depending on their nature. Since the cross-couplings are usually implemented by external elements instead of coupling paths, they are considered as additional NRNs, so their frequency dependence can be considered in the band-pass coupling matrix approximation.

3.7.1 Coupling Matrix Definition

The coupling matrix is a suitable representation of a 2-port network composed of coupled resonators. The common $N+2$ coupling matrix of a filter refers to the extended prototype including source and load nodes [50]. It allows to consider fully canonical structures with direct source to load coupling.

In Chapter 2, it has been presented the nodal diagram of an acoustic resonator, made of a resonant and a non-resonant nodes. Therefore, the common $N+2$ coupling matrix needs a formulation extension in order to introduce the NRNs, leading to a $2N+2$ coupling matrix, where N is the number of acoustic resonators.

For cross-coupled topologies, in which the cross-couplings are represented by NRNs, the size of the coupling matrix increase to $(2N+2+X_P+X_0)$, where X_P is the number of cross-couplings realized by lumped elements, i.e. inductors or capacitors, and X_0 is the number of NRNs forced to 0. The latter nodes are required in specific positions of the nodal prototype as connection points between resonators. For example, when a shunt resonator is connected in series to a ground inductor, the required low-pass model of the shunt resonator becomes the same than that of a series resonator, i.e. a dangling resonator placed between two inverters. In those cases, a zero NRN is used for the connection of the series and the shunt resonators, since all of them requires their own inverters. In Figure 3.16 there is the equivalence between the NRN and the band-pass element used to realize the cross-coupling, subject to the position of the NRN in the network and its sign.

In order to simplify the management of the general coupling matrix, which can result in a large symmetrical matrix given that not only resonant nodes are considered, it can be divided into smaller sub-matrices depending on the connections between the nodes:

- $\boldsymbol{M}_{SL} \in \Re^{2\times 2}$: sub-matrix of source and load nodes. The diagonal $[M_{SL}]_{ii}$ represents the matching elements of the input and output ports. In general, $[M_{SL}]_{12} = [M_{SL}]_{21} = 0$, although the EMF between ports can be placed here.
- $\boldsymbol{M}_{R} \in \Re^{N\times N}$: sub-matrix of resonant nodes. The diagonal elements $[M_R]_{ii}$ are the self-couplings of the resonators, that is the FIR elements b_i in parallel with the unitary capacitors.
- $\boldsymbol{M}_{N} \in \Re^{N\times N}$: sub-matrix of the NRN nodes that are part of an acoustic resonator. The diagonal elements $[M_N]_{ii}$ are the susceptances of the NRNs B_i. In this sub-matrix, the inline connections between the different NRNs have to be also specified.
- $\boldsymbol{M}_{SL\_N} \in \Re^{2\times N}$: sub-matrix of the connections between source and load nodes, and the dangling resonators NRNs. Usually, the NRN of the first resonator B_1 is connected to source, and the NRN of the last resonator B_N is connected to load, both of them by

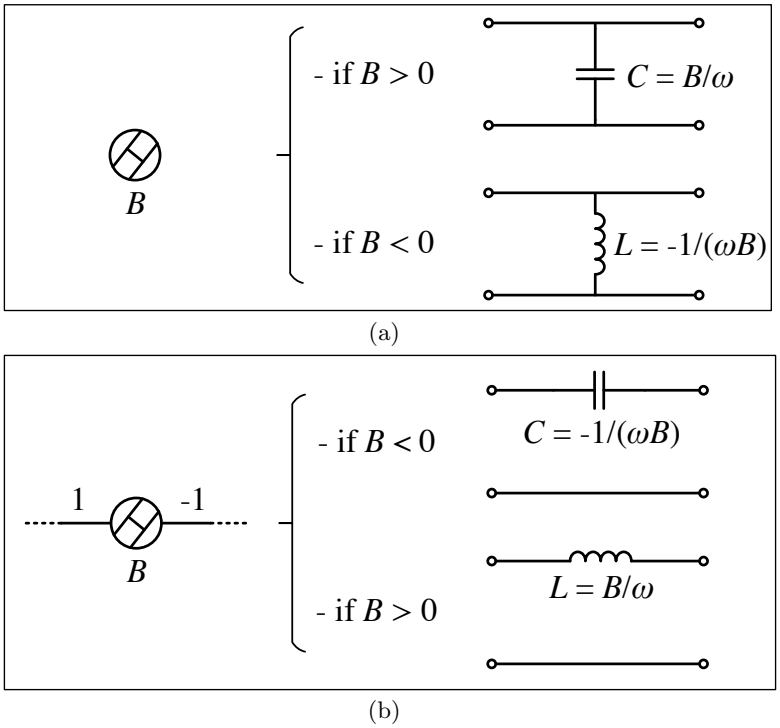

Figure 3.16: NRNs and its band-pass equivalent elements: (a) NRN without inverters and (b) NRN with inverters.

unitary inverters.

- $\boldsymbol{M}_{R\_N} \in \Re^{N\times N}$: sub-matrix of connections between the resonant nodes and the NRNs of the acoustic resonators, i.e. the couplings J_{Ri} in the main diagonal $[M_{R\_N}]_{ii}$.
- $\boldsymbol{M}_X \in \Re^{(X_P+X_0)\times(X_P+X_0)}$: sub-matrix of NRNs that are not part of the acoustic resonators. They can be either part of a cross-coupling or zero.
- $\boldsymbol{M}_{SL\_X} \in \Re^{2\times(X_P+X_0)}$: sub-matrix with the connections between the cross-couplings NRNs and the source and load ports, in case they exist.
- $\boldsymbol{M}_{N\_X} \in \Re^{N\times(X_P+X_0)}$: sub-matrix with the connections between the cross-couplings and the NRNs of the acoustic resonators.

The general coupling matrix defined by the sub-matrices specified above results in

$$\boldsymbol{M} = \begin{bmatrix} \boldsymbol{M}_{SL} & \boldsymbol{0}^{2\times N} & \boldsymbol{M}_{SL\_N} & \boldsymbol{M}_{SL\_X} \\ \boldsymbol{0}^{N\times 2} & \boldsymbol{M}_R & \boldsymbol{M}_{R\_N} & \boldsymbol{0}^{N\times(X_P+X_0)} \\ \boldsymbol{M}_{SL\_N}^T & \boldsymbol{M}_{R\_N}^T & \boldsymbol{M}_N & \boldsymbol{M}_{N\_X} \\ \boldsymbol{M}_{SL\_X}^T & \boldsymbol{0}^{(X_P+X_0)\times N} & \boldsymbol{M}_{N\_X}^T & \boldsymbol{M}_X \end{bmatrix}, \tag{3.36}$$

where $\boldsymbol{0}$ is a zero sub-matrix. It is located in the sub-matrices that represent the connections between the resonant nodes of the acoustic resonators with terminals and cross-coupling NRNs,

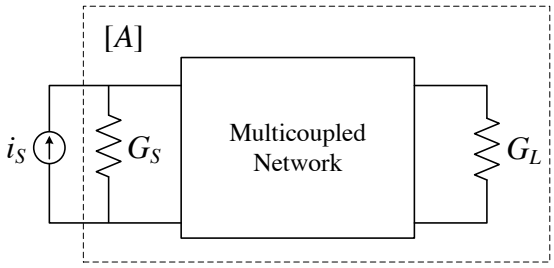

Figure 3.17: Network defined by the admittance matrix $[A]$ including the conductance of source G_S and load G_L.

because these connections have no physical realization. It is interesting to observe that the coupling matrix is symmetrical about its main diagonal, because a filter is a passive and reciprocal network.

The narrowband approximation of the coupling matrix model, which assumes the couplings frequency independent, is its main drawback. The coupling matrix use extents to narrow bandwidths up to 5% approximately.

3.7.2 Analysis of the Network Represented by the Coupling Matrix

The coupling matrix contains most of the relevant information about the network, although it is not a complete representation of it. Additional elements such as the conductance of each port and the parallel unitary capacitors of the resonant nodes are included in external matrices.

The two-port network to be analyzed is fed with a current source i_S of internal conductance G_S and loaded with a conductance G_L, as depicted in Figure 3.17. The multicoupled circuit is arranged with admittance nodes, whether they are resonant or non-resonant. The voltage at each node is denoted by v_i, all of them grouped in the vector $\boldsymbol{v}$ of length $(2N+2+X_P+X_0)$. The source is the only node to be excited, resulting in an excitation vector of $\boldsymbol{i} = [1, 0, \ldots, 0]^T$. Therefore, the nodes equations resulting from Kirchhoff's law can be formulated in matrix notation as

$$[A][v] = [-j\boldsymbol{G} + \Omega\boldsymbol{W} + \boldsymbol{M}][v] = -j[i], \tag{3.37}$$

where $\boldsymbol{G}$ is an $N_T \times N_T$ diagonal matrix ($N_T = 2N + 2 + X_P + X_0$) of conductances, with $G_{11} = G_S$, $G_{N_T,N_T} = G_L$ and $G_{ii} = 0$ otherwise. G_S and G_L are usually considered unitary. The normalized low-pass angular frequency is denoted by Ω. $\boldsymbol{W}$ is an $N_T \times N_T$ diagonal matrix such that $W_{11} = W_{N_T,N_T} = 0$, $W_{kk} = 1$ if node k is resonating, and $W_{kk} = 0$ if it is non-resonating.

The voltage of each node can be computed by solving the lineal system in (3.37). The response of the circuit at the two ports is fully specified by the voltages at the input and output nodes,

i.e., v_1 and v_2. Therefore, the S-parameters are found to be as follows:

$$S_{11} = -1 - 2jG_S \left[A^{-1}\right]_{11} \tag{3.38a}$$

$$S_{22} = -1 - 2jG_L \left[A^{-1}\right]_{22} \tag{3.38b}$$

$$S_{21} = -2j\sqrt{G_S G_L} \left[A^{-1}\right]_{21} \tag{3.38c}$$

Our definition of the coupling matrix has the input and output ports represented by the first and second rows and columns, respectively. The results can be expanded to a multi-port network following the proper formulation [88]. That multi-port interpretation might be a good solution to the synthesis of multiplexers for the near-future systems based on carrier aggregation.

3.7.3 Coupling Matrix Local Optimization

The design of filtering devices based on acoustic resonators usually becomes a challenging task due to the increasingly stringent technological requirements. Therefore, we can define the problem as nonlinear and constrained, and make use of the sequential quadratic programming (SQP) algorithm through the NLPQL code of Prof. Schittkowski [89]. The definition of the problem can be expressed as

$$\min_x f(x) \text{ such that } \begin{cases} c(x) \geq 0 \\ c_{eq}(x) = 0 \\ x_l \leq x \leq x_u \end{cases} \tag{3.39}$$

where x is a vector with the optimization variables, f is the objective function, c and c_{eq} contains the inequality and equality constraints, respectively, and x_l and x_u are the lower and upper bounds of the optimization variables.

The aim of this synthesis procedure based in local optimization is to find the parameters of a given topology that can be implemented with acoustic resonators, i.e., accommodates the technological requirements, and that best satisfy the mask specifications. Meanwhile, an arbitrary coupling matrix should fit into a generalized Chebyshev filtering function, which is also part of the optimization. Our optimization variables are therefore the coupling matrix parameters m_x, the transmission zeros Ω_k, and the return loss RL. In m_x vector there are specified all nodes, whether they are resonant nodes or NRNs, and the J_R couplings of the dangling resonators. Notice that the main line couplings are set always to unity and, therefore, they are not considered as optimization variables.

The inequality constraint vector c can contain the difference between the mask specifications and the coupling matrix response, so the transmission level is always lower than the specification at the corresponding frequencies. Other restrictions such as maximum static capacitors or ground inductors can also be specified here. On the other hand, in the equality constraint vector c_{eq} we impose the required coupling coefficient restriction, in order to assure technological feasibility.

Finally, the lower and upper bounds are used to reduce the space of solutions. They are set depending on the sign of the coupling matrix parameters. For example, it has been shown in Chapter 2 that the NRN B_i and the FIR b_i of the ith resonator positioned in series have to be always negative. Then, the bounds of this resonator are specified accordingly.

In spite of only the relationships between the problem variables and the design parameters are given in this work, more information about SQP optimization can be found in [89].

General class of Chebyshev filtering functions are rational functions of frequency, and they are uniquely specified by the location of their poles and zeros and an additional scaling constant. The zeros and poles of the transmission function are identical to the zeros of S_{11} and S_{21} parameters, respectively. An arbitrary response represented in a coupling matrix will tend to the desired transfer function by vanishing the S-parameters at the corresponding frequencies. To determine the additional scaling constant, the return loss is evaluated at $\Omega = \pm 1$ to get $|S_{11}(\Omega = \pm 1)| = \varepsilon/\sqrt{1+\varepsilon^2}$. The cost function used for the coupling matrix optimization is therefore defined as [87]

$$\begin{aligned} f = &\sum_{i=1}^{N} |S_{11}(\Omega_{zi})|^2 + \sum_{i=1}^{P} |S_{21}(\Omega_{pi})|^2 \\ &+ \left(|S_{11}(\Omega = -1)| - \frac{\varepsilon}{\sqrt{1+\varepsilon^2}} \right)^2 + \left(|S_{11}(\Omega = 1)| - \frac{\varepsilon}{\sqrt{1+\varepsilon^2}} \right)^2 . \end{aligned} \tag{3.40}$$

Here, Ω_{zi} are the zeros of the filtering function $C_N(\Omega)$, i.e., the reflection zeros or roots of $F(\Omega)$. Meanwhile, Ω_{pi} are the poles of the filtering function, that is, the transmission zeros Ω_k or roots of $P(\Omega)$. Notice that, in (3.40), it is assumed that $C_N(\Omega)$ has N zeros and P poles. For fully canonical filters based in acoustic resonators, P is equal to N. More information about the filtering function can be found in Chapter 2.

3.7.4 Numerical Results

In order to verify the optimization method presented above, the synthesis of a seventh-order Band-25 receiver filter is realized in this section. The band-pass circuit to synthesize is shown in Figure 3.18 (a). Three ground inductors L_{xR2}, L_{xR4}, and L_{xR6} are connected to the shunt resonators and a cross-coupling capacitor C_{xS4} between source and the bottom of resonator 4 is considered. A hypothetical parasitic capacitance $C_{Par} = 0.05$ pF is contemplated between resonators 2 and 6.

The corresponding low-pass nodal diagram is presented in Figure 3.18 (b). The acoustic resonators are modeled by means of dangling resonators and the external elements as NRNs. It is interesting to observe that the shunt resonators are not directly connected to ground because of the ground inductors. Therefore, their low-pass model becomes the same than the series resonators one, a dangling resonator placed between unitary inverters. The nodes B_0 are

Table 3.5: Resonator Parameters of the Synthesized Band-25 RX Cross-Coupled Filter.

Parameters	**Res 1**	**Res 2**	**Res 3**	**Res 4**	**Res 5**	**Res 6**	**Res 7**
f_s (GHz)	1.98	1.91	1.96	1.91	1.96	1.91	1.98
k^2_{eff} (%)	6.58	6.58	6.58	6.58	6.58	6.58	6.58
C_0 (pF)	0.71	4.50	0.71	4.50	0.70	4.50	0.68

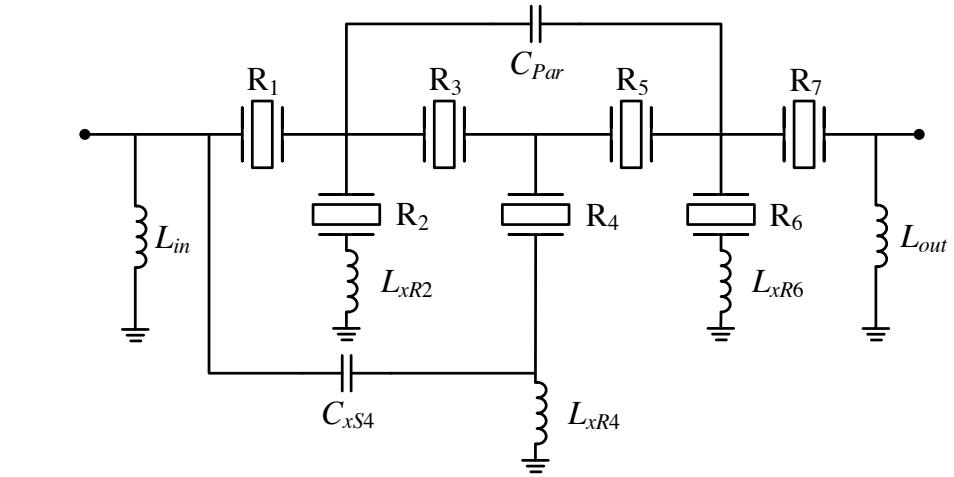

(a)

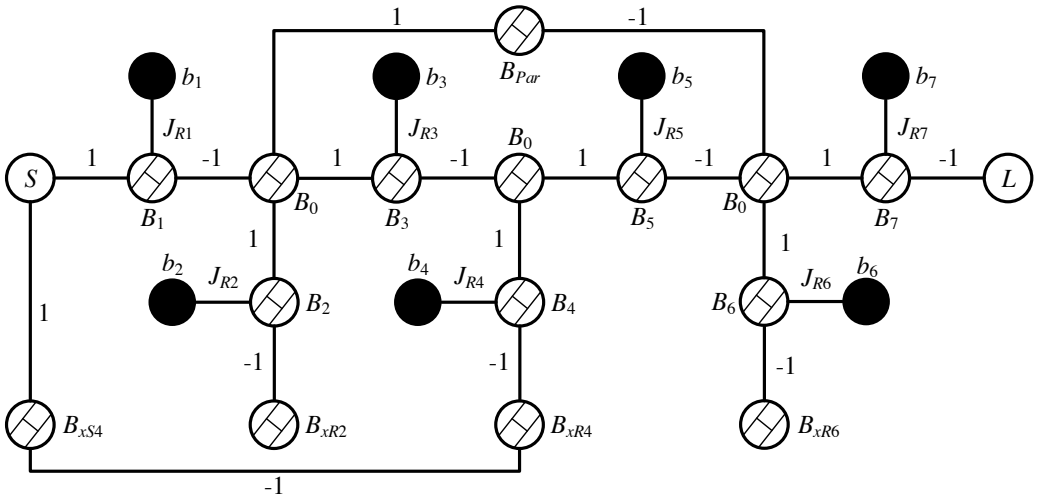

(b)

Figure 3.18: Prescribed topology of the Band-25 RX cross-coupled filter: (a) band-pass circuit and (b) low-pass nodal scheme.

NRNs with zero susceptance, included only as a hypothetical connection between resonators. The number of cross-coupling elements is $X_P = 5$ and the number of NRNs equal to zero is $X_0 = 3$. Therefore, the coupling matrix of the proposed network results in an $N_T \times N_T$ matrix

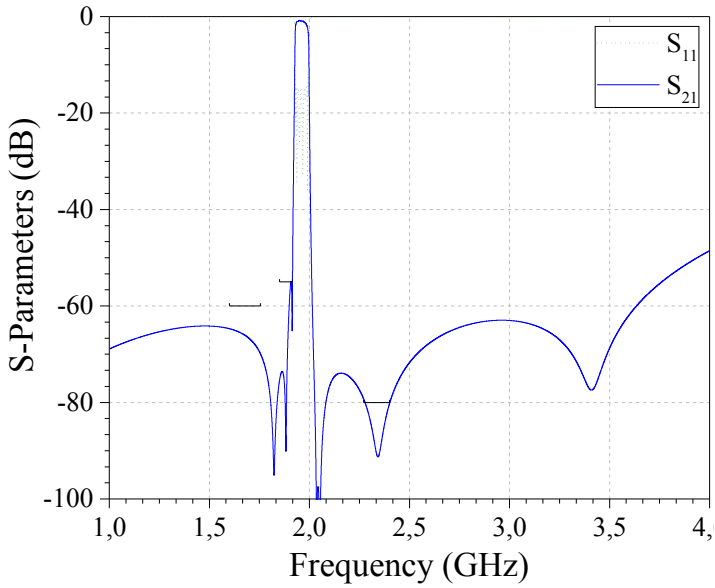

Figure 3.19: Transmission and reflection responses of the Band-25 synthesized filter by coupling matrix optimization. A quality factor of $Q = 1500$ and a electrode resistance of $R_S = 0.1$ have been considered.

where $N_T = 24$.

During the optimization procedure of the coupling matrix, the hypothetical parasitic element B_{Par} is not considered as an optimization variable, whereas the other parameters are. The objective coupling coefficient of all acoustic resonators is expected to be of 6.58 % and only 3 distinct resonant frequencies are allowed. Table 3.5 shows the resonator parameters of the synthesized filter. The external elements are found to be $L_{in} = 4.7$ nH, $L_{out} = 5.27$ nH, $L_{xR2} = 0.41$ nH, $L_{xR4} = 0.28$ nH, $L_{xR6} = 0.41$ nH, and $C_{xS4} = 0.26$ pF.

Figure 3.19 depicts the band-pass response of the synthesized filter. To check the capabilities of this methodology, some stringent attenuation masks have been introduced. It is interesting to observe that the characteristic frequencies, i.e. the transmission zeros and the reflection zeros, tends to an equiripple general class of Chebyshev transfer function, due to the definition of the objective function.

The OoB transmission zeros are introduced by the ground inductors. They allow for good rejection at higher frequencies, although they also generate transmission poles at very high frequencies, between 6 to 10 GHz in this case.

The time cost of the proposed synthesis based in the coupling matrix optimization is of a few minutes. Obviously, it depends on the number of parameters to optimize, the mask specifications, and the technological requirements. The initial guess plays an important role in the process and

has to be properly managed in order to obtain the best solution in the shortest amount of time. From several studies, we have realized that the best starting point is an ideal equiripple Chebyshev filter satisfying the maximum number of technological restrictions. By using the synthesis techniques presented in Chapter 2 a ladder-type filter based in acoustic wave resonators can be simply synthesized. Adding to the ladder structure the desired cross-coupling elements, but with a low coupling strength so the ideal response is not highly damaged, becomes the best starting guess. The cross-coupling elements along with the resonators are then optimized to satisfy the mask specifications while maintaining the technological feasibility.

3.8 Chapter Summary

In this chapter, synthesis techniques for the design of cross-coupled filtering networks based on acoustic resonators have been presented. A methodology based on the parameter extraction of the resonators and the desired cross-inverters is useful to synthesize a limited number of topologies. However, it is an interesting methodology because it relates the cross-couplings with the resonant frequencies of the resonators, which can become complex. When complex singularities arise, further cross-couplings are required to be extracted. Otherwise, the filter characteristics are damaged because the dangling resonator (or acoustic resonator) is unable to implement complex roots.

Studies on the response behavior due to potential parasitic elements, such as the electromagnetic feedthrough between ports, have also been developed in this chapter. During the extraction procedure, the cross-inverter is not present because we desire it, but forced by the physical structure. Then, the resonance frequencies of the resonators are not equal to the transmission zeros as expected. The appropriate procedure of design in those cases has been presented through an example.

Finally, an additional synthesis methodology of cross-coupled topologies by means of the coupling matrix optimization has also been proposed. The coupling matrix arrangement to simplify its management and a cost function based on the characteristic frequencies have been introduced. By means of an example, the advantages of this technique that provides a feasible solution and accept any cross-coupled topology has been successfully shown.

CHAPTER 4

Synthesis of Ladder-Type Acoustic Filters in the Band-Pass Domain

Conventional synthesis techniques usually derives filtering polynomials from the general Chebyshev low-pass filtering function. Coupling matrices or low-pass prototype networks are derived and transformed into the band-pass domain for practical application. Unfortunately, these procedures are based on a narrowband approximation where poles and zeros of the transfer function that are far away from the passband, including those around the negative band, are neglected [46]. Frequency-invariant reactances or frequency-independent coupling coefficients in the low-pass models can only be successfully approximated over a narrow band of frequencies in the microwave region.

In Chapters 2 and 3 these synthesis techniques have been applied for the design of filters based on acoustic resonators. Ladder-type structures and cross-coupled topologies have been successfully synthesized taking into account the technological restrictions. However, for future designs with more and more stringent specifications, the out-of-band (OoB) frequency behavior of all elements in the network may be essential to address the requirements. Furthermore, accuracy on the phase parameters could be determining for the design of the imminent carrier aggregation multiplexer devices.

The aim of this chapter is to introduce fundamental theory on the required band-pass filtering functions for filters based on acoustic resonators. The singularities in the origin and infinite frequencies determines the matching elements of the resulting network, which are carefully analyzed in this chapter. The extraction procedure realized directly in the band-pass domain is also presented, which can be done from the open- and/or short-circuit reactance parameters. Finally, an example of the Band 42 is realized in order to validate the proposed methodology.

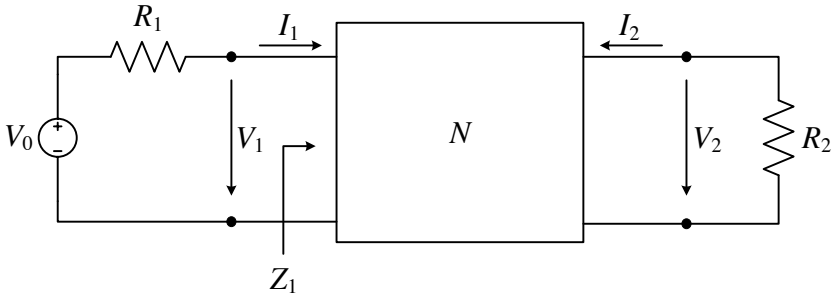

Figure 4.1: A two-port network terminated in R_1 and R_2 at port-1 and port-2, respectively, and its typical operating conditions.

4.1 Double-Terminated Network Analysis

The synthesis of transfer functions in the band-pass domain is the main objective of this chapter. The problem is to find a two-port terminated network such that its transfer function has a desired frequency response. The problem can be approached in two steps. The first is to obtain a rational function of s whose frequency response approximates the desired transfer function. The second step is to synthesize the rational function as the transfer function of a two-port network, and it is the subject of this section. The latter is an equivalence of the Darlington's method, also discussed in [90, 91].

A transfer function describes certain input/output relation, and in circuits, it is usually the ratio of the maximum available power P_{max} from the ideal voltage source to the power delivered to the load P_2. The output port is usually terminated in a load impedance, and the voltage source usually has an internal impedance associated with it. The case of resistive termination at both ports is depicted in Figure 4.1. The transfer function $H(s)$ is defined as [58]

$$|H(s)|^2 = \frac{P_{max}}{P_2} = \left| \frac{1}{2} \sqrt{\frac{R_2}{R_1}} \frac{V_0(s)}{V_2(s)} \right|^2 . \tag{4.1}$$

For passive lossless two-port networks it is usually more convenient to define a characteristic function $K(s)$ given by the Feldtkeller equation as

$$|H(s)|^2 = 1 + |K(s)|^2 \tag{4.2}$$

In order to derive the conditions for a rational function $H(s)$ to be realizable as the transfer function of a two-port network comprising capacitors and inductors, we need to relate the transfer function to some physical properties of the two-port network. To this end, it is most convenient to characterize the network by its scattering matrix.

The transmission coefficient S_{21} represents the ratio of the transmitted wave to the incident

wave, and it is expressed in terms of the two-port voltages as

$$S_{21}(s) = 2\sqrt{\frac{R_1}{R_2}}\frac{V_2(s)}{V_0(s)} = \frac{1}{H(s)}. \tag{4.3}$$

Meanwhile, the reflection coefficient S_{11} is defined as the ratio of the reflected wave to the incident wave. It results in terms of the two-port network voltages as [92]

$$S_{11}(s) = \frac{2V_1(s) - V_0(s)}{V_0(s)}. \tag{4.4}$$

The voltage V_1 may be determined from the source and the divider voltage ratio as

$$V_1(s) = V_0(s)\frac{Z_1(s)}{Z_1(s) + R_1}. \tag{4.5}$$

From (4.4) and (4.5) the reflection coefficient is derived as

$$S_{11}(s) = \frac{Z_1(s) - R_1}{Z_1(s) + R_1}. \tag{4.6}$$

Equation (4.6) establishes a relation between the input impedance and the reflection coefficient of a two-port network. Given $S_{11}(s)$, the input impedance is found to be

$$Z_1(s) = R_1\frac{1 + S_{11}(s)}{1 - S_{11}(s)}. \tag{4.7}$$

This relation will be used during the transfer function synthesis in the following sections.

4.1.1 Two-Port Parameters

There are other characterizations of a two-port network besides scattering matrix. These are strictly circuit parameters derived in terms of voltages and currents at the terminals, and are independent of their terminations.

With reference to Figure 4.1, the terminal voltages V_1 and V_2 are linearly related to the terminal currents I_1 and I_2 through the open-circuit impedance matrix as

$$\begin{bmatrix} V_1 \\ V_2 \end{bmatrix} = \begin{bmatrix} Z_{11}(s) & Z_{12}(s) \\ Z_{21}(s) & Z_{22}(s) \end{bmatrix} \begin{bmatrix} I_1 \\ I_2 \end{bmatrix}. \tag{4.8}$$

The open-circuit impedance coefficients are given by

$$Z_{11}(s) = \left.\frac{V_1}{I_1}\right|_{I_2=0}, \tag{4.9a}$$

$$Z_{12}(s) = \left.\frac{V_1}{I_2}\right|_{I_1=0}, \tag{4.9b}$$

$$Z_{21}(s) = \left.\frac{V_2}{I_1}\right|_{I_2=0}, \tag{4.9c}$$

$$Z_{22}(s) = \left.\frac{V_2}{I_2}\right|_{I_1=0}. \tag{4.9d}$$

Coefficients $Z_{11}(s)$ and $Z_{22}(s)$ are input impedance parameters when the opposite port is open-circuited ($R_i = \infty$). According to Foster's theorem [93], any combination of pure reactances in complex two-port networks can be expressed by a reactance function $Z(s)$ with the following properties: the reactance function must be a rational function of the frequency s with positive real coefficients; $Z(s)$ has poles only on the $j\omega$-axis, and at least either a pole or zero at $s = \infty$ and a pole or zero at $s = 0$; $Z(s)$ is always an odd function and the reactance always increases in value with frequency. By reciprocity it is also derived that $Z_{12}(s) = Z_{21}(s)$.

A different representation of network values can be given by the chain matrix as

$$\begin{bmatrix} V_1 \\ I_1 \end{bmatrix} = \begin{bmatrix} A(s) & B(s) \\ C(s) & D(s) \end{bmatrix} \begin{bmatrix} V_2 \\ I_2 \end{bmatrix}, \tag{4.10}$$

where the chain matrix is related with the open-circuit impedance matrix as

$$\begin{bmatrix} A(s) & B(s) \\ C(s) & D(s) \end{bmatrix} = \frac{1}{Z_{12}(s)} \begin{bmatrix} Z_{11}(s) & Z_{11}(s)Z_{22}(s) - Z_{12}^2(s) \\ 1 & Z_{22}(s) \end{bmatrix}. \tag{4.11}$$

Since impedance coefficients $Z_{11}(s)$, $Z_{22}(s)$, and $Z_{12}(s)$ are odd polynomials for a network made of reactive elements, $A(s)$ and $D(s)$ are always even, while $B(s)$ and $C(s)$ are always odd, rational functions [94].

From (4.10), the following equations can be derived:

$$V_1 = V_2 A(s) + I_2 B(s), \tag{4.12a}$$

$$I_1 = V_2 C(s) + I_2 D(s). \tag{4.12b}$$

The input impedance $Z_1(s)$ can be expressed from the chain equation (4.12) by

$$Z_1(s) = \frac{V_1}{I_1} = \frac{A(s) + B(s)/R_2}{C(s) + D(s)/R_2}. \tag{4.13}$$

For further discussion it is advantageous to introduce normalized impedances related to R_1 by

$$z_{ik} = \frac{Z_{ik}}{R_1}, \tag{4.14}$$

and the following chain coefficients relations:

$$\begin{aligned} a &= A\sqrt{\frac{R_2}{R_1}} \qquad b = \frac{B}{\sqrt{R_1 R_2}} \\ c &= C\sqrt{R_1 R_2} \qquad d = D\sqrt{\frac{R_1}{R_2}} \end{aligned} \tag{4.15}$$

The transfer function and the characteristic function can be written in terms of the chain matrix coefficients as follows [92]:

$$H(s) = \frac{a(s) + b(s) + c(s) + d(s)}{2}, \tag{4.16}$$

and

$$K(s) = \frac{a(s) + b(s) - c(s) - d(s)}{2}. \tag{4.17}$$

4.1.2 Polynomial Definition of Transmission and Filtering Functions

The transmission and the characteristic functions are rational functions that can be expressed in terms of polynomials $P(s)$, $F(s)$, and $E(s)$ by

$$H(s) = \frac{E(s)}{P(s)}, \tag{4.18}$$

and

$$K(s) = \frac{F(s)}{P(s)}. \tag{4.19}$$

In order that the functions correspond to a realizable, reactive network, polynomials $P(s)$, $F(s)$, and $E(s)$ have to meet the following conditions:

1. $P(s)$, $F(s)$, and $E(s)$ must be real, rational functions of s.
2. $E(s)$ must be a Hurwitz polynomial whose singularities should necessarily lie in the left s half-plane.
3. $P(s)$ should be an even or odd polynomial whose degree is lower or at most equal to that of $E(s)$.
4. The condition $|H(s)| \geq 1$ must be satisfied. Its physical meaning is that the power at the output end P_2, in case of passive networks, cannot be greater than the maximum deliverable power P_{max} of the source.

Since the polynomials $E(s)$ and $F(s)$ are rational functions, they can be subdivided into even and odd parts. Equations (4.18) and (4.19) can be written in the following form:

$$H(s) = \frac{E_e(s) + E_o(s)}{P(s)}, \tag{4.20}$$

and

$$K(s) = \frac{F_e(s) + F_o(s)}{P(s)}. \tag{4.21}$$

With the aid of the previous equations and equations (4.16) and (4.17), the polynomials $E(s)$ and $F(s)$ become

$$E(s) = E_e(s) + E_o(s) = \frac{P(s)\,(a(s) + b(s) + c(s) + d(s))}{2}, \tag{4.22}$$

and

$$F(s) = F_e(s) + F_o(s) = \frac{P(s)\,(a(s) + b(s) - c(s) - d(s))}{2}. \tag{4.23}$$

It has been seen from (4.11) that coefficients $a(s)$ and $d(s)$ are even, while $b(s)$ and $c(s)$ are odd. Therefore, two cases can be considered according to $P(s)$ is an even or an odd polynomial.

1. If $P(s)$ is an even function:

$$E_e(s) = \frac{P(s)\,(a(s) + d(s))}{2}, \tag{4.24a}$$

$$E_o(s) = \frac{P(s)\,(b(s) + c(s))}{2}, \tag{4.24b}$$

$$F_e(s) = \frac{P(s)\,(a(s) - d(s))}{2}, \tag{4.24c}$$

$$F_o(s) = \frac{P(s)\,(b(s) - c(s))}{2}. \tag{4.24d}$$

The chain matrix is therefore given by

$$\begin{bmatrix} a(s) & b(s) \\ c(s) & d(s) \end{bmatrix} = \frac{1}{P(s)} \begin{bmatrix} E_e(s) + F_e(s) & E_o(s) + F_o(s) \\ E_o(s) - F_o(s) & E_e(s) - F_e(s) \end{bmatrix}. \tag{4.25}$$

2. If $P(s)$ is an odd function:

$$E_e(s) = \frac{P(s)\,(b(s) + c(s))}{2}, \tag{4.26a}$$

$$E_o(s) = \frac{P(s)\,(a(s) + d(s))}{2}, \tag{4.26b}$$

$$F_e(s) = \frac{P(s)\,(b(s) - c(s))}{2}, \tag{4.26c}$$

$$F_o(s) = \frac{P(s)\,(a(s) - d(s))}{2}. \tag{4.26d}$$

The chain matrix is therefore given by

$$\begin{bmatrix} a(s) & b(s) \\ c(s) & d(s) \end{bmatrix} = \frac{1}{P(s)} \begin{bmatrix} E_o(s) + F_o(s) & E_e(s) + F_e(s) \\ E_e(s) - F_e(s) & E_o(s) - F_o(s) \end{bmatrix}. \tag{4.27}$$

The open-circuit impedance coefficients can be calculated as functions of the frequency parameters from the transmission function $H(s)$ and the characteristic function $K(s)$ using (4.11) as given in Table 4.1. The network can be fully determined by these reactances together with the complete set of zeros of $P(s)$. The circuit parameters can be calculated by partial or full removal at these poles.

It is interesting to observe that the reactance parameters in Table 4.1 describe a circuit that we named Z-equivalent network. The reason is that the network to be realized is best described by the open-circuit impedance parameters because the first and last circuital elements are positioned in series. However, it could be possible to realize the dual network, in which the first and last elements are in shunt and the network is best described by the admittance parameters. Furthermore, a combination of both realizations is also possible, in which the first element is in series and the last one in shunt, or vice versa. In Appendix A all open- and short-circuit reactance parameters are derived from the transmission and characteristic functions $H(s)$ and $K(s)$, respectively, and polynomials $P(s)$, $F(s)$, and $E(s)$.

Table 4.1: Network Open-Circuit Impedance Parameters as Functions of Polynomials $P(s)$, $F(s)$, and $E(s)$.

Coefficient	$P(s)$ is even	$P(s)$ is odd
$z_{11}(s)$	$\frac{E_e(s)+F_e(s)}{E_o(s)-F_o(s)}$	$\frac{E_o(s)+F_o(s)}{E_e(s)-F_e(s)}$
$z_{22}(s)$	$\frac{E_e(s)-F_e(s)}{E_o(s)-F_o(s)}$	$\frac{E_o(s)-F_o(s)}{E_e(s)-F_e(s)}$
$z_{12}(s)$	$\frac{P(s)}{E_o(s)-F_o(s)}$	$\frac{P(s)}{E_e(s)-F_e(s)}$

4.1.3 Realization of the Filter Network

The low-pass nodal network of a ladder-type filter based on acoustic resonators has been presented in Chapter 2. If the resonator is represented by the dangling resonator model, which is mainly composed of a resonant node coupled to a NRN, the network simply becomes a cascading of several dangling resonators.

In the band-pass domain, the nodal diagram shape can remain the same, as depicted in Figure 4.2. However, the frequency invariant elements are replaced by either inductors or capacitors. The NRN are replaced by reactive nodes [95], increasing the accuracy of the practical realization. Admittance inverters are considered as ideal components because their role in ladder-type filter based on acoustic resonators is to serialize a shunt resonator and, therefore, no admittance inverters are physically implemented. Source and load nodes are reactive nodes that can be either inductive or capacitive. Their nature is given by the transfer function to implement and its poles and zeros at the origin and infinite frequencies.

Figure 4.3 shows the circuital equivalence between the nodal diagram and the BVD model for both a shunt and a series resonator. It is interesting to observe that, where in the low-pass domain there was a NRN, in the band-pass domain there is a capacitive reactive node for a shunt resonator and an inductive reactive node for a series resonator. This, in turn, is a constrain on the topology for a realizable network.

Furthermore, they are essential during the extraction procedure for the preparation of the following finite transmission zeros removal. This consist in enforcing the remaining admittance $Y_{i+1}(\omega)$ after the extraction of the reactive node B_i to be zero at $\omega = \pm j\omega_{i+1}$, which can be achieved by shunt inductors or capacitors. Those reactive nodes also imply the existence of transmission zeros at infinity and the origin, which have to be considered during the determination of the characteristic function.

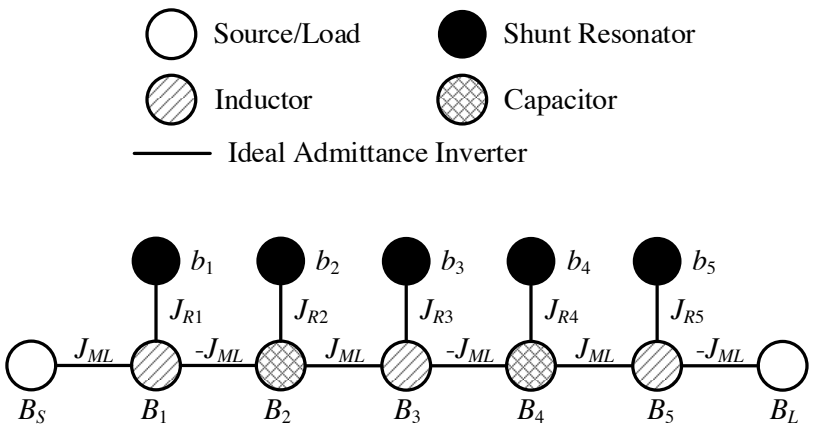

Figure 4.2: Inline filter of order $N = 5$ with reactive nodes. All components are shunt connected.

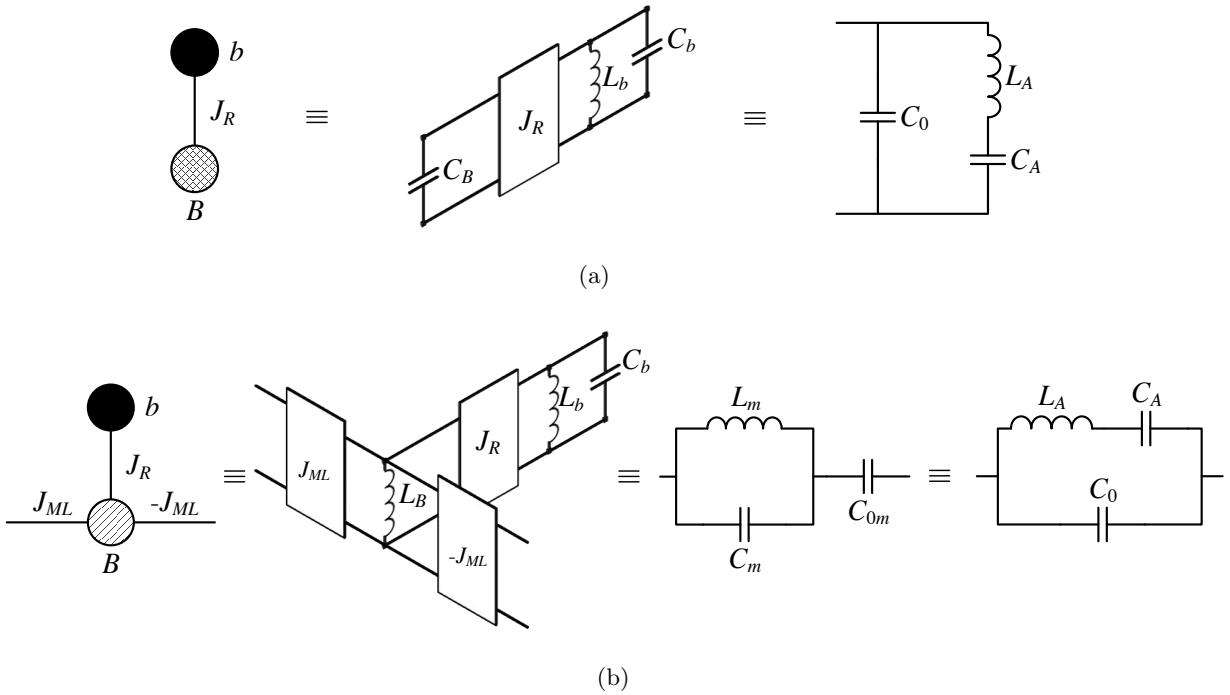

Figure 4.3: Band-pass equivalent circuit of an acoustic resonator positioned in (a) shunt and (b) series.

By means of the input admittance parameters, a set of extraction iterations is performed to obtain the nodal elements. The extraction strategies for different types of nodes are summarized next. The procedure will focus on shunt connected elements, though similar considerations apply to series connections. Furthermore, the following nodal theory is completely equivalent with the circuital extraction of traditional techniques [96].

Capacitive Reactive Node

A shunt capacitor introduces a transmission zero at $\omega = \infty$. Therefore, the extraction of the reactive node of Figure 4.4 (a) is carried out by evaluating the admittance parameter at infinity as follows:

$$B_C = \left.\frac{y_{in}(s)}{s}\right|_{s=\infty}, \qquad y\prime(s) = y_{in}(s) - sB_C. \tag{4.28}$$

Inductive Reactive Node

A shunt inductor introduces a transmission zero at the origin ($\omega = 0$). Thus, the extraction of the reactive node depicted in Figure 4.4 (b) is completed by

$$B_L = \left.\frac{1}{s \cdot y_{in}(s)}\right|_{s=0}, \qquad y\prime(s) = y_{in}(s) - \frac{1}{sB_L}. \tag{4.29}$$

Shunt Acoustic Dangling Resonator

Previous to the extraction of a dangling resonator connected to a capacitive node, an inductive reactive node had to be extracted in order to prepare the ith transmission zero ω_i annihilation. If it has been extracted correctly, the admittance $y_{in}(s)$ in Figure 4.4 (c) should have a zero at $\pm j\omega_i$. If the resonant node b_i is made of a shunt resonator with an inductor L_b and a capacitor C_b, as shown in Figure 4.3 (a), and it is considered that $J_{Ri} = 1$, it is obtained that

$$C_b = \left.\frac{s}{y_{in}(s)\left(s^2 + \omega_i^2\right)}\right|_{s=j\omega_i}, \qquad y_1(s) = y_{in}(s) - \frac{s/C_b}{s^2 + \omega_i^2}, \tag{4.30}$$

and

$$L_b = \frac{1}{\omega_i^2 C_b}. \tag{4.31}$$

Next, the capacitive reactive node B_i prepares the extraction of the following TZ ω_{i+1}. It is accomplished as

$$B_i = \left.\frac{y_1(s)}{s}\right|_{s=j\omega_{i+1}}, \qquad y\prime(s) = y_1(s) - sB_i. \tag{4.32}$$

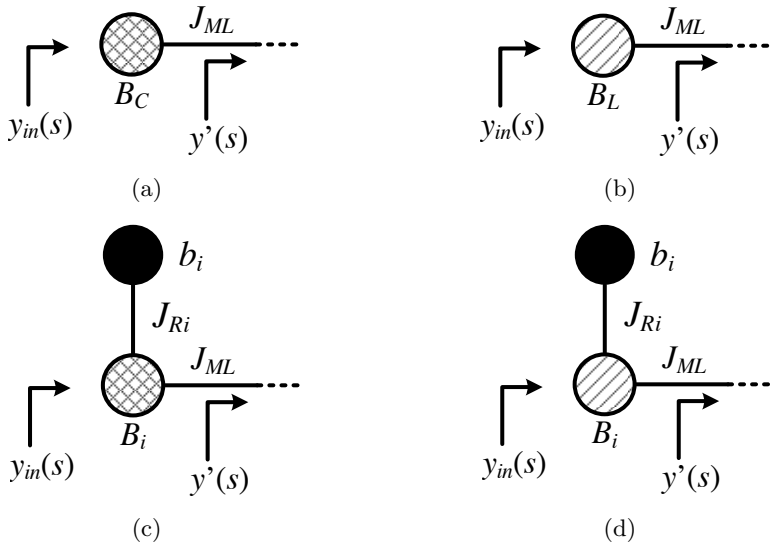

Figure 4.4: Some basic blocks to be extracted during the band-pass synthesis: (a) shunt capacitor, (b) shunt inductor, (c) shunt acoustic dangling resonator, and (d) series acoustic dangling resonator.

Series Acoustic Dangling Resonator

Finally, previous to the extraction of a dangling resonator connected to an inductive node, a capacitive reactive node had to be extracted. Therefore, the extraction of the transmission zero ω_i has been already prepared and the admittance $y_{in}(s)$ in Figure 4.4 (d) have a zero at $\pm j\omega_i$. Same than before, if the resonator is made of an inductor L_b and a capacitor C_b, and it is considered that $J_{Ri} = 1$, the resonant node parameters are extracted using (4.30) and (4.31).

However, the reactive node B_i, which is inductive in this case, is obtained by evaluating the admittance at the next TZ as follows:

$$B_i = \left.\frac{1}{s \cdot y_1(s)}\right|_{s=j\omega_{i+1}}, \qquad y\prime(s) = y_1(s) - \frac{1}{sB_i}. \tag{4.33}$$

4.1.4 Synthesis Rules

In this section, several rules for the practical realization of the filter are discussed. The number of TZs and their location constrain the topology and the type of reactive nodes, specially those that are not part of a dangling resonator, i.e., source and load nodes in ladder-type networks based on acoustic resonators (see Figure 4.2).

Two different interpretations for the same problem can be derived: for a given characteristic polynomials, the proper realization of the network able to accommodate them, and, on the other

hand, if the topology is fixed, the knowledge of the characteristic frequencies in order to derive correctly the transfer function. Nevertheless, the designer must understand the location of the transmission zeros and their multiplicity in a given structure. To this end, the following rules should be considered [97]:

- Regarding reactive nodes (TZs at the origin or infinity):
  - After a partial extraction in $s_i = j\omega_i$, where ω_i is either zero or infinity, another extraction in s_i can only occur within an even number of inverters.
  - After a complete extraction in $s_i = j\omega_i$, where ω_i is either zero or infinity, another extraction in s_i can only occur within an odd number of inverters.
- Regarding dangling resonators (TZs at finite frequencies):
  - To prepare the extraction of a TZ $s_i = \pm j\omega_i$ above the passband, a partial extraction of a TZ at infinity is previously required via a capacitive reactive node.
  - To prepare the extraction of a TZ $s_i = \pm j\omega_i$ below the passband, a partial extraction of a TZ in the origin is previously required via an inductive reactive node.

From these rules, it can be stated that the number of TZs in the origin (or at infinity) of a ladder-type network is equal to the number of shunt inductors (or capacitors) separated from the previous one by an odd number of inverters. Those connected within an even number of inverters actually operate on the same TZ, thus not increasing its multiplicity. Further constraints can also be derived from these rules: if there is at least one TZ above the passband, then there must be at least one TZ at infinity, and if there is at least one TZ below the passband, then there must be at least one TZ in the origin.

Concerning ladder-type filters based on acoustic resonators, all reactive nodes that are part of a dangling resonator are partial extraction of TZs in the origin or at infinity, that prepare the extraction of the following finite TZ. Therefore, the reactive node of a series acoustic resonator is a shunt inductor, in order to prepare the TZ below the passband introduced by the following shunt resonator. Similarly, the reactive node of a shunt acoustic resonator is a shunt capacitor, to prepare in this case the TZ above the passband introduced by the following series resonator.

Following these rules, source (and load) must be a reactive node that prepare the annihilation of the first (and the last) TZ. If we consider a typical odd order filter starting in series resonator, source and load nodes are supposed to be shunt capacitors, as depicted in Figure 4.5 (a). Those will be partial extractions of a TZ at infinity. It can be observed that this network introduces one TZ in the origin and one TZ at infinity, both of them implemented by shunt inductors and shunt capacitors, respectively, connected within an even number of inverters.

Meanwhile, it is known that acoustic ladder-type filters can be realized with a matching

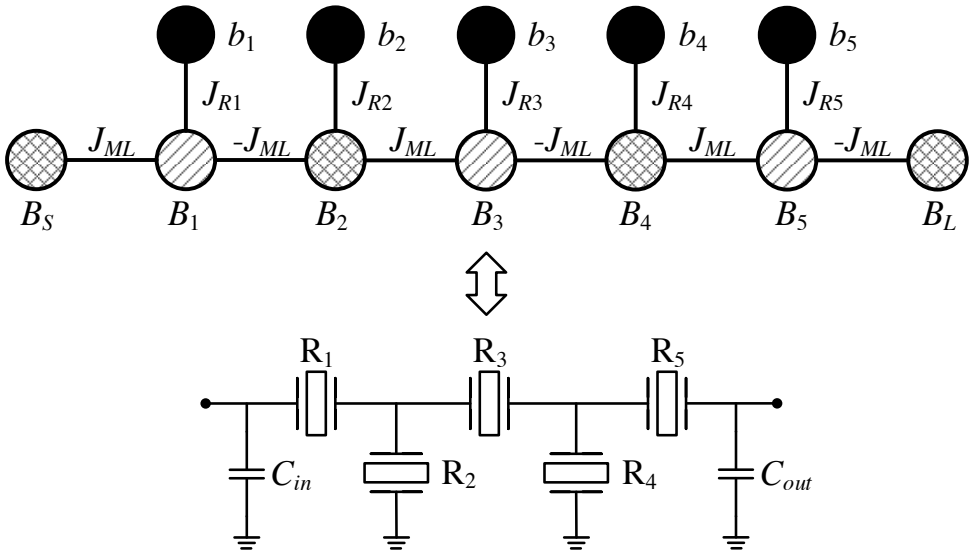

(a)

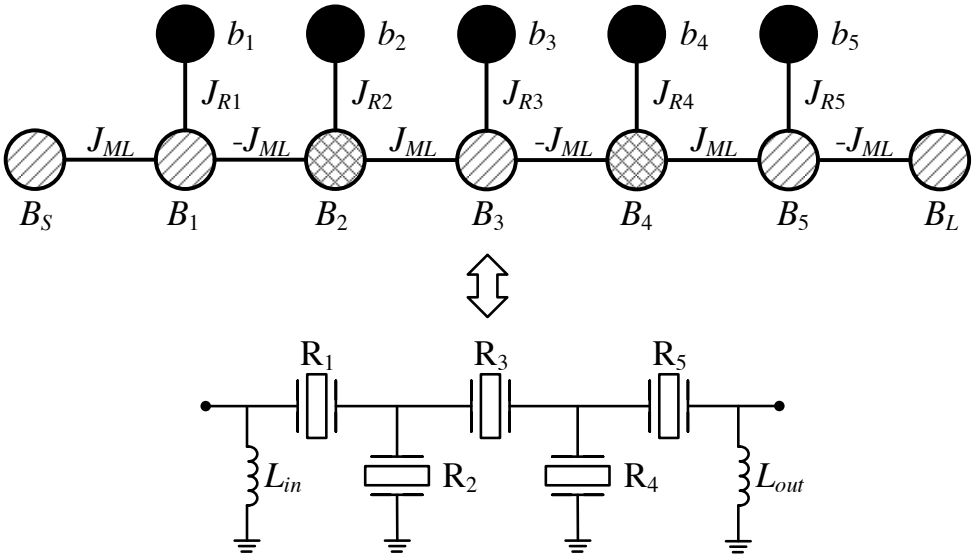

(b)

Figure 4.5: Ladder-type network with different source and load reactive nodes: (a) capacitive and (b) inductive natures.

inductor at both ports, even if the first and last resonators are in series, therefore introducing TZs above the passband. That type of topology, depicted in Figure 4.5 (b), has some special requirements that must be considered in order to be a realizable network. Following the rules mentioned above, the input and output inductor B_S and B_L, respectively, must be completed extractions of TZs in the origin, because there are other extractions in the origin by the nodes B_1 and B_5 within an odd number of inverters. Therefore, that network introduces three TZs in the origin (two implemented by the input and output inductors, and the other one partially implemented by the nodes B_1, B_3, and B_5, connected within an even number of inverters), and one TZ at infinity, generated by nodes B_2 and B_4.

In [98] there are derived the conditions for situations in which an inductor extracts a TZ above the passband, which is actually possible although not usual. These should also be satisfied for topologies such that represented in Figure 4.5 (b).

4.2 Determination of the Characteristic Function $K(s)$

In Chapter 2 a characteristic function $C_N(\Omega)$ has been derived for the synthesis of low-pass filters. It has been used for the synthesis of ladder-type filters based on acoustic resonators, where each resonator introduces a TZ resulting in a fully-canonical network. Therefore, the characteristic function has been determined from the low-pass finite TZs. After a frequency transformation, a band-pass network based on BVD resonators is obtained. The equivalence between the low-pass and the band-pass responses is only valid for frequencies near the passband, because the frequency transformation is a narrowband approximation. The out of band characteristics, i.e. additional TZs due to ground inductors, TZs at origin and infinite frequencies, etc., are not considered during the low-pass synthesis, and they are noticeable only after the band-pass transformation.

To determine the new characteristic function $K(s)$ we are going to analyze the characteristics of a band-pass ladder-type filter made of BVD resonators. Figure 4.6 shows the transmission and reflection parameters of a 7th degree filter based on acoustic resonators. By simple inspection of the figures, the requirements that the characteristic function has to meet are:

- A dual-passband response at $B = [\omega_1, \omega_2]$ and $-B = [-\omega_2, -\omega_1]$ directly achieved with mirror to the origin.
- For an Nth-order filter, it is capable of having N finite transmission zeros with reference to one passband.
- For an Nth-order filter, the reflection parameters have N reflection zeros with reference to one passband.
- At least one TZ is at the origin ($\omega = 0$) and one at infinity ($\omega = \infty$), and, what is most

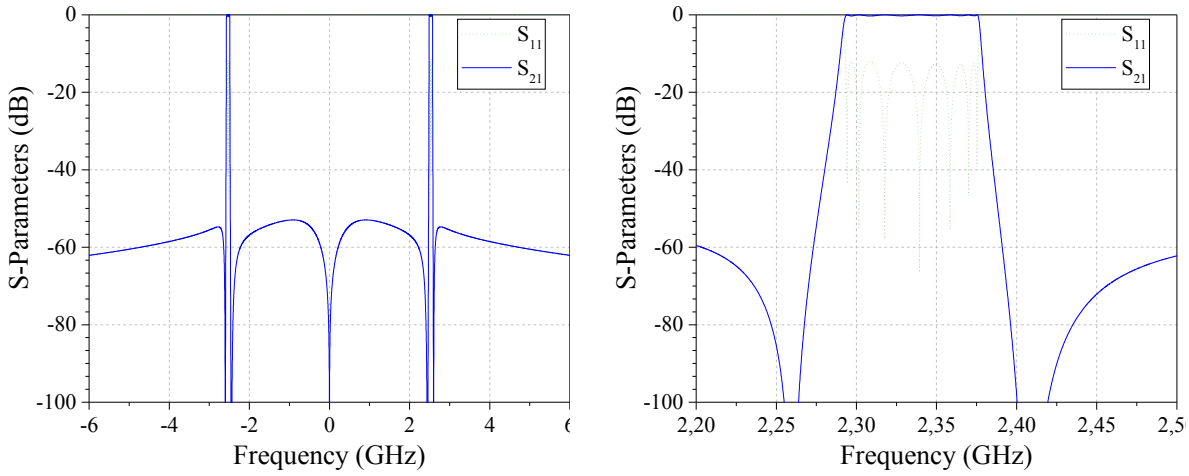

(a) (b)

Figure 4.6: Filter characteristics of a ladder-type filter based on acoustic resonators: (a) out of band and (b) passband representation.

important, they do not introduce additional reflection zeros inside the passband.

The construction of the filtering function to meet these specifications builds on the classical approach, which is summarized next.

4.2.1 Classical General Chebyshev Low-Pass Filtering Function

One of the most widely used filtering function for an Nth-order general Chebyshev low-pass prototype is [58]

$$C_N(\Omega) = \cosh\left[\sum_{n=1}^{N} \cosh^{-1}\left(x_n\left(\Omega\right)\right)\right], \tag{4.34}$$

where

$$x_n(\Omega) = \frac{\Omega - 1/\Omega_n}{1 - \Omega/\Omega_n}. \tag{4.35}$$

In (4.35), Ω_n stands for a normalized location of a transmission zero in the complex plane, including infinity, and Ω is the low-pass frequency variable. The properties of $x_n(\Omega)$ to describe a Chebyshev characteristic are:

- $x_n(\Omega_n) = \pm\infty$, where Ω_n is a TZ.
- $x_n(\Omega = \pm 1) = \pm 1$.
- Between $\Omega = -1$ and $\Omega = 1$, $1 \geq x_n(\Omega) \geq -1$.

It is interesting to observe that $x_n(\Omega)$ is a function capable of introducing one reflection zero in the passband as well as one TZ in the rejection band.

4.2.2 Band-Pass Filtering Function for Filters Based on Acoustic Resonators

In view of the requirements that the new band-pass filtering function has to meet, the low-pass general class of Chebyshev filtering function summarized above is modified accordingly. The definition of the filtering function becomes [99]:

$$K(\omega) = \cosh\left[\cosh^{-1}\left(T_0\left(\omega\right)\right) + \sum_{n=1}^{N} \cosh^{-1}\left(X_n\left(\omega\right)\right)\right]. \tag{4.36}$$

The function $X_n(\omega)$ should meet the following requirements:

- At $\omega = \omega_n$, where ω_n is a finite-position TZ at both positive and negative frequencies, $X_n(\omega) = \pm\infty$.
- At the passband edges of both positive and negative bands, $X_n(\pm\omega_1) = -X_n(\pm\omega_2) = -1$.
- Between $\omega = \pm\omega_1$ and $\omega = \pm\omega_2$ (both positive and negative passband frequency range), $1 \geq X_n(\omega) \geq -1$.

In view of these specifications, the following $X_n(\omega)$ is derived:

$$X_n(\omega) = \frac{T_1(\omega) - 1/T_1(\omega_n)}{1 - T_1(\omega)/T_1(\omega_n)}, \tag{4.37}$$

where $T_1(\omega)$ is found to be

$$T_1(\omega) = \frac{2\omega^2 - \left(\omega_1^2 + \omega_2^2\right)}{\omega_2^2 - \omega_1^2}. \tag{4.38}$$

This definition of band-pass filtering function is in agreement with that derived in [99] for the synthesis of filters with arbitrary bandwidth. The function $X_n(\omega)$ is the band-pass equivalent function of the low-pass $x_n(\Omega)$ and introduce a reflection zero and a TZ at a finite frequency in reference to one passband.

Additionally, the term $T_0(\omega)$ in (4.36) should introduce a TZ at dc ($\omega = 0$), but no reflection zero in any of the two passbands. In [100], a filtering function able to accommodate a source-load coupling is derived, with a term that introduces a TZ in the origin and no resonance in the passband. To determine $T_0(\omega)$ the following requirements have to be satisfied:

- $T_0(\omega = 0) = \pm\infty$ to introduce a TZ in the origin.
- At the passband edges of both positive and negative bands, $T_0(\pm\omega_1) = T_0(\pm\omega_2) = \pm 1$.

By further development of these requirements, $T_0(\omega)$ is found to be

$$T_0(\omega) = \frac{T_2(\omega)}{\omega}, \qquad T_2(\omega) = \frac{\omega^2 + \omega_1\omega_2}{\omega_1 + \omega_2}. \tag{4.39}$$

Different from the frequency function of $T_2(\omega)/\omega$ in [99], the term $T_0(\omega)$ in (4.39) introduces no resonances in the passband, but it forms a TZ at zero frequency. This is a required specification in order to realize ladder-type filters based on acoustic resonators, as discussed above. However, according to our experience, all of the realized networks encountered after several examples present an attenuation pole above the passband, between a finite TZ and infinity, resulting in a poor OoB attenuation at high frequencies.

We propose in this work two different solutions to best accommodate the characteristics of a ladder-type filter based on acoustic resonators depending on the number of TZs in the origin: one if there is only 1 TZ, thus resulting in a capacitive matching network, and another for 3 TZs placed in the origin, resulting then in an inductive matching network (see Section 4.1.4).

Case 1. Capacitive Matching

The proposed term $T_0(\omega)$ if there is only one TZ in the origin has been encountered by mixing the conditions derived in [99] and [100], so it introduces a TZ in the origin, no resonance in the passband, and no attenuation pole above the passband. It has been derived as

$$T_0(\omega) = \frac{T_2(\omega)}{\omega}, \qquad T_2(\omega) = \frac{\omega^2 + \omega_1\omega_2}{\omega_2 - \omega_1}. \tag{4.40}$$

Figure 4.7 shows a comparison between the terms $T_0(\omega)$ derived by Amari in [99], by Zhang in [100], and the proposed one in this work. The one derived by Amari crosses zero at a frequency inside the passband, thus introducing a resonance, i.e., a reflection zero. However, the function increases fast to infinity at high frequencies, improving the OoB attenuation. The term derived by Zhang does not cross zero inside the passband, but the slope of the curve at high frequencies is relatively flat. The proposed term, as can be observed, does not cross zero, thus introducing no resonance in the passband, and it presents a step slope at high frequencies, approximating to the function derived by Amari as the frequency increases. Thus, the proposed function is the best suited one for the design of ladder-type filters based on acoustic resonators.

The fact that the term $T_0(\omega)$ in (4.40) introduces only one TZ in the origin is a limitation on the network realization, because this TZ has to be partially extracted during the parameter extraction procedure. Some networks may require complete extractions of TZs at the origin, as discussed in Section 4.1.4. This case, which is valid for network with inductive matching elements, is detailed next.

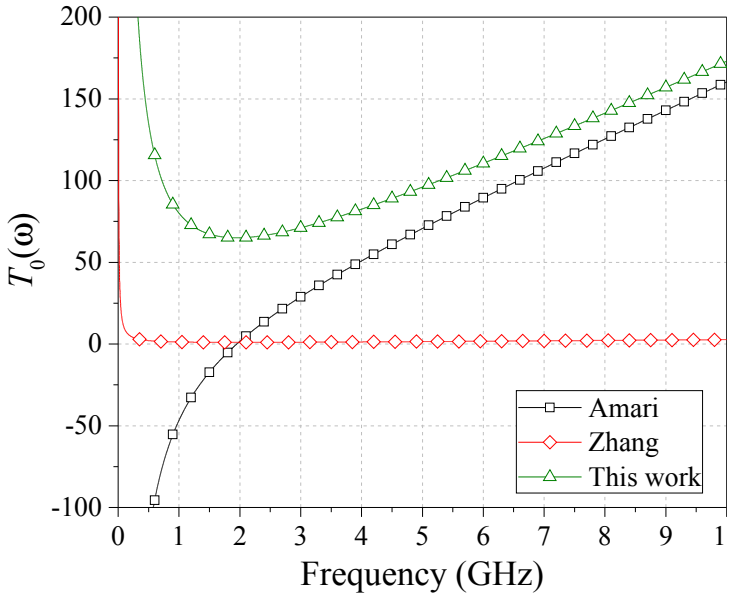

Figure 4.7: Comparison of the terms $T_0(\omega)$ derived by Amari, Zhang, and the one proposed in this work for a ladder-type filter based on acoustic resonators. The passband edges used in this example have been defined at $f_1 = 1.92$ GHz and $f_2 = 1.98$ GHz.

Case 2. Inductive Matching

The proposed filtering function with three TZs in the origin, one TZ at infinity, and N finite TZs with reference to one passband has been found to be

$$K(\omega) = \cosh\left[\cosh^{-1}\left(T_0\left(\omega\right)\right) + \cosh^{-1}\left(T_0'\left(\omega\right)\right) + \sum_{n=1}^{N}\cosh^{-1}\left(X_n\left(\omega\right)\right)\right], \tag{4.41}$$

where $X_n(\omega)$ is given by (4.37).

The term $T_0(\omega)$ can be either the one in (4.39) or the one in (4.40). Differences in the out of band frequencies are found depending on the chosen $T_0(\omega)$. These difference are translated in differences in the network realization. By using the $T_0(\omega)$ derived in this work, the attenuation at high frequencies becomes much better than using the term proposed by Zhang. However, it may be necessary to extract an additional capacitor at source and load nodes to accommodate the following TZs during the extraction. Then, an inductor and a capacitor will be necessary at both ports to properly fit the transfer function. On the other hand, by using the term $T_0(\omega)$ proposed by Zhang, the network may be realized with only an inductor as a matching element.

Finally, the new term $T_0'(\omega)$ is derived according to $T_0'(\omega^2 = 0) = \pm\infty$, so two TZs lie in the origin. Therefore, $T_0'(\omega)$ is found to be

$$T_0'(\omega) = \frac{T_2'(\omega)}{\omega^2}, \qquad T_2'(\omega) = \frac{-\omega^3 - \omega_1\omega_2\omega}{\omega_2 - \omega_1}. \tag{4.42}$$

The term $T_0'(\omega)$ introduces now two additional TZs in the origin, which should be completely removed by the input and output inductors. After that, it might be necessary to extract a shunt capacitance in order to prepare the following extraction of a TZ above the passband, unless an inverse (or dual) extraction becomes possible [98].

The filtering functions derived in this section are ready to accommodate band-pass ladder-type filters based on acoustic resonators, either if the matching elements are capacitors or inductors. Different definitions of the characteristic frequencies yielding distinct filtering functions may result in other filter topologies. Furthermore, TZs introduced by ground inductors or additional cross-couplings should be considered during the definition of the filtering function in order to obtain a realizable network. In other words, the transfer function has to contemplate every characteristic frequency present in the network to realize. This might be a complex task as the number of elements and cross-couplings increase, making difficult to derive a general technique for the calculation of the band-pass transfer and characteristic functions.

4.2.3 Determination of the Characteristic Polynomials $P(\omega)$, $F(\omega)$, and $E(\omega)$

In this section the characteristic polynomials $P(\omega)$ and $F(\omega)$ are determined from the filtering function, whereas the polynomial $E(\omega)$ is derived from the conservation of energy equation once the other two polynomials are known. Two different cases are detailed for the two filtering functions derived above: the first with one TZ in the origin and another at infinity, and the second with three TZs in the origin and one TZ at infinity. The recursive method derived to find $F(\omega)$ adopts the strategy used in [58] for the synthesis of low-pass prototypes.

To determine the characteristic polynomials, the band-pass filtering function is written in a rational form as the ratio of two polynomials:

$$K(\omega) = \frac{F(\omega)}{P(\omega)}, \tag{4.43}$$

where the roots of $F(\omega)$ are the reflection zeros and the roots of $P(\omega)$ are the transmission zeros.

The following derivation of the polynomials take under consideration an odd order filter starting in a series resonator. Two different networks can be obtained depending on the nature of the input/output matching elements.

Capacitive Matching Elements

Further analysis of the characteristic function $K(\omega)$ using (4.36), (4.37), and (4.40) yields

$$K(\omega) = \frac{1}{2}\frac{(c_0 + d_0)\prod_{n=1}^{N}(c_n + d_n) + (c_0 - d_0)\prod_{n=1}^{N}(c_n - d_n)}{\omega\prod_{n=1}^{N}(1 - s_n T_1(\omega))} \tag{4.44}$$

where

$$c_0 = T_2(\omega), \tag{4.45a}$$

$$d_0 = \sqrt{T_2^2(\omega) - \omega^2}, \tag{4.45b}$$

$$c_n = s_n T_1(\omega), \tag{4.45c}$$

$$d_n = \sqrt{1 - s_n^2}\sqrt{T_1^2(\omega) - 1}, \tag{4.45d}$$

$$s_n = 1/T_1(\omega_n). \tag{4.45e}$$

It can be observed by simple analysis of equation (4.44) that the roots of the denominator correspond to the overall set of transmission zeros, including those in the negative frequencies and that in the origin. Therefore, polynomial $P(\omega)$ can be determined by

$$P(\omega) = \omega \prod_{n=1}^{N} \left(1 - T_1(\omega)/T_1(\omega_n)\right), \tag{4.46}$$

where ω_n are the finite transmission zeros in respect to one passband, and N the filter degree.

To derive the coefficients of $F(\omega)$, a recursive technique where the solution for the nth degree polynomial is built up from the results of the $(n-1)$th one is developed. To this end, the new polynomials $U(\omega)$ and $V(\omega)$ used during the iterative procedure are defined as

$$U_N(\omega) = u_{2N}\omega^{2N} + u_{2N-1}\omega^{2N-1} + \ldots + u_1\omega + u_0, \tag{4.47a}$$

$$V_N(\omega) = \omega' \left(v_{2N}\omega^{2N} + v_{2N-1}\omega^{2N-1} + \ldots + v_1\omega + v_0\right), \tag{4.47b}$$

where the transformed variable ω' is defined as

$$\omega' = \sqrt{T_1^2(\omega) - 1}. \tag{4.48}$$

Polynomials $U_0(\omega)$ and $V_0(\omega)$ at first iteration of the process are derived from the term introducing the TZ in the origin as

$$U_0(\omega) = c_0 = T_2(\omega) = \frac{\omega^2 + \omega_1\omega_2}{\omega_2 - \omega_1}, \tag{4.49a}$$

$$V_0(\omega) = d_0 = \sqrt{T_2^2(\omega) - \omega^2} = \omega' \left(\frac{\omega_1 - \omega_2}{2}\right). \tag{4.49b}$$

The following Nth iterations are performed with the prescribed finite transmission zeros ω_n with reference to one passband. The remaining cycles use the following equations to update polynomials $U_i(\omega)$ and $V_i(\omega)$ at ith iteration:

$$U_i(\omega) = U_{i-1}(\omega)\left(T_1(\omega) - s_i\right) + \omega'\sqrt{1 - s_i^2}V_{i-1}(\omega), \tag{4.50a}$$

$$V_i(\omega) = \omega'\sqrt{1 - s_i^2}U_{i-1}(\omega) + V_{i-1}(\omega)\left(T_1(\omega) - s_i\right). \tag{4.50b}$$

At the end of the recursive technique, the numerator of the filtering function $F(\omega)$ is equal to $U_N(\omega)$, and their roots are the reflection zeros. For a general class of Chebyshev function, the reflection zeros in the complex s plane must be either real or come in conjugate imaginary pairs.

After the characteristic function $K(s)$ has been completely determined according to the requirements, the transmission function $H(s)$ is then to be calculated. According to the Feldtkeller equation given by

$$|H(s)|^2 = 1 + |K(s)|^2 , \tag{4.51}$$

the Hurwitz polynomial $E(s)$ can be calculated as

$$|E(s)|^2 = |F(s)|^2 + |P(s)|^2 . \tag{4.52}$$

Inductive Matching Elements

The second case of study covers filtering functions including three TZs in the origin, in order to realize a network with inductive input and output matching elements. Therefore, an additional term T_0' has been included in the filtering function in respect with that of only one TZ in the origin.

Further development of the filtering function in (4.41) yields

$$K(\omega) = \frac{1}{2} \frac{(c_0 + d_0)(c_0' + d_0') \prod_{n=1}^{N} (c_n + d_n) + (c_0 - d_0)(c_0' - d_0') \prod_{n=1}^{N} (c_n - d_n)}{\omega^3 \prod_{n=1}^{N} (1 - s_n T_1(\omega))} \tag{4.53}$$

where

$$c_0 = T_2(\omega), \tag{4.54a}$$

$$d_0 = \sqrt{T_2^2(\omega) - \omega^2}, \tag{4.54b}$$

$$c_0' = T_2'(\omega), \tag{4.54c}$$

$$d_0' = \sqrt{T_2'^2(\omega) - \omega^4}, \tag{4.54d}$$

$$c_n = s_n T_1(\omega), \tag{4.54e}$$

$$d_n = \sqrt{1 - s_n^2} \sqrt{T_1^2(\omega) - 1}, \tag{4.54f}$$

$$s_n = 1/T_1(\omega_n). \tag{4.54g}$$

It is interesting to observe that in this case the denominator of the filtering function has three transmission zeros at $\omega = 0$, as expected. Similar than before, polynomial $P(\omega)$ is determined by

$$P(\omega) = \omega^3 \prod_{n=1}^{N} (1 - T_1(\omega)/T_1(\omega_n)) . \tag{4.55}$$

The numerator of the filtering function $F(\omega)$ is calculated with a recursive technique similar to that proposed above, but taking into account the additional term $T_0'(\omega)$. Polynomials $U(\omega)$ and $V(\omega)$ are also used during the procedure, as well as the transformed variable ω' defined in (4.48).

The first iteration contemplates the first term $T_0(\omega)$. Here, we are going to use the term proposed by Zhang in [100], although the term proposed in this work can also be used. Polynomials $U_0(\omega)$ and $V_0(\omega)$ are therefore obtained as

$$U_0(\omega) = c_0 = T_2(\omega) = \frac{\omega^2 + \omega_1\omega_2}{\omega_2 + \omega_1}, \tag{4.56a}$$

$$V_0(\omega) = d_0 = \sqrt{T_2^2(\omega) - \omega^2} = \omega' \left(\frac{\omega_1 - \omega_2}{2}\right). \tag{4.56b}$$

In the second iteration the term $T_0'(\omega)$ is introduced, and polynomials $U_0'(\omega)$ and $V_0'(\omega)$ are derived as

$$U_0'(\omega) = U_0(\omega)T_2'(\omega) + \omega' V_0(\omega) \left(\frac{\omega\,(\omega_1 - \omega_2)}{2}\right), \tag{4.57a}$$

$$V_0'(\omega) = V_0(\omega)T_2'(\omega) + \omega' U_0(\omega) \left(\frac{\omega\,(\omega_1 - \omega_2)}{2}\right). \tag{4.57b}$$

The following N cycles are completed by using (4.50) and the finite TZs ω_n with respect to one passband. At the end of the recursive procedure, $F(\omega) = U_N(\omega)$, and their roots are the reflection zeros. Polynomial $E(\omega)$ can be derived from the Fedtkeller equation according to (4.52).

4.2.4 Normalization

When dealing with passband polynomials, the usual units of the elements, e.g., hertz, henry, farad, etc., are not suitable for computation purposes because the large magnitude differences may cause numerical problems, specially for high-frequency and large-degree filters. In order to overcome this issue, a normalizing constant ω_c is used for scaling purposes.

Typical bands to be designed by acoustic devices lie in the range of a few GHz. Therefore, a constant $\omega_c = 2\pi 10^9$ rad/s may be suitable. Without loss of generality, other normalizing constant values can be chosen, like the geometrical mean of the cutoff frequencies ω_1 and ω_2, i.e., $\omega_c = \omega_0 = \sqrt{\omega_1\omega_2}$.

It is also possible to normalize the impedance with a reference resistance R_c, that could be taken as the internal resistance of the signal source R_1.

The normalized values for the circuit elements obtained at the end of the synthesis l_i and c_i, and the normalized frequencies Ω_i may then be converted to the desired frequency range and

impedance level by means of

$$\omega_i = \omega_c \Omega_i \text{ [rad/s]}, \tag{4.58a}$$

$$L_i = \frac{R_c}{\omega_c} l_i \text{ [H]}, \tag{4.58b}$$

$$C_i = \frac{1}{R_c \omega_c} c_i \text{ [F]}. \tag{4.58c}$$

Transfer and characteristic functions, and consequently all reactance functions expressed in terms of expanded polynomials, tend to be inherently ill-conditioned. This means that small perturbations in the coefficients of the polynomials can result in large changes in their roots. For example, the zeros of $K(\omega)$ are all inside the passband, with small difference on the roots. Hence, this function is ill-conditioned in terms of ω and it becomes worse as the passband gets narrower or the filter degree increases [101]. During the parameter extraction procedure, where the reactance functions may be converted to partial fraction expansion representation, it is prudent to avoid ill-conditioning because it can increase sensitivity to round-off errors.

One potential way to avoid ill-conditioning is to replace the frequency variable, so perturbations on the new polynomials coefficients do not affect the roots considerably. Another option, that may work even in the case of polynomials with closely spaced roots, is to define and use the polynomials by their roots rather than by their coefficients.

Ladder-type filters based on acoustic resonators have finite TZs close to each other and not far from the band, because of the coupling coefficient restrictions. Thus, both the numerator and denominator roots of the characteristic function, i.e., reflection and transmission zeros, are closely spaced, increasing the probability of ill-conditioning. According to our experience, the synthesis of a fifth degree band-pass filter based on acoustic resonators can be straightforward realized from the input reactance parameter. However, for a seventh degree filter, numerical instabilities can be found, and it is recommended to perform the extraction from both the input and output port simultaneously.

4.3 Numerical Examples

In this section, we present two numerical examples of ladder-type filters synthesized directly in the band-pass domain. The examples highlights the conditions required to determine the filtering function from the characteristic frequencies, in order to realize a network based on acoustic resonators. The first one is for the case of capacitive matching elements, whereas the second example demonstrates the inductive matching elements case.

Both examples are a fifth-order Chebyshev filter with 12 dB return loss. The examples are realized in the Band 42, with a passband extending from 3.4 to 3.6 GHz. It has been conscien-

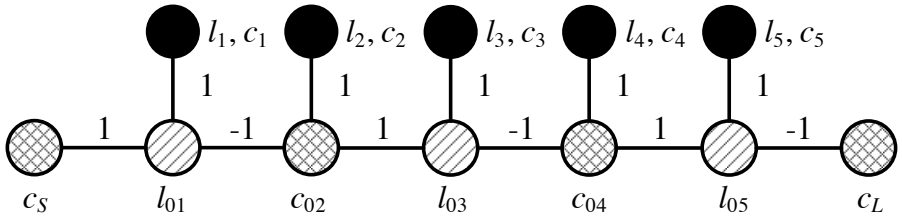

Figure 4.8: Ladder-type network to realize.

tiously designed at this band because of the high frequencies and large bandwidth specifications it presents. The finite TZs have been prescribed at 3.726, 3.314, and 3.67 GHz (the first and the second have multiplicity two).

First of all, we have to define a normalizing constant, in this case of $\omega_c = 2\pi 10^9$ rad/s. The normalized passband frequencies result then in $\omega_1 = \pm 3.4$ and $\omega_2 = \pm 3.6$ rad/s, and the finite transmission zeros as $\omega_n = [\pm 3.726,\ \pm 3.314,\ \pm 3.67,\ \pm 3.314,\ \pm 3.726]$.

4.3.1 Example 1. Capacitive Matching

In this example we define only one TZ in the origin and one TZ at infinity. Therefore, the resulting matching elements from the synthesis will be capacitors. The network to realize is depicted in Figure 4.8. Dangling resonators 1, 3, and 5 are connected to inductive reactive nodes, being series acoustic resonators after the circuital transformation. Meanwhile, resonators 2 and 4 are connected to capacitive reactive nodes, thus being shunt resonators.

Filtering Function

The band-pass generalized Chebyshev filtering function $K(s)$ has been defined as the ratio of two polynomials, $F(s)$ over $P(s)$. Its zeros are the reflection zeros, and its poles the transmission zeros. Polynomial $P(s)$ can therefore be derived from $s_n = j\omega_n$, the finite TZs, and the TZ in the origin. In Table 4.2 there are the coefficients of the obtained polynomial $P(s)$.

In order to find the numerator of the filtering function, $F(s)$, the recursive technique derived in Section 4.2.3 for the capacitive matching elements (because there is only one TZ in the origin) is used. The resulting coefficients of $F(s)$ are shown in Table 4.2, and the reflection zeros are found to lie at $\omega_r = [\pm 3.6j,\ \pm 3.4042,\ \pm 3.4409,\ \pm 3.5095,\ \pm 3.5693,\ \pm 3.5968]$. It can be observed that there are ten reflection zeros inside the positive and negative passbands, and two imaginary reflection zeros that do not create a notch in the passband, as expected.

Finally, the polynomial $E(s)$ is derived because it is necessary for the reactance calculation. It is obtained by means of the Fedtkeller equation, and its coefficients are also presented in Table

Table 4.2: Coefficients of the calculated polynomials $P(s)$, $F(s)$, and $E(s)$.

Degree	Coefficient of $P(s)$	Coefficient of $F(s)$	Coefficient of $E(s)$
12		1.0	1.0
11	1.0		7.47
10		48.46	76.37
9	63.20		459.36
8		712.39	2 402.14
7	1 593.02		11 289.16
6		−1 035.50	39 864.44
5	20 017.07		138 621.25
4		−126 380.77	368 263.52
3	125 374.57		850 456.93
2		−1 193 373.65	1 795 694.70
1	313 120.58		2 085 538.30
0		−3 610 044.50	3 610 044.50

4.2.

Reactance Function and Extraction Procedure

The extraction procedure will be performed from both the input and the output ports, in order to obtain a more accurate solution. For the removal of attenuation poles from the input, the primary open-circuit reactance X_{1o} is used. Because $P(s)$ is odd, X_{1o} is calculated as

$$X_{1o} = \frac{E_o - F_o}{E_e + F_e} =$$

$$= \frac{7.47s^{11} + 459.36s^9 + 11289.16s^7 + 138621.25s^5 + 850456.93s^3 + 2085538.30s}{2s^{12} + 124.83s^{10} + 3114.53s^8 + 38828.94s^6 + 241882.75s^4 + 602321.05s^2}. \quad (4.59)$$

Similarly, for the removal of attenuation poles from the output, the secondary open-circuit reactance X_{2o} is calculated. In this case, it is obtained by

$$X_{2o} = \frac{E_o + F_o}{E_e + F_e} = X_{1o}, \quad (4.60)$$

since $F(s)$ is pure even.

The first node to be extracted is a capacitive reactive node c_S, that accommodates the annihilation of the first TZ $\omega_1 = \pm 3.726$. For $y_1 = 1/X_{1o}$, c_S is obtained as

$$c_S = \left.\frac{y_1}{s}\right|_{s=3.726j} = 0.1365.$$

The remainder function is

$$y_2 = y_1 - s \cdot c_S = \frac{0.13s^{12} + 8.32s^{10} + 210.69s^8 + 2665.44s^6 + 16843.02s^4 + 42529.80s^2}{s^{11} + 61.48s^9 + 1511.05s^7 + 18554.35s^5 + 113833.01s^3 + 279147.70s}.$$

The unitary inverter is extracted by $y_3 = 1/y_2$, and then, a full removal at $s = \pm j\omega_1 = \pm j3.726$ is performed by

$$c_1 = \left.\frac{s}{y_3\left(s^2+3.726^2\right)}\right|_{s^2=-3.726^2} = 1.0681, \qquad l_1 = \frac{1}{\omega_1^2 c_1} = 0.0674.$$

To complete the extraction of the first TZ, the remainder admittance becomes

$$y_4 = y_3 - \frac{s/c_1}{s^2+\omega_1^2} = \frac{6.68s^9 + 329.35s^7 + 6081.56s^5 + 49868.49s^3 + 153217.75s}{s^{10} + 49.50s^8 + 918.17s^6 + 7563.12s^4 + 23343.63s^2}.$$

Next, a partial removal to prepare the annihilation of the following TZ $\omega_2 = \pm 3.314$ is necessary. The element to be extracted is an inductor, because the following TZ is below the passband, and it is extracted as

$$l_{01} = \left.\frac{1}{s\cdot y_4}\right|_{s=3.314j} = 0.1842.$$

The remainder admittance is

$$y_5 = y_4 - \frac{1}{s\cdot l_{01}} = \frac{1.25s^9 + 60.63s^7 + 1097.29s^5 + 8812.01s^3 + 26496.59s}{s^{10} + 49.50s^8 + 918.17s^6 + 7563.12s^4 + 23343.63s^2}.$$

A unitary inverter yields $y_6 = 1/y_5$, and then, a complete extraction at $s = \pm j\omega_2 = \pm j3.314$ can be realized by means of

$$c_2 = \left.\frac{s}{y_6\left(s^2+3.314^2\right)}\right|_{s^2=-3.314^2} = 1.2217, \qquad l_2 = \frac{1}{\omega_2^2 c_2} = 0.0745.$$

Similarly than before, the remainder admittance becomes

$$y_7 = y_6 - \frac{s/c_2}{s^2+\omega_2^2} = \frac{0.80s^8 + 29.88s^6 + 373.03s^4 + 1550.57s^2}{s^7 + 37.35s^5 + 464.38s^3 + 1922.59s}.$$

To prepare the annihilation of the third TZ $\omega_3 = 3.67$, the capacitor c_{02} has to be extracted by

$$c_{02} = \left.\frac{y_7}{s}\right|_{s=3.67j} = 0.7008,$$

and the remainder admittance is

$$y_8 = y_7 - s\cdot c_{02} = \frac{0.0963s^8 + 3.71s^6 + 47.60s^4 + 203.27s^2}{s^7 + 37.35s^5 + 464.38s^3 + 1922.59s}.$$

From the admittance after the unitary inverter $y_9 = 1/y_8$, the third TZ is completely removed:

$$c_3 = \left.\frac{s}{y_9\left(s^2+3.67^2\right)}\right|_{s^2=-3.67^2} = 1.2452, \qquad l_3 = \frac{1}{\omega_3^2 c_3} = 0.0596,$$

and

$$y_{10} = y_9 - \frac{s/c_3}{s^2+\omega_3^2} = \frac{9.58s^5 + 238.62s^3 + 1482.42s}{s^6 + 25.07s^4 + 156.73s^2}.$$

Finally, and before start the extraction from the output port, the following TZ $\omega_4 = 3.314$ annihilation is prepared by the extraction of the inductor l_{03}, given by

$$l_{03} = \left.\frac{1}{s\cdot y_{10}}\right|_{s=3.314j} = 0.1207.$$

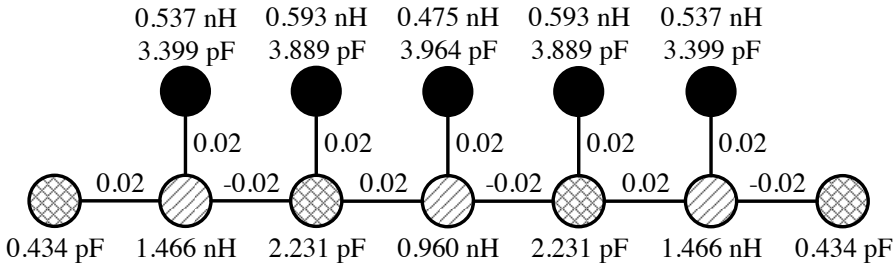

Figure 4.9: Synthesized band-pass filter for a reference impedance of 50 Ohm.

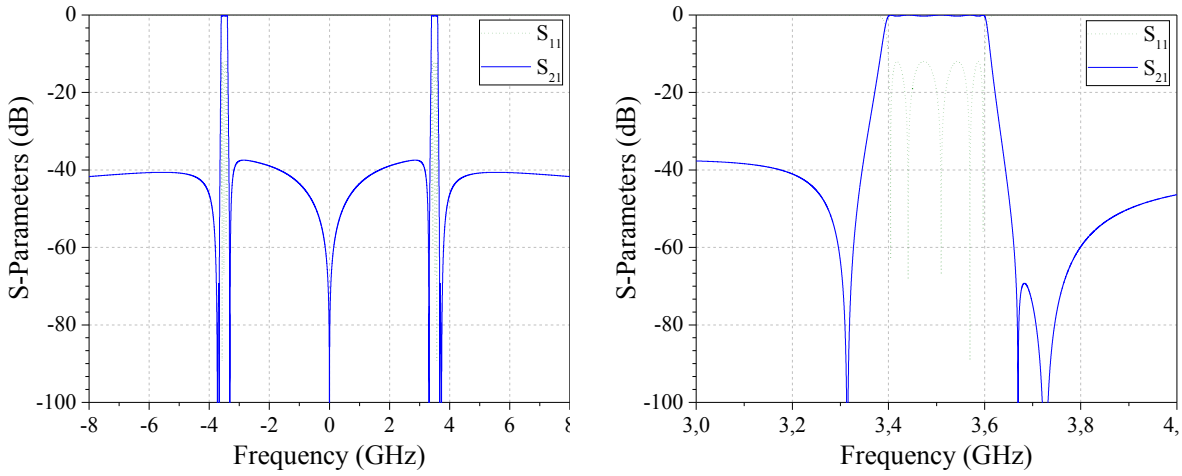

(a) (b)

Figure 4.10: Response of the synthesized band-pass filter with capacitive matching elements for (a) out of band and (b) near the passband frequencies.

Since the arrangement of the prescribed TZs is symmetrical, and so is the network to realize ($X_{1o} = X_{2o}$), the extraction process from the output is exactly the same than that already realized from the input, thus yielding the same circuital parameters.

The resulting inline topology and the synthesized parameters after denormalization are shown in Figure 4.9. From that nodal network the ladder-type circuit made of BVD resonators can be straightforward derived. Its response is shown in Figure 4.10. It can be observed that there is one TZ in the origin, one TZ at infinity, $N = 5$ finite TZs, and $N = 5$ reflection zeros inside the passband, as expected for a ladder-type filter based on acoustic resonators with capacitive matching elements.

4.3.2 Example 2. Inductive Matching

In this second example we are going to consider three TZs in the origin, one TZ at infinity, and the same finite TZs used during the example above. Therefore, the response of both examples near the passband will be the same, and differences will only be found at frequencies far from the band. The transmission slope to the origin will be steeper for the inductive case, because there are two more TZs at this frequency. However, the slope to infinity will be flatter compared to the capacitive case.

Filtering Function

The set of band-pass generalized Chebyshev polynomials have been calculated using the expressions derived in Section 4.2.3. The resulting coefficients of polynomials $P(s)$, $F(s)$, and $E(s)$ are shown in Table 4.3.

Polynomial $P(s)$ has been calculated from the finite set of TZs and the TZs in the origin. Because the finite TZs are the same in both examples but there are two more TZs in the origin in this case compared with the capacitive one, the coefficients of $P(s)$ remain the same but the degree has increased by two.

On the other hand, the calculation of $F(s)$ polynomial uses a different recursive technique because of the additional terms included in the filtering function. Thus, the polynomial is not expected to be the same than in the capacitive case, although the in-band reflection zeros are almost equal. The roots of $F(s)$ polynomial are found to lie at $\omega_r = [\pm 30.52j,\ \pm 0.46j,\ \pm 3.4042,\ \pm 3.4405,\ \pm 3.5089,\ \pm 3.5691,\ \pm 3.5968]$, where two purely imaginary reflection zeros are lying outside each band, therefore not introducing a notch inside the passband. From the coefficients of $F(s)$, it can be noticed that the sign of the first and last coefficients is the same. This is a necessary condition for the realisability of the band-pass filter with an inverse extraction, i.e., extracting an inductive reactive node to generate a TZs above the passband [98].

The last polynomial $E(s)$ has been calculated from the Fedtkeller equation and used later to calculate the reactance function used during the extraction procedure.

Reactance Function and Extraction Procedure

In this example, the extraction will be also performed from both the input and output ports. The extraction from the input makes use of the primary open-circuit reactance X_{1o}. Since $P(s)$

Table 4.3: Coefficients of the calculated polynomials $P(s)$, $F(s)$, and $E(s)$.

Degree	Coefficient of $P(s)$	Coefficient of $F(s)$	Coefficient of $E(s)$
14		1.0	1.0
13	1.0		62.32
12		−870.29	1 066.64
11	63.20		4 971.26
10		−5 5510.08	63 510.51
9	1 593.02		161 034.35
8		−1 374 152.11	1 549 574.80
7	20 017.07		2 720 998.11
6		−16 825 728.89	19 063 769.99
5	125 374.57		25 342 173.53
4		−101 757 304.73	118 389 771.76
3	313 120.58		123 432 589.17
2		−236 549 222.88	303 287 796.51
1			245 519 973.12
0		55 831 718.68	55 831 718.68

is an odd polynomial, the reactance function is derived as

$$X_{1o} = \frac{E_o - F_o}{E_e + F_e} =$$

$$= \frac{62.3s^{13} + 497.1s^{11} + 161034s^9 + 2720998s^7 + 25342173s^5 + 123432589s^3 + 245519973s}{2s^{14} + 196.4s^{12} + 8000s^{10} + 175422s^8 + 2238041s^6 + 16632467s^4 + 66738573s^2 + 111663437}. \tag{4.61}$$

Because polynomial $F(s)$ is even, the open-circuit reactance from the output port X_{2o} is the equal to the reactance looking to the input port X_{1o}.

To start the extraction procedure, the first step is a complete extraction of an inductor, thus annihilating a TZs in the origin. For $y_1 = 1/X_{1o}$, it can be accomplished using

$$l_S = \left.\frac{1}{s \cdot y_1}\right|_{s=0} = 2.1987.$$

The admittance after the complete extraction reminds

$$y_2 = y_1 - \frac{1}{s \cdot l_S} =$$

$$= \frac{0.032s^{13} + 2.7s^{11} + 92.1s^9 + 1639.7s^7 + 16054.9s^5 + 81945.8s^3 + 170108.9s}{s^{12} + 79.77s^{10} + 2584.05s^8 + 43662.68s^6 + 406654.94s^4 + 1980669.59s^2 + 3939753.25}.$$

It might be possible that the annihilation of the following TZ requires the extraction of a shunt capacitor in order to accommodate the admittance function. This step is the same than the first

step in the previous example, where the source capacitor accommodates the extraction of the first finite TZ. This capacitor is obtained as

$$c_S = \left.\frac{y_2}{s}\right|_{s=3.726j} = -0.0605,$$

and extracted from the admittance function as

$$y_3 = y_2 - s \cdot c_S =$$

$$= \frac{0.093s^{13} + 7.53s^{11} + 248.56s^9 + 4283.4s^7 + 40676.8s^5 + 201869.9s^3 + 408650.3s}{s^{12} + 79.77s^{10} + 2584.05s^8 + 43662.68s^6 + 406654.94s^4 + 1980669.59s^2 + 3939753.25}.$$

It is important no observe that the capacitor c_S resulted in a negative value. Therefore, it has to be implemented with a positive inductor of value $l'_S = -1/\left(\omega_0^2 \cdot c_S\right)$.

Next, the unitary inverter is extracted by $y_4 = 1/y_3$. Then, a full removal of the pole $\pm j\omega_1 = \pm j3.726$ is performed by

$$c_1 = \left.\frac{s}{y_4\left(s^2 + 3.726^2\right)}\right|_{s^2=-3.726^2} = 0.9878, \qquad l_1 = \frac{1}{\omega_1^2 c_1} = 0.0729.$$

To complete the extraction of the first TZ, the remainder admittance becomes

$$y_5 = y_4 - \frac{s/c_1}{s^2 + \omega_1^2} =$$

$$= \frac{9.78s^{10} + 657.1s^8 + 17002.03s^6 + 213055.7s^4 + 1296315.4s^2 + 3063581.4}{s^{11} + 67.36s^9 + 1747.99s^7 + 21971.4s^5 + 134084.1s^3 + 317769.5s}.$$

From this point, the second and third resonators are extracted following the same procedure. Then, the extraction is performed from the output port in order to avoid numerical errors. Because the network is symmetrical, the same resonator values have to be obtained. For asymmetrical realizations, an inverter may result in a value different than 1, and either a transformer or a matching network is required to maintain the filter characteristics.

Figure 4.11 depicts the band-pass nodal diagram of the synthesized network. The matching elements at both input and output ports are the parallel of the two inductors l_S and l'_S. The values of the network parameters have been calculated for a normalizing constant of $\omega_c = 2\pi 10^9$ rad/s and a reference impedance of 50 Ohms.

Finally, the out of band and the passband responses of the synthesized network are shown in Figures 4.12 (a) and (b), respectively. As expected, the passband, the transmission zeros, and the reflection zeros are exactly the same than in the capacitive case. However, big differences can be found on the out of band frequencies. At low frequencies close to the origin the inductive case provides more attenuation, due to the two additional TZs at dc. At higher frequencies, although a TZ is placed at infinity, the attenuation slope is not as steeper as in the capacitive case.

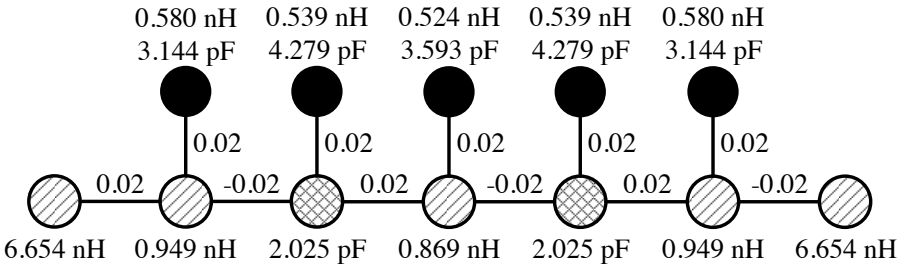

Figure 4.11: Synthesized band-pass filter for a reference impedance of 50 Ohms.

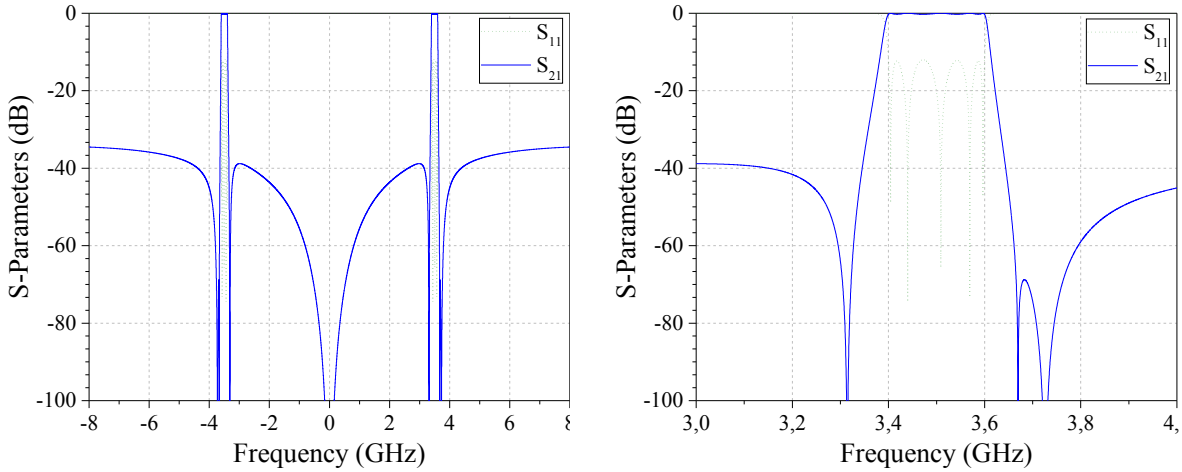

(a) (b)

Figure 4.12: Response of the synthesized band-pass filter with inductive matching elements for (a) out of band and (b) near the passband frequencies.

The two examples provided in this section demonstrates the theory introduced in this chapter for the design of filters directly in the band-pass domain. The proposed filtering functions and the realized topologies are ready to accommodate the acoustic technology, and only the proper set of transmission zeros and return loss has to be found to satisfy the technological constraints.

4.4 Chapter Summary

A theory for the band-pass synthesis of ladder-type filter based on acoustic resonators has been presented in this chapter. The synthesis realized directly in the band-pass domain overcomes the narrowband approximation in which is based the low-pass classical theory. This could be essential for the design of the upcoming band-pass filters with more and more stringent specifications in both the passband and OoB frequencies. Also for the upcoming design of multiplexer modules, in which the phase control over a wide range of frequencies is imperative.

The proper network definition and reactance parameters have been first derived, from which the circuital extraction can be performed. The definition of the network to synthesize is very important, because it determines the number of TZs in the origin, infinity, and finite frequencies. Since ladder-type filters present N finite TZs, the prescribed number of TZs in the origin determines the matching elements at input and output ports.

With the network and all TZs completely determined, it has been presented a recursive technique for the derivation of the transfer and characteristic functions. These functions accommodates the main properties existing in ladder-type filters based on acoustic resonators, so the resulting reactance parameters define the expected network. Finally, a Band 42 example has been realized in order to validate the proposed technique.

Further work on band-pass synthesis is necessary since some problems may arise during the procedure. Numerical instabilities and accumulative round-off errors may be present during the extraction procedure, in which the poles and zeros of large polynomials are constantly calculated. The main issues are found when the transfer and characteristic functions are ill-conditioned, which is common in ladder-type acoustic filters because all poles are very close to each other, mainly because of the coupling coefficient requirements. Additional work can also be done for cross-coupled topologies synthesis or ladder-type filters taking ground inductors into account, which effectively introduce TZs above the passband but no reflection zeros inside it.

CHAPTER 5

Conclusions and Future Work

The user segment of wireless and mobile communication systems is taking advantage of the outstanding performance given by filtering devices based on micro-acoustic resonators. With the deployment of 4G and the upcoming 5G systems, the number of supported bands in the front-end of a handset device has increased exponentially. The coexistence of more than 20 filters and duplexers in a front-end module within a very limited space, along with an exceptional performance, would be impossible without micro-acoustic technologies. This is why SAW and BAW technologies have dominated the market of wireless telecommunications RF filters, and it is expected to continue with this trend for the future mobile communications systems.

Carrier aggregation has changed the paradigm of the front-end architectures. Whereas during the last years a duplexer approach in conjunction with a switch was the main structural design, a multiplexer approach codesigned with power amplifiers is best suited for CA systems, improving the performance and reducing costs. However, in the multiplexer approach, maintaining cross-isolation between multiple bands below -55 dB is very challenging. The use of suitable filter design techniques becomes more and more necessary as the specifications eventually are more stringent and difficult to achieve.

In this work, we have provided systematic methodologies for the design of filters based on acoustic resonators. Synthesis techniques for the design of ladder-type filters, as well as cross-coupled prototypes, have been proposed. These can also be used to analyze and understand the behavior of the filtering network and its effects. However, the main benefit of the proposed methodologies is that their connect the synthesis techniques with the stringent constraints required by micro-acoustic technologies. The most important one is the effective coupling coefficient, or equivalently the capacitance ratio, which is required to be uniform for all the resonators making the filter. The quality factor, resonant frequencies, power handling, among others, are

also essential and must be contemplated during the design procedure. The aim of the provided methodologies is to simplify the design, enable the analysis of the networks, and make the design more efficient compared with the commonly used optimization methods.

In Chapter 2, a general class of Chebyshev filtering function has been linked with an inline topology, whose parameters can be obtained by means of the extracted pole technique. This low-pass prototype, made of a cascading of dangling resonators, can be transformed into a band-pass network made of BVD model resonators, which are commonly accepted as 1D models of a micro-acoustic resonator. The input variables to the synthesis procedure are the location of the finite TZs, the return loss, and the band specifications. An automatic search engine of the input variables that yields a network satisfying both the required technological constraints and the frequency specifications becomes the best solution to obtain starting guesses for further processes in a minimum time and computational costs. In other words, the methodology is time efficient and precise in the outcomes, and the filtering network is completely and automatically determined assuming a set of electrical specifications and technological constraints.

Furthermore, with the proposed synthesis techniques the phase parameters can be easily controlled. This has been enabled the design of duplexers and multiplexers with the minimum number of matching components. The relationship between the external elements required to satisfy the phase conditions has been analytically obtained. We have also demonstrated that by synthesizing each stand-alone filter with the proper phase condition, the multiplexer structure can be simply achieved by the connection of all filters at the common port, without a noticeable damage on the filter characteristics.

In Chapter 3, the same idea has been applied for the synthesis of cross-coupled prototype filters. A limited number of cross-coupled topologies in which the cross-couplings do not cross each other and they are connected only on the NRNs of the shunt resonators can be synthesized with the given technique. However, more important has been the understanding of the network characteristics after a cross-coupling extraction. Complex roots may appear in specific cases, which have been accurately analyzed. This synthesis technique has allowed the understanding of common effects in fabricated devices from a methodological point of view, and it has opened solutions that were impossible to obtain by optimization techniques.

The methodology has also been used to understand a potential parasitic electro-magnetic feedthrough between the ports of a filter. This feedthrough can be modeled by an inverter between source and load nodes in the low-pass prototype, and can be extracted at the beginning of the synthesis assuming that the level of signal leakage is known. Then, the required resonant frequencies for a given response are different than the prescribed TZs and the complete network can be easily synthesized, even if additional cross-couplings are necessary due to complex singularities.

At the end of Chapter 3, the synthesis of cross-coupled prototypes by the optimization of the coupling matrix has been presented. This technique allows the design of any cross-coupled topology, whatever the filter degree and the number of couplings. A suitable definition of the coupling matrix for filters based on acoustic resonators has been introduced. The cost function employed during the optimization is based on the characteristic frequencies of a general class of Chebyshev function. The difference between the poles and zeros of the filtering function and those of the optimized coupling matrix are minimized, therefore pressing the prototype response to be as Chebyshev as possible while satisfying the mask specifications and assuring technological feasibility. This technique has been proved to be successful through an example, although it requires of good starting guesses for a proper operation of the optimization procedure.

Finally, in Chapter 4 the synthesis of ladder-type filters directly in the band-pass domain has been introduced. The aim of this chapter was to overcome possible inaccuracies during the low-pass to band-pass frequency transformation, which is a narrowband equivalence between the low-pass and band-pass domains. First, the double-terminated network has been analyzed in order to obtain the analytical expressions of the two-port reactance parameters. Then, capacitive and inductive reactive nodes have been introduced, which are the equivalent nodes of the low-pass NRNs. However, reactive nodes are capable of introducing TZs in the origin or infinite frequencies. These TZs, along with the ones located at both positive and negative finite frequencies, have to be contemplated for a proper definition of the band-pass filtering function. Two different cases have been contemplated in this chapter: when the matching elements are capacitive and when they are inductive. Two definitions of the filtering functions, as well as the correspondent analysis of band-pass polynomials, have been proposed for each case. The main difference is the number of TZs in the origin, and the network to realize depend completely on them.

This band-pass synthesis technique will be useful for the upcoming multiplexer systems, because the band-pass characteristics are directly prescribed by the designer at the beginning of the design and no differences appear after the parameter extraction procedure. Although numerical inaccuracies may be found during the parameter extraction if the polynomial functions are ill-conditioned, two examples have shown the capabilities of the technique, which still has a lot of potential to be discovered.

Along with all theory presented in this thesis, different software tools including all advantages of the proposed synthesis techniques have been developed. The automation of the solution search for ladder-type and cross-coupled filtering networks based on the synthesis approaches presented in this work are able to combine frequency mask specifications fulfillment with networks ready to accommodate the technological constraints given by micro-acoustic technologies.

5.1 Future Work

This work includes a lot of theoretical content for the design and synthesis of microwave filters based on acoustic resonators. Although the methodologies have been validated by one of the most important manufacturers of acoustic devices, measures have not been included because of intellectual property limitations. The manufacturing of acoustic devices entails a complex process in which the design must be determined by the fabrication process requirements. A deep knowledge of these requirements can be used to approximate the results of the synthesis to a more realistic ones or include constraints into the methodology to obtain more feasible solutions. Many further processes on the design of an acoustic device are necessary behind the methodologies proposed in this work. However, they provide huge improvements in terms of network analysis, phase and magnitude characteristics management, technological feasibility checking, investigation of novel topologies, to get really good starting points for further optimization processes, and so on.

Even though fabrication is essential for further research on synthesis techniques of acoustic devices, some theoretical future work lines can also be identified:

1. The coupling matrix representation has proved to be very advantageous for the design of microwave filters. The coupling matrix has the capacity to include nodes of different nature, like resonant and non-resonant nodes. However, the general application of similarity transformations for coupling matrices with mixed nodes is not allowed. Different rank, determinant, and eigenvalues between two matrices with the same response and degree invalidate the application of similarity transformations. But we have realized that the matrices are congruent, and lineal transformations can be applied to move from one matrix to another. We have not obtained a general solution, and sometimes we have not been able to obtain one matrix by transformations on another. Further work can be done in this field in order to configure topologies efficiently and systematically by matrix transformations.

2. The synthesis of cross-coupled prototypes can be extended to take into consideration the most common cross-couplings in acoustic devices, like a shared ground inductor between two shunt resonators. Admittance blocks with the specified cross-couplings configurations should be analyzed to compare its characteristic frequencies with those of the filtering function.

3. In this work, the use of band-pass polynomials for the synthesis of acoustic devices has been introduced, but there is still a long way to cover in this field. When external inductors are considered in the network, additional TZs must be contemplated in the transfer function definition. The calculation of the polynomials should also be updated for each case, and a general procedure is difficult to foresight at this moment. Many work in this field can also be done to improve possible numerical instabilities during the band-pass extraction

procedure.

4. It is well-known in the microwave theory that singly-terminated filters are useful for the design of multiplexing devices, because of its reactance characteristics. Moreover, singly-terminated filters have a port of impedance zero, which is very advantageous for the connection of power amplifiers of low output impedance without the need of complex matching networks. Further work to synthesize singly-terminated filters that satisfy the acoustic technological constraints can be investigated, therefore offering a valuable methodology for the design of the future 5G systems.

Acoustic is the unique technology available nowadays ready to satisfy the stringent performance specifications of the current and future mobile standards while occupying a compact footprint. Therefore, a lot of improvements are expected to see the light in the near future in terms of synthesis, design, and fabrication of acoustic devices. The acoustic is becoming a fascinating field for researchers, and this is just the beginning of the golden age for acoustic filter design.

APPENDIX A

Transducer and Reactance Parameters Relationship

Transmission properties of a two-port network are usually specified in terms of the transducer parameters $H(s)$ and $K(s)$. However, the network is completely determined during the realization procedure by a reactance parameter. It is therefore necessary to establish the relationship between the open- and short-circuit reactance parameters X_o and X_s, respectively, and the transducer functions $H(s)$ and $K(s)$.

From the circuit depicted in Figure A.1, the following relations can be stated:

$$V_1 = V_0 - I_1 R_1 \tag{A.1a}$$

$$V_2 = -I_2 R_2 \tag{A.1b}$$

If the sub-network N is described by the open-circuit impedance parameters, the input and output voltages can be expressed as

$$V_1 = Z_{11} I_1 + Z_{12} I_2 \tag{A.2a}$$

$$V_2 = Z_{21} I_1 + Z_{22} I_2 \tag{A.2b}$$

Solving (A.1) and (A.2) for currents I_1 and I_2 it is obtained that

$$I_1 = V_0 \frac{Z_{22} + R_2}{(Z_{11} + R_1)(Z_{22} + R_2) - Z_{12}^2} \tag{A.3a}$$

$$I_2 = -V_0 \frac{Z_{12}}{(Z_{11} + R_1)(Z_{22} + R_2) - Z_{12}^2} \tag{A.3b}$$

The transfer function can be written as

$$H(s) = \frac{1}{2}\sqrt{\frac{R_2}{R_1}}\frac{V_0}{V_2} = \frac{1}{2}\sqrt{\frac{R_2}{R_1}}\frac{V_0}{-I_2 R_2}. \tag{A.4}$$

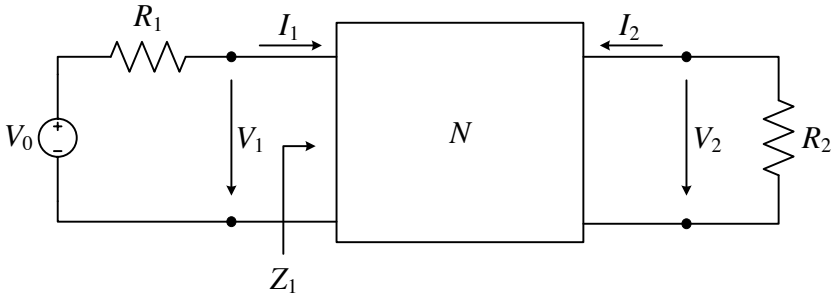

Figure A.1: A two-port network terminated in R_1 and R_2 at port-1 and port-2, respectively, and its typical operating conditions.

With the aid of equation (A.3) the transfer function of (A.4) becomes:

$$H(s) = \frac{(Z_{11} + R_1)(Z_{22} + R_2) - Z_{12}^2}{2Z_{12}\sqrt{R_1 R_2}}. \tag{A.5}$$

The input impedance is given by

$$Z_1 = \frac{V_1}{I_1} = \frac{V_0 - I_1 R_1}{I_1} = \frac{V_0}{I_1} - R_1, \tag{A.6}$$

and by substitution in the previous expression for the current I_1 of (A.3),

$$Z_1 = \frac{(Z_{11} + R_1)(Z_{22} + R_2) - Z_{12}^2}{Z_{22} + R_2} - R_1 = Z_{11} - \frac{Z_{12}^2}{Z_{22} + R_2}. \tag{A.7}$$

The reflection coefficient $\rho(s)$ is defined as

$$\rho(s) = \pm\frac{Z_1 - R_1}{Z_1 + R_1}, \tag{A.8}$$

where the $\pm$ sign appears because of the square root definition of the reflection coefficient $|\rho(s)|^2 = P_r/P_{max}$. P_r is the reflected power at the input port and P_{max} is the maximum available power from the source.

Solving for Z_1 in (A.8) it is obtained:

$$Z_1 = R_1\frac{1 \pm \rho(s)}{1 \mp \rho(s)}. \tag{A.9}$$

It is interesting to observe that the ambiguity of the sign only implies to modify Z_1 by $1/Z_1$ leading to a dual circuit. Next, we are going to solve the transducer functions and the reactance parameters for both cases, when the sign is taken positive and when it is negative, yielding different but equivalent networks.

A.1 Z-Equivalent Circuit

In this section, the equivalent circuit represented by an impedance matrix is considered. An example of symmetrical network is depicted in Figure A.2. Since this network is going to be

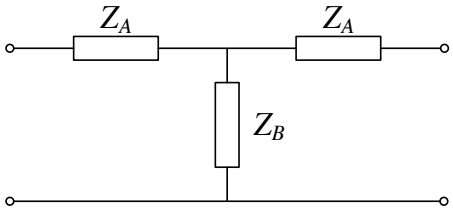

Figure A.2: Impedance Equivalent Network.

realized from an input impedance Z_1, the positive sign of the reflection coefficient is taken. With the aid of equation (A.7) the reflection coefficient of (A.8) becomes:

$$\rho(s) = \frac{Z_1 - R_1}{Z_1 + R_1} = \frac{(Z_{11} - R_1)(Z_{22} + R_2) - Z_{12}^2}{(Z_{11} + R_1)(Z_{22} + R_2) - Z_{12}^2}. \tag{A.10}$$

The characteristic function $K(s)$ can be obtained from the transfer function $H(s)$ and the reflection coefficient $\rho(s)$ as [58]

$$K(s) = H(s)\rho(s) = \frac{(Z_{11} - R_1)(Z_{22} + R_2) - Z_{12}^2}{2Z_{12}\sqrt{R_1 R_2}}. \tag{A.11}$$

Since the open-circuit impedance parameters Z_{11}, Z_{22}, and Z_{12} are odd polynomials in s [93], the functions $H(s)$ and $K(s)$ given by equations (A.5) and (A.11), respectively, can be divided into their even and odd parts:

$$H_e(s) = \frac{Z_{11}R_2 + Z_{22}R_1}{2Z_{12}\sqrt{R_1 R_2}}\,, \qquad H_o(s) = \frac{Z_{11}Z_{22} - Z_{12}^2 + R_1 R_2}{2Z_{12}\sqrt{R_1 R_2}} \tag{A.12a}$$

$$K_e(s) = \frac{Z_{11}R_2 - Z_{22}R_1}{2Z_{12}\sqrt{R_1 R_2}}\,, \qquad K_o(s) = \frac{Z_{11}Z_{22} - Z_{12}^2 - R_1 R_2}{2Z_{12}\sqrt{R_1 R_2}} \tag{A.12b}$$

Applying the addition and subtraction to the functions it is obtained:

$$H_e + K_e = \sqrt{\frac{R_2}{R_1}}\frac{Z_{11}}{Z_{12}} \tag{A.13a}$$

$$H_e - K_e = \sqrt{\frac{R_1}{R_2}}\frac{Z_{22}}{Z_{12}} \tag{A.13b}$$

$$H_o + K_o = \frac{Z_{11}Z_{22} - Z_{12}^2}{Z_{12}\sqrt{R_1 R_2}} \tag{A.13c}$$

$$H_o - K_o = \frac{\sqrt{R_1 R_2}}{Z_{12}} \tag{A.13d}$$

From (A.13d) it is derived that

$$Z_{12} = \frac{\sqrt{R_1 R_2}}{H_o - K_o}. \tag{A.14}$$

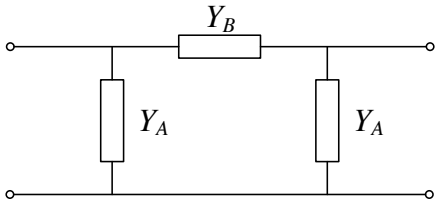

Figure A.3: Impedance Equivalent Network.

Substituting (A.14) in (A.13a) and (A.13b) the input and output open-circuit parameters are obtained as

$$Z_{11} = R_1 \frac{H_e + K_e}{H_o - K_o} \tag{A.15a}$$

$$Z_{22} = R_2 \frac{H_e - K_e}{H_o - K_o} \tag{A.15b}$$

The same study can be realized with the short-circuit admittance parameters, thus obtaining the following expressions:

$$Y_{12} = -\frac{1}{\sqrt{R_1 R_2}} \frac{1}{H_o + K_o} \tag{A.16a}$$

$$Y_{11} = \frac{1}{R_1} \frac{H_e - K_e}{H_o + K_o} \tag{A.16b}$$

$$Y_{22} = \frac{1}{R_2} \frac{H_e + K_e}{H_o + K_o} \tag{A.16c}$$

A.2 Y-Equivalent Circuit

In this section it is considered a network that it is better described by the admittance parameters, as the one shown in Figure A.3. However, the aim is to obtain the impedance parameters from the transducer parameters. The reflection coefficient is taken negative in this case, resulting in

$$\rho(s) = \frac{R_1 - Z_1}{R_1 + Z_1} = \frac{(R_1 - Z_{11})(Z_{22} + R_2) + Z_{12}^2}{(R_1 + Z_{11})(Z_{22} + R_2) - Z_{12}^2}. \tag{A.17}$$

The characteristic function is therefore obtained as

$$K(s) = H(s)\rho(s) = \frac{(R_1 - Z_{11})(Z_{22} + R_2) + Z_{12}^2}{2Z_{12}\sqrt{R_1 R_2}}. \tag{A.18}$$

Since the open-circuit impedance parameters Z_{11}, Z_{22}, and Z_{12} are odd polynomials in s [93], the functions $H(s)$ and $K(s)$ given by equations (A.5) and (A.18), respectively, can be divided

into their even and odd parts:

$$H_e(s) = \frac{Z_{11}R_2 + Z_{22}R_1}{2Z_{12}\sqrt{R_1R_2}}\,, \qquad H_o(s) = \frac{Z_{11}Z_{22} - Z_{12}^2 + R_1R_2}{2Z_{12}\sqrt{R_1R_2}} \tag{A.19a}$$

$$K_e(s) = \frac{Z_{22}R_1 - Z_1R_2}{2Z_{12}\sqrt{R_1R_2}}\,, \qquad K_o(s) = \frac{-Z_{11}Z_{22} + Z_{12}^2 + R_1R_2}{2Z_{12}\sqrt{R_1R_2}} \tag{A.19b}$$

Same than before, by applying the addition and subtraction to the functions it is obtained:

$$H_e + K_e = \sqrt{\frac{R_1}{R_2}}\frac{Z_{22}}{Z_{12}} \tag{A.20a}$$

$$H_e - K_e = \sqrt{\frac{R_2}{R_1}}\frac{Z_{11}}{Z_{12}} \tag{A.20b}$$

$$H_o + K_o = \frac{\sqrt{R_1R_2}}{Z_{12}} \tag{A.20c}$$

$$H_o - K_o = \frac{Z_{11}Z_{22} - Z_{12}^2}{Z_{12}\sqrt{R_1R_2}} \tag{A.20d}$$

From (A.20c) it is derived that

$$Z_{12} = \frac{\sqrt{R_1R_2}}{H_o + K_o}. \tag{A.21}$$

Substituting (A.21) in (A.20b) and (A.20a) the input and output open-circuit parameters are obtained as

$$Z_{11} = R_1\frac{H_e - K_e}{H_o + K_o} \tag{A.22a}$$

$$Z_{22} = R_2\frac{H_e + K_e}{H_o + K_o} \tag{A.22b}$$

The same study can be realized with the short-circuit admittance parameters, thus obtaining the following expressions:

$$Y_{12} = -\frac{1}{\sqrt{R_1R_2}}\frac{1}{H_o - K_o} \tag{A.23a}$$

$$Y_{11} = \frac{1}{R_1}\frac{H_e + K_e}{H_o - K_o} \tag{A.23b}$$

$$Y_{22} = \frac{1}{R_2}\frac{H_e - K_e}{H_o - K_o} \tag{A.23c}$$

Table A.1: Network Open- and Short-Circuit Reactance Parameters Looking at the Network from its Input and Back from the Output Terminals.

	Z-Equivalent Circuit		**Y-Equivalent Circuit**	
	P even	P odd	P even	P odd
X_{1o}	$R_1\frac{E_e+F_e}{E_o-F_o}$	$R_1\frac{E_o+F_o}{E_e-F_e}$	$R_1\frac{E_e-F_e}{E_o+F_o}$	$R_1\frac{E_o-F_o}{E_e+F_e}$
X_{1s}	$R_1\frac{E_o+F_o}{E_e-F_e}$	$R_1\frac{E_e+F_e}{E_o-F_o}$	$R_1\frac{E_o-F_o}{E_e+F_e}$	$R_1\frac{E_e-F_e}{E_o+F_o}$
X_{2o}	$R_2\frac{E_e-F_e}{E_o-F_o}$	$R_2\frac{E_o-F_o}{E_e-F_e}$	$R_2\frac{E_e+F_e}{E_o+F_o}$	$R_2\frac{E_o+F_o}{E_e+F_e}$
X_{2s}	$R_2\frac{E_o+F_o}{E_e+F_e}$	$R_2\frac{E_e+F_e}{E_o+F_o}$	$R_2\frac{E_o-F_o}{E_e-F_e}$	$R_2\frac{E_e-F_e}{E_o-F_o}$

A.3 Polynomial Definition of the Open- and Short-Circuit Reactance Parameters

The transducer parameters $H(s)$ and $K(s)$ are even or odd rational functions of s. Therefore, they can be expressed in polynomial form as

$$H(s) = \frac{E_e + E_o}{P} \tag{A.24a}$$

$$K(s) = \frac{F_e + F_o}{P} \tag{A.24b}$$

Since $P(s)$ is either an even or odd function [92], the open- and short-circuit reactance parameters obtained in sections A.1 and A.2 can be divided in two cases for each equivalent circuit. Table A.1 contains all possible open- and short-circuit reactance parameters for both equivalent circuits and depending on function $P(s)$. The network to be synthesized is completely determined by one or more of these reactances together with the complete set of transmission zeros or roots of $P(s)$. The circuit elements can be calculated by partial or full removal of the residues at these poles.

Bibliography

[1] Cisco VNI Forecast, "Cisco visual networking index: Global mobile data traffic forecast update, 2015-2020," *Cisco Public Information*, February 2016, [Online]. Available: www.cisco.com.

[2] J. G. Andrews, S. Buzzi, W. Choi, S. V. Hanly, A. Lozano, A. C. K. Soong, and J. C. Zhang, "What will 5g be?," *IEEE Journal on Selected Areas in Communications*, vol. 32, no. 6, pp. 1065–1082, June 2014.

[3] J. Wannstrom, "LTE-Advanced," *3GPP: The Mobile Broadband Standard*, June 2013, [Online]. Available: www.3gpp.org/technologies/keywords-acronyms/97-lte-advanced.

[4] "4G Americas: 4G Mobile Broadband Evolution: Release 10, Release 11 and Beyond - HSPA+, SAE/LTE and LTE-Advanced," October 2012.

[5] C. E. Shannon, "Communication in the presence of noise," *Proc. IRE.*, vol. 37, no. 1, 1949.

[6] G. Yuan, X. Zhang, W. Wang, and Y. Yang, "Carrier aggregation for LTE-Advanced mobile communication systems," *IEEE Communications Magazine*, vol. 48, no. 2, pp. 88–93, February 2010.

[7] K. I. Pedersen, F. Frederiksen, C. Rosa, H. Nguyen, L. G. U. Garcia, and Y. Wang, "Carrier aggregation for LTE-Advanced: functionality and performance aspects," *IEEE Communications Magazine*, vol. 49, no. 6, pp. 89–95, June 2011.

[8] Q. Li, G. Li, W. Lee, M. i. Lee, D. Mazzarese, B. Clerckx, and Z. Li, "MIMO techniques in WiMAX and LTE: a feature overview," *IEEE Communications Magazine*, vol. 48, no. 5, pp. 86–92, May 2010.

[9] "4G Americas: 4G Mobile Broadband Evolution Towards 5G: Rel 12 & Rel 13 and Beyond," June 2015.

[10] E. Schmidhammer, T. Metzger, and C. Hoffmann, "Multiplexers: a necessary extension for 4G/5G systems," in *2016 IEEE MTT-S International Microwave Symposium IMS2016*, May 2016.

[11] G. G. Fattinger, A. Volatier, M. Al-Joumayly, Y. Yusuf, R. Aigner, N. Khlat, and M. Granger-Jones, "Carrier aggregation and its challenges - or: The golden age for acoustic filters," in *2016 IEEE MTT-S International Microwave Symposium IMS2016*, May 2016.

[12] W. Mueller and R. Ruby, "Multiplexers as a method of supporting same-frequency-range down link carrier aggregation," in *2016 IEEE MTT-S International Microwave Symposium IMS2016*, May 2016.

[13] T. Takai, H. Iwamoto, Y. Takamine, T. Wada, M. Hiramoto, M. Koshino, and N. Nakajima, "Investigations on design technologies for SAW quadplexer with narrow duplex gap," in *2016 IEEE MTT-S International Microwave Symposium IMS2016*, May 2016.

[14] "Leveraging advanced filter technology for regional demands," February 2015, [Online]. Available: http://cn.qorvo.com/docs/brochures/qorvo-filter-technology.pdf.

[15] C. C. W. Ruppel, L. Reindl, and R. Weigel, "Saw devices and their wireless communications applications," *IEEE Microwave Magazine*, vol. 3, no. 2, pp. 65–71, Jun 2002.

[16] K.-Y. Hashimoto, *RF Bulk Acoustic Wave Filters for Communications*, Artech House, 2009.

[17] T. Bauer, C. Eggs, K. Wagner, and P. Hagn, "A bright outlook for acoustic filtering: A new generation of very low-profile saw, tc saw, and baw devices for module integration," *IEEE Microwave Magazine*, vol. 16, no. 7, pp. 73–81, Aug 2015.

[18] R. Ruby, "11E-2 Review and Comparison of Bulk Acoustic Wave FBAR, SMR Technology," in *Ultrasonics Symposium, 2007. IEEE*, Oct 2007, pp. 1029–1040.

[19] R. Ruby, P. Bradley, J. D. Larson, and Y. Oshmyansky, "Pcs 1900 mhz duplexer using thin film bulk acoustic resonators (fbars)," *Electronics Letters*, vol. 35, no. 10, pp. 794–795, May 1999.

[20] R. Ruby, P. Bradley, D. Clark, D. Feld, T. Jamneala, and Kun Wang, "Acoustic fbar for filters, duplexers and front end modules," in *Microwave Symposium Digest, 2004 IEEE MTT-S International*, June 2004, vol. 2, pp. 931–934 Vol.2.

[21] R. Aigner, J. Ella, H. J. Timme, L. Elbrecht, W. Nessler, and S. Marksteiner, "Advancement of mems into rf-filter applications," in *Electron Devices Meeting, 2002. IEDM '02. International*, Dec 2002, pp. 897–900.

[22] "Energy loss mechanisms in SMR-type BAW devices," in *IEEE MTT-S International Microwave Symposium Digest, 2005.*, June 2005, pp. 4 pp.–.

[23] S. Marksteiner, J. Kaitila, G. G. Fattinger, and R. Aigner, "Optimization of acoustic mirrors for solidly mounted BAW resonators," in *IEEE Ultrasonics Symposium, 2005.*, Sept 2005, vol. 1, pp. 329–332.

[24] S. Marksteiner, G. Fattinger, R. Aigner, and J. Kaitila, "Acoustic reflector for a BAW resonator providing specified reflection of both shear waves and longitudinal waves," August 2005, US Patent 6,933,807.

[25] R. Ruby, "A snapshot in time: The future in filters for cell phones," *IEEE Microwave Magazine*, vol. 16, no. 7, pp. 46–59, Aug 2015.

[26] R. Aigner, "SAW and BAW technologies for RF filter applications: A review of the relative strengths and weaknesses," in *2008 IEEE Ultrasonics Symposium*, Nov 2008, pp. 582–589.

[27] S. V. Krishnaswamy, J. Rosenbaum, S. Horwitz, C. Vale, and R. A. Moore, "Film bulk acoustic wave resonator technology," in *Ultrasonics Symposium, 1990. Proceedings., IEEE 1990*, Dec 1990, pp. 529–536 vol.1.

[28] J. D. Larson, P. D. Bradley, S. Wartenberg, and R. C. Ruby, "Modified butterworth-van dyke circuit for fbar resonators and automated measurement system," in *Ultrasonics Symposium, 2000 IEEE*, Oct 2000, vol. 1, pp. 863–868 vol.1.

[29] Jordi Verdú Tirado, "Bulk acoustic wave resonators and their application to microwave devices," *PhD, Universitat Antonoma de Barcelona*, 2010.

[30] Warren P Mason and Hans Baerwald, "Piezoelectric crystals and their applications to ultrasonics," *Physics Today*, vol. 4, pp. 23, 1951.

[31] J. F. Rosenbaum, *Bulk Acoustic Wave Theory and Devices*, Artech House, Boston, 1988.

[32] M. J. S. Lowe, "Matrix techniques for modeling ultrasonic waves in multilayered media," *IEEE Transactions on Ultrasonics, Ferroelectrics, and Frequency Control*, vol. 42, no. 4, pp. 525–542, July 1995.

[33] G. Tobolka, "Mixed matrix representation of saw transducers," *IEEE Transactions on Sonics and Ultrasonics*, vol. 26, no. 6, pp. 426–427, Nov 1979.

[34] K.-Y. Hashimoto, *Surface Acoustic Wave Devices in Telecommunications: Modelling and Simulation*, Berlin: Springer, 2000.

[35] C. C. W. Ruppel, W. Ruile, G. Scholl, K. C. Wagner, and O. Manner, "Review of models for low-loss filter design and applications," in *Ultrasonics Symposium, 1994. Proceedings., 1994 IEEE*, Oct 1994, vol. 1, pp. 313–324 vol.1.

[36] R. Lerch, "Simulation of piezoelectric devices by two- and three-dimensional finite elements," *IEEE Transactions on Ultrasonics, Ferroelectrics, and Frequency Control*, vol. 37, no. 3, pp. 233–247, May 1990.

[37] T. Makkonen, A. Holappa, J. Ella, and M. M. Salomea, "Finite element simulations of thin-film composite baw resonators," *IEEE Transactions on Ultrasonics, Ferroelectrics, and Frequency Control*, vol. 48, no. 5, pp. 1241–1258, Sept 2001.

[38] M. Solal, L. Chen, and J. Gratier, "Measurement and fem/bem simulation of transverse effects in saw resonators on lithium tantalate," *IEEE Transactions on Ultrasonics, Ferroelectrics, and Frequency Control*, vol. 60, no. 11, pp. 2404–2413, November 2013.

[39] J. Kaitila, M. Ylilammi, J. Ella, and R. Aigner, "Spurious resonance free bulk acoustic wave resonators," in *Ultrasonics, 2003 IEEE Symposium on*, Oct 2003, vol. 1, pp. 84–87 Vol.1.

[40] N. Finger, G. Kovacs, J. Schoberl, and U. Langer, "Accurate fem/bem-simulation of surface acoustic wave filters," in *Ultrasonics, 2003 IEEE Symposium on*, Oct 2003, vol. 2, pp. 1680–1685 Vol.2.

[41] F. M. Pitschi, J. E. Kiwitt, R. D. Koch, B. Bader, K. Wagner, and R. Weigel, "High performance microwave acoustic components for mobile radios," in *2009 IEEE International Ultrasonics Symposium*, Sept 2009, pp. 1–10.

[42] J. Verdu, O. Menendez, and P. De Paco, "Ladder-type filter based on bulk acoustic wave resonators with improved out-of-band rejection," *Microwave and Optical Technology Letters*, vol. 50, no. 1, pp. 103–107, 2008.

[43] P. Warder and A. Link, "Golden age for filter design: Innovative and proven approaches for acoustic filter, duplexer, and multiplexer design," *IEEE Microwave Magazine*, vol. 16, no. 7, pp. 60–72, Aug 2015.

[44] K. M. Lakin, "Modeling of thin film resonators and filters," in *Microwave Symposium Digest, 1992., IEEE MTT-S International*, June 1992, pp. 149–152 vol.1.

[45] Jia-Shen G Hong and Michael J Lancaster, *Microstrip filters for RF/microwave applications*, vol. 167, John Wiley & Sons, 2004.

[46] R. Baum, "Design of unsymmetrical band-pass filters," *IRE Transactions on Circuit Theory*, vol. 4, no. 2, pp. 33–40, Jun 1957.

[47] R. J. Cameron and J. D. Rhodes, "Asymmetric realizations for dual-mode bandpass filters," *IEEE Transactions on Microwave Theory and Techniques*, vol. 29, no. 1, pp. 51–58, Jan 1981.

[48] R. J. Cameron, "General coupling matrix synthesis methods for chebyshev filtering functions," *IEEE Transactions on Microwave Theory and Techniques*, vol. 47, no. 4, pp. 433–442, Apr 1999.

[49] A. E. Atia and A. E. Williams, "Narrow-bandpass waveguide filters," *IEEE Transactions on Microwave Theory and Techniques*, vol. 20, no. 4, pp. 258–265, Apr 1972.

[50] R. J. Cameron, "Advanced coupling matrix synthesis techniques for microwave filters," *IEEE Transactions on Microwave Theory and Techniques*, vol. 51, no. 1, pp. 1–10, Jan 2003.

[51] H. C. Bell, "Canonical asymmetric coupled-resonator filters," *IEEE Transactions on Microwave Theory and Techniques*, vol. 30, no. 9, pp. 1335–1340, Sep 1982.

[52] U. Rosenberg and W. Hagele, "Advanced multimode cavity filter design using source/load-resonance circuit cross couplings," *IEEE Microwave and Guided Wave Letters*, vol. 2, no. 12, pp. 508–510, Dec 1992.

[53] Ching-Ku Liao and Chi-Yang Chang, "Design of microstrip quadruplet filters with source-load coupling," *IEEE Transactions on Microwave Theory and Techniques*, vol. 53, no. 7, pp. 2302–2308, July 2005.

[54] S. Amari and G. Macchiarella, "Synthesis of inline filters with arbitrarily placed attenuation poles by using nonresonating nodes," *IEEE Transactions on Microwave Theory and Techniques*, vol. 53, no. 10, pp. 3075–3081, Oct 2005.

[55] R. J. Cameron, A. R. Harish, and C. J. Radcliffe, "Synthesis of advanced microwave filters without diagonal cross-couplings," *IEEE Transactions on Microwave Theory and Techniques*, vol. 50, no. 12, pp. 2862–2872, Dec 2002.

[56] S. Amari, U. Rosenberg, and J. Bornemann, "Singlets, cascaded singlets, and the nonresonating node model for advanced modular design of elliptic filters," *IEEE Microwave and Wireless Components Letters*, vol. 14, no. 5, pp. 237–239, May 2004.

[57] Mercedes Jimenez Blasco and Pedro de Paco, *A coupling matrix vision for mobile filtering devices with micro-acoustic wave technologies. A systematic approach*, Ph.D. thesis, Universitat Autònoma de Barcelona, 2015.

[58] Richard J Cameron, Raafat Mansour, and Chandra M Kudsia, *Microwave filters for communication systems: fundamentals, design and applications*, Wiley-Interscience, 2007.

[59] R. J. Cameron, "Fast generation of Chebyshev filter prototypes with asymmetrically-prescribed transmission zeros," *ESA Journal*, vol. 6, pp. 83–95, 1982.

[60] Robert Aigner, "Bringing baw technology into volume production: The ten commandments and the seven deadly sins," in *IEEE Int. Symp. Acoust. Wave. Dev. for Future Mobile Communication Syst*, 2007.

[61] S. Gong and G. Piazza, "Design and analysis of lithium-niobate-based high electromechanical coupling rf-mems resonators for wideband filtering," *IEEE Transactions on Microwave Theory and Techniques*, vol. 61, no. 1, pp. 403–414, Jan 2013.

[62] A. Tag, V. Chauhan, R. Weigel, A. Hagelauer, B. Bader, C. Huck, M. Pitschi, and D. Karolewski, "Multiphysics modeling of baw filters," in *Ultrasonics Symposium (IUS), 2015 IEEE International*, Oct 2015, pp. 1–4.

[63] J. Galipeau and R. E. Chang, "Design considerations for high power baw duplexers for base station applications," in *Ultrasonics Symposium (IUS), 2015 IEEE International*, Oct 2015, pp. 1–4.

[64] Y. Satoh, T. Nishihara, O. Ikata, M. Ueda, and H. Ohomori, "Saw duplexer metallizations for high power durability," in *Ultrasonics Symposium, 1998. Proceedings., 1998 IEEE*, 1998, vol. 1, pp. 17–26 vol.1.

[65] R. Takayama, M. Furukawa, Y. Murashima, T. Sakuragawa, N. Yuda, and K. Nomura, "High power saw filter with new al-sc-cu/ti/al-sc-cu/ti electrodes," in *Ultrasonics Symposium, 1998. Proceedings., 1998 IEEE*, 1998, vol. 1, pp. 5–8 vol.1.

[66] O. Nakagawara, M. Saeki, N. Tsubaki, N. Taniguchi, K. Ikada, M. Watanabe, K. Inoue, T. Hagi, T. Makino, and S. Arai, "High power durable saw antenna duplexers for w-cdma with epitaxially grown aluminum electrodes," in *Ultrasonics Symposium, 2002. Proceedings. 2002 IEEE*, Oct 2002, vol. 1, pp. 43–46 vol.1.

[67] T. Matsuda, H. Uchishiba, O. Ikata, T. Nishihara, and V. Satoh, "L and s band low-loss filters using saw resonators," in *Ultrasonics Symposium, 1994. Proceedings., 1994 IEEE*, Oct 1994, vol. 1, pp. 163–167 vol.1.

[68] C. Ernst, V. Postoyalko, and N. G. Khan, "Relationship between group delay and stored energy in microwave filters," *IEEE Transactions on Microwave Theory and Techniques*, vol. 49, no. 1, pp. 192–196, Jan 2001.

[69] J. D. Rhodes and R. J. Cameron, "General extracted pole synthesis technique with applications to low-loss te011 mode filters," *IEEE Transactions on Microwave Theory and Techniques*, vol. 28, no. 9, pp. 1018–1028, Sep 1980.

[70] G. Macchiarella, M. Oldoni, and S. Tamiazzo, "Narrowband microwave filters with mixed topology," *IEEE Transactions on Microwave Theory and Techniques*, vol. 60, no. 12, pp. 3980–3987, Dec 2012.

[71] S. Tamiazzo and G. Macchiarella, "Synthesis of cross-coupled prototype filters including resonant and non-resonant nodes," *IEEE Transactions on Microwave Theory and Techniques*, vol. 63, no. 10, pp. 3408–3415, Oct 2015.

[72] S. Amari and M. Bekheit, "Physical interpretation and implications of similarity transformations in coupled resonator filter design," *IEEE Transactions on Microwave Theory and Techniques*, vol. 55, no. 6, pp. 1139–1153, June 2007.

[73] J. Tsutsumi, S. Inoue, M. Iwaki, M. Hara, H. Nakamura, K. Matsumoto, M. Ueda, and Y. Satoh, "A design technique to enhance isolation of duplexer in single-ended and differential modes," in *2011 IEEE International Ultrasonics Symposium*, Oct 2011, pp. 1833–1836.

[74] P. Selmeier, R. Grunwald, A. Przadka, H. Kruger, G. Feiertag, and C. Ruppel, "Recent advances in saw packaging," in *Ultrasonics Symposium, 2001 IEEE*, 2001, vol. 1, pp. 283–292 vol.1.

[75] R. E. Jones, C. Ramiah, T. Kamgaing, S. K. Banerjee, Chi-Taou Tsai, H. G. Hughes, A. P. De Silva, J. Drye, Li Li, W. Blood, Qiang Li, C. R. Vaughan, R. Miglore, D. Penunuri, R. Lucero, D. R. Frear, and M. F. Miller, "System-in-a-package integration of saw rf rx filter stacked on a transceiver chip," *IEEE Transactions on Advanced Packaging*, vol. 28, no. 2, pp. 310–319, May 2005.

[76] J. Tsutsumi and K. Matsumoto, "Super-isolation duplexer aiming for removing rx interstage filter in w-cdma handsets," in *Microwave Conference, 2008. EuMC 2008. 38th European*, Oct 2008, pp. 1066–1069.

[77] M. Iwaki, J. Tsutsumi, Y. Endo, H. Nakamura, and Y. Satoh, "An attenuation improvement technology for ladder saw/fbar filters and duplexers employing cancellation circuit," in *Microwave Conference (EuMC), 2011 41st European*, Oct 2011, pp. 751–754.

[78] F. Moller and W. Buff, "Electromagnetic feedthrough in si/zno-saw-devices," in *Ultrasonics Symposium, 1992. Proceedings., IEEE 1992*, Oct 1992, pp. 245–248 vol.1.

[79] T. Makkonen, V. P. Plessky, S. Kondratiev, and M. M. Salomaa, "Electromagnetic modeling of package parasitics in saw-duplexer," in *Ultrasonics Symposium, 1996. Proceedings., 1996 IEEE*, Nov 1996, vol. 1, pp. 29–32 vol.1.

[80] A. Venema and R. F. Humphryes, "Equivalent circuit for a saw idt in multi-layer media with an electrically conductive silicon substrate," in *Ultrasonics Symposium, 1977*, Oct 1977, pp. 637–641.

[81] H. Yatsuda, "Modeling of parasitic effects for flip-chip saw filters," in *Ultrasonics Symposium, 1997. Proceedings., 1997 IEEE*, Oct 1997, vol. 1, pp. 143–146 vol.1.

[82] P. Dufilie and J. Desbois, "Modeling of feedthrough and ground loops in saw filters," in *Ultrasonics Symposium, 1993. Proceedings., IEEE 1993*, Oct 1993, pp. 223–226 vol.1.

[83] G. Fischerauer, D. Gogl, R. Weigel, and P. Russer, "Investigation of parasitic effects in multi-transducer saw rf filters," in *Ultrasonics Symposium, 1994. Proceedings., 1994 IEEE*, Oct 1994, vol. 1, pp. 241–244 vol.1.

[84] E. Iborra, L. Vergara, J. Sangrador, M. Clement, A. Sanz-Hervas, and J. Olivares, "Circuital model for the analysis of the piezoelectric response of aln films using saw filters," *IEEE Transactions on Ultrasonics, Ferroelectrics, and Frequency Control*, vol. 54, no. 11, pp. 2367–2375, Nov 2007.

[85] A Atia and A Williams, "New types of waveguide bandpass filters for satellite transponders," *Comsat Tech. Review*, vol. 1, no. 1, pp. 21–43, 1971.

[86] W. A. Atia, K. A. Zaki, and A. E. Atia, "Synthesis of general topology multiple coupled resonator filters by optimization," in *Microwave Symposium Digest, 1998 IEEE MTT-S International*, June 1998, vol. 2, pp. 821–824 vol.2.

[87] S. Amari, "Synthesis of cross-coupled resonator filters using an analytical gradient-based optimization technique," *IEEE Transactions on Microwave Theory and Techniques*, vol. 48, no. 9, pp. 1559–1564, Sep 2000.

[88] A. Garcia-Lamperez, M. Salazar-Palma, and T. K. Sarkar, "Analytical synthesis of microwave multiport networks," in *Microwave Symposium Digest, 2004 IEEE MTT-S International*, June 2004, vol. 2, pp. 455–458 Vol.2.

[89] Klaus Schittkowski, "Nlpql: A fortran subroutine solving constrained nonlinear programming problems," *Annals of operations research*, vol. 5, no. 2, pp. 485–500, 1986.

[90] George Lawrence Matthaei, Leo Young, and Edward McClung Thompson Jones, *Microwave filters, impedance-matching networks, and coupling structures*, Artech house, 1980.

[91] Harry YF Lam, *Analog and digital filters: design and realization*, Englewood Cliffs, NJ: Prentice-Hall, 1979.

[92] Anatol I Zverev, *Handbook of filter synthesis*, Wiley-Blackwell, 2005.

[93] R. M. Foster, "A reactance theorem," *The Bell System Technical Journal*, vol. 3, no. 2, pp. 259–267, April 1924.

[94] A. Talbot, "A new method of synthesis of reactance networks," *Proceedings of the IEE - Part IV: Institution Monographs*, vol. 101, no. 6, pp. 73–90, February 1954.

[95] G. Macchiarella, M. Oldoni, F. Seyfert, and S. Amari, "Synthesis of microwave filters with reactive nodes," in *Microwave Conference (EuMC), 2012 42nd European*, Oct 2012, pp. 467–470.

[96] R. Saal and E. Ulbrich, "On the design of filters by synthesis," *IRE Transactions on Circuit Theory*, vol. 5, no. 4, pp. 284–327, Dec 1958.

[97] Matteo Oldoni, Giuseppe Macchiarella, and Fabien Seyfert, *Synthesis and modelling techniques for microwave filters and diplexers: advances in analytical methods with applications to design and tuning*, Scholars' Press, 2014.

[98] J. Neirynck and D. Manh Cuong, "Realisability of bandpass filters," *Electronics Letters*, vol. 11, no. 12, pp. 256–258, June 1975.

[99] S. Amari, F. Seyfert, and M. Bekheit, "Theory of coupled resonator microwave bandpass filters of arbitrary bandwidth," *IEEE Transactions on Microwave Theory and Techniques*, vol. 58, no. 8, pp. 2188–2203, Aug 2010.

[100] R. Zhang and L. Zhu, "Synthesis of dual-wideband bandpass filters with source-load coupling network," *IEEE Transactions on Microwave Theory and Techniques*, vol. 62, no. 3, pp. 441–449, March 2014.

[101] G. Szentirmai, "Filsyn - a general purpose filter synthesis program," *Proceedings of the IEEE*, vol. 65, no. 10, pp. 1443–1458, Oct 1977.